



**HAL**  
open science

# Numerical simulation of elastic wave propagation in honeycomb core sandwich plates

Biyu Tian

► **To cite this version:**

Biyu Tian. Numerical simulation of elastic wave propagation in honeycomb core sandwich plates. Other. Ecole Centrale Paris, 2012. English. NNT : 2012ECAP0033 . tel-01064030

**HAL Id: tel-01064030**

**<https://theses.hal.science/tel-01064030>**

Submitted on 15 Sep 2014

**HAL** is a multi-disciplinary open access archive for the deposit and dissemination of scientific research documents, whether they are published or not. The documents may come from teaching and research institutions in France or abroad, or from public or private research centers.

L'archive ouverte pluridisciplinaire **HAL**, est destinée au dépôt et à la diffusion de documents scientifiques de niveau recherche, publiés ou non, émanant des établissements d'enseignement et de recherche français ou étrangers, des laboratoires publics ou privés.



**ÉCOLE CENTRALE DES ARTS  
ET MANUFACTURES  
« ÉCOLE CENTRALE PARIS »**

**THÈSE**  
présentée par

**Biyu Tian**

pour l'obtention du

**GRADE DE DOCTEUR**

**Document provisoire**

**Spécialité: Mécanique**

**Laboratoire d'accueil: Mécanique des Sols Structures et Matériaux (MSSMat)**

**SUJET: Numerical simulation of elastic wave propagation in honeycomb core sandwich plates**

# Table of contents

<b>Introduction</b> .....	<b>4</b>
<b>1 Industrial and academic issues</b> .....	<b>7</b>
1.1 Honeycomb core sandwich panel.....	8
1.2 Qualification of the homogenized models.....	10
1.2.1 Homogenized models .....	10
1.2.2 Theoretical analysis of wave propagation in homogenized model .....	10
1.2.3 Numerical simulation analysis of homogenized models .....	12
1.3 Research work on periodic networks .....	16
Conclusion .....	17
<b>2 Bloch wave analysis on periodic networks</b> .....	<b>19</b>
2.1 Bloch wave approach .....	20
2.1.1 Direct and inverse Bloch wave transforms .....	21
2.1.2 Bloch wave analysis of elastic wave propagation in periodic networks .....	22
2.1.3 Brillouin zone.....	22
2.2 Explicit analysis of dispersion relation in 1D periodic beam network .....	24
2.2.1 Longitudinal wave propagation.....	25
2.2.2 Bending and transverse shear wave propagation .....	30
2.3 2D periodic beam networks .....	32
2.3.1 Hexagonal network.....	32
2.3.2 Periodic rectangular network .....	38
2.4 3D periodic plate networks.....	39
2.4.1 Honeycomb thin layer.....	39
2.4.2 Honeycomb core sandwich plate.....	42
Conclusion .....	44
<b>3 Wave propagation in 1D and 2D periodic networks</b> .....	<b>45</b>
3.1 Analysis of the frequency bandgaps in 1D periodic beam network.....	46
3.1.1 Dispersion relation.....	46
3.1.2 Influence of structural and geometric characteristics on frequency bandgaps .....	47
3.1.3 Bloch wave eigenmodes .....	50
3.2 2D hexagonal and rectangular beam networks .....	50
3.2.1 Dispersion relation.....	51
3.2.2 Influence of structural and geometric characteristics on frequency bandgaps of hexagonal network .....	54
3.2.3 Bloch wave eigenmodes .....	62

3.3 Wave propagation velocities analysis in hexagonal beam network.....	65
3.3.1 Membrane S-mode and P-mode.....	65
3.3.2 Bending mode .....	67
Conclusion .....	71
<b>4 Wave propagation in honeycomb core sandwich plate.....</b>	<b>73</b>
4.1 Dispersion relation and Bloch wave eigenmodes .....	74
4.1.1 Discussion on the modeling of the junction conditions in the primitive cell.....	74
4.1.2 Dispersion relation.....	75
4.1.3 Influence of structural and geometric characteristics on dispersion relation.....	77
4.1.4 Bloch wave eigenmodes .....	79
4.2 Wave propagation velocities analysis .....	81
4.2.1 Membrane S-mode and bending modes of honeycomb thin layer.....	81
4.2.2 1 <sup>st</sup> Bloch wave mode of the honeycomb core sandwich plate .....	84
Conclusion .....	86
<b>Conclusion .....</b>	<b>87</b>
<b>Reference .....</b>	<b>89</b>
<b>Appendix A.....</b>	<b>94</b>

# Introduction

Stage separation and cap jettison for space launcher are often performed by pyrotechnic cut process. The heavy pyrotechnic process triggers a high level shock wave. Since the location of the cut line is close to the payload adaptor, the high level shock wave can reach it directly and induce strong vibrations in it. The payload adaptor is assembled with and to support the satellite (payload) and the electronic equipments inside the space launcher. It is composed of two main parts. The upper part is connected to the payload directly. It is a cone structure (ACU) mainly made of honeycomb core sandwich composite shells expanded 100% or not. The lower one is a cylinder structure (Virole) of different aluminum shells. If the certain strong vibration propagates through the payload adaptor, it will probably damage the payload and the electronic equipments. To reduce the vibration in the payload adaptor and then protect all the equipments, it is mandatory to understand the vibration properties in it. Based on the above industrial requirements, research work on the dynamic behaviors of the payload adaptor of Ariane5 under a shock loading has already been presented (Inqui  t   2008, Boullard 2009, Tie and all 2009, Legay and De   2009).

The industrial background of this topic comes partly from the research work on ACU. It is a complementary study based on J. M. Lecl  re, A. Boullard and A. Gr  de's theses, which have already solved problems in three aspects: first is the development of adaptive and parallel dynamic solvers based on time discontinuous space-time Galerkin method; second is the analysis of wave propagation in media with honeycomb cores; third is the analysis of wave propagation in plates and shells (Lecl  re 2001, Boullard 2009, Gr  d   2009).

The objective of the present work first focuses on studying the wave transmission, reflection and attenuation in honeycomb core sandwich composite plate/shell, more particularly in the honeycomb thin layer that is the middle layer of the sandwich structure. Furthermore, we look for an efficient and more appropriate way to model honeycomb sandwich plates/shells.

As one kind of composite materials, honeycomb core sandwich plates/shells have been widely used in aerospace and automotive industry as they have lightweight physical but high strength mechanical properties. In previous work, to simulate the honeycomb core sandwich shells in ACU, classical homogenized models plus orthotropic plate/shell models have been considered to represent honeycomb sandwich structures. Because the considered honeycomb core sandwich shell is a structure with diameter of 2m and height of 1m, while the characteristics length of the honeycomb cells is about 5mm, for which we have a very large sandwich shell size compared with a very small honeycomb cell size. Obviously, if we apply a model that describes all the microstructures of the honeycomb cells of the core layer, the calculation will be very expensive or even prohibitive for the whole sandwich shell structure. The homogenized models take advantage of neglecting the micro-structural of the honeycomb core thin layer by using an equivalent constitutive law with continuous mechanical characteristics instead so that the models can save a large amount of calculation.

However, it has been discussed in Gr  d  's thesis and in our other previous work (Gr  d   2009, Tie and all 2009) that the classical homogenized models offer an efficient and reliable solution to investigate the static or low frequency (LF) dynamic behaviors of the honeycomb core sandwich, but for the high frequency (HF) bending wave propagation, they fail to give appropriate simulation results.

It has been analyzed that on one hand, for the HF ranges, the involved wavelengths are as

short as or even shorter than each honeycomb cellular characteristic length, so it is not reasonable any more to consider the whole middle layer as a homogeneous structure as the interactions between the waves and the honeycomb cellular microstructure become important. These interactions result in some complex deformation modes of the cellular walls that cannot be taken into account by the classical homogenized models. Besides, it is known that the periodicity of the honeycomb cells also influences the way waves propagate. For example it constrains the direction and the frequencies of the wave propagation. On the other hand, for the honeycomb sandwich structure, the two skin layers are thin and rigid and the honeycomb thin layer is relatively thick and flexible. The two skins play a major role in membrane waves propagation but the honeycomb thin layer is much more important for bending wave propagation when compared with the skins. Thus in HF range, the accuracy of the bending wave simulation is more affected. As a result, it is essential to investigate the wave propagation in the sandwich structure, especially the interactions between the waves and the cell walls within or when the waves cross the honeycomb cells, first and then try to provide a better sandwich plates/shells.

In order to reach the above aims, it is believed that the model should consider and integrate the influence of the honeycomb cellular microstructure. Because the honeycomb thin layer is composed of topological isomorphic thin-walled hexagonal cells, we propose to take advantage of its periodicity to apply the Bloch wave theory to the modeling.

The Bloch wave theory is largely employed in quantum mechanics and photonics crystal, and recently it has been applied in periodic mechanic structures as well. According to the theory, any non-periodic function defined on a periodic structure can be decomposed into its Bloch wave modes that are periodic functions and have the same periodicity as the periodic structure, so that the domain to be analyzed and modeled can be reduced from the entire structure to one primitive cell. That means the wave propagation phenomena through the honeycomb thin layer can be understood by investigating the Bloch wave functions only in one honeycomb cell, and lots of efforts can be saved. In addition, with the help of Bloch wave theorem, it is possible to obtain and study the detailed HF wave propagation phenomena in each cell. Since the honeycomb thin layer is discontinuous in geometry, it has been observed that special wave phenomena, such as frequency bandgaps, exist when wave propagating in the structure.

Our research considers first the numerical modeling of elastic wave propagation in one-dimensional (1D) periodic network and then two-dimensional (2D) periodic networks with rectangular and hexagonal cells. Finally the numerical model is applied to the honeycomb thin layer and the honeycomb sandwich as well. The dispersion relation, of each network, between the Bloch wave vectors and the eigenvalues is obtained and analyzed. The dispersive characteristics and the anisotropic behaviors of the periodic networks are observed by analyzing the phase and group wave velocities of several main modes. The first six Bloch eigenmodes of the networks are investigated.

For the 1D periodic network, the dependency of the frequency bandgaps on the mismatch of the characteristic acoustic impedances within a primitive cell is highlighted. The diffracted waves caused by the periodic cells are also analytically calculated and the wave amplification phenomena are observed. For the 2D periodic networks and the honeycomb thin layer, the influence of the geometric and mechanical characteristics, such as the Young's modulus, the internal angle, the double-thickness horizontal cellular wall on the frequency band-gap is studied. Besides, by comparing the wave velocities of several main wave modes with the equivalent homogenized model, we check whether and in which range the homogenized models work.

The thesis is organized as follows:

Chapter 1 is first concentrated on introducing the honeycomb core sandwich panels, such as the manufacturing process and the classical cell types. Then it pays attention to analytically and numerically aspects of the dynamic behaviors of the homogenized models. The membrane and the bending and transverse shear behaviors comparisons between the homogenized models and the honeycomb sandwich reference model are given. In the end, a very brief view is proposed put on the recent researches on periodic networks.

The second chapter is devoted to the theoretical Bloch wave analysis respectively on the 1D periodic beam network, the 2D periodic hexagonal and rectangular cell type beam networks, the honeycomb thin layer and finally the honeycomb sandwich plate. The corresponding first Brillouin zone of each periodic network is built, with special emphasis given on explaining the design of the zone for the 2D hexagonal network. The complete definition of the Bloch eigenproblem that combines the Bloch transform of equilibrium equation, the interface condition within the primitive cell and the periodic boundary condition at the end of the primitive cell is developed and explained for each periodic network.

The third chapter focuses on the numerical results of the elastic wave propagation in the 1D and the 2D periodic hexagonal and rectangular networks. For the 1D network, the analytical dispersion curves are obtained respectively for the longitudinal and the bending and transverse shear waves. Then for the 2D networks, the numerical dispersion curves as well as the dispersion surfaces are obtained. The Bloch wave eigenmodes are analyzed for both the 1D and 2D networks. The influence of the mechanical and geometric characteristics of the networks, such as the Young's modulus, the beam thickness and the internal angle, on the bandgaps is looked into through parametric studies which can no doubt bring new ideas for the design of periodic networks in the future. Finally, the phase and group wave velocities of several main wave modes of the periodic hexagonal beam network are analyzed to study the anisotropic and dispersive behaviors of the networks.

In the end, in the fourth chapter, the numerical results of the elastic wave propagation in the honeycomb thin layer and the sandwich plate are presented. Important information as the dispersion relation and the Bloch wave eigenmodes are obtained. The influence of the double thickness horizontal plate and the internal angle on the dispersion curves are investigated by the parametric studied. The wave propagation velocities of several main modes are calculated and compared with the equivalent homogenized model.

# Chapter 1

## Industrial and academic issues

*In this chapter, the aim is to introduce the industrial and research background of the present work. Therefore, a brief view of honeycomb core sandwich panels is given at first. Then the considered honeycomb core sandwich shell is presented, for which we have a multi-scale problem when doing the numerical simulation. Thirdly, the classical homogenized models usually applied to simulate honeycomb sandwiches are introduced and discussed. Their membrane and bending and transverse shear behaviors are studied analytically and then compared numerically to a reference model that keeps all the detailed information of the microstructure of the honeycomb sandwich. In the end, we get a very brief review of the theorems and the calculation methods that have been developed to look into the wave propagation in periodic networks.*

### Summary

---

<b>1.1 Honeycomb core sandwich panel</b> .....	<b>8</b>
<b>1.2 Qualification of the homogenized models</b> .....	<b>10</b>
1.2.1 Homogenized models.....	10
1.2.2 Theoretical analysis of wave propagation in homogenized model.....	10
1.2.3 Numerical simulation analysis of homogenized models.....	12
<b>1.3 Research work on periodic networks</b> .....	<b>16</b>
<b>Conclusion</b> .....	<b>17</b>

---

## 1.1 Honeycomb core sandwich panel

Honeycomb core sandwich panel is three-layered composite structure. The two cover layers are respectively a top skin and a bottom skin. The one in the middle is a honeycomb core thin layer, which usually contains repetitive regular cavities (Figure 1.1). Honeycomb core sandwich panels have been widely used in various engineering requirements as in one hand they can minimize amount of used material to reach special high bending stiffness and strength to weight and material cost ratio; in the other hand they can be easily manufactured from a large range of materials and their mechanical characteristics can be easily adapted.

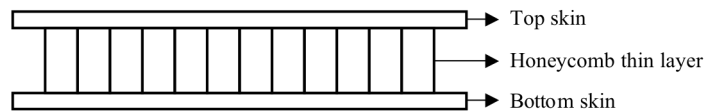


Figure 1.1 Honeycomb core sandwich panel

Nowadays, numbers of cellular shapes and connection methods have been developed to have different kinds of honeycomb core thin layers. Generally, hexagonal, rectangle, triangle or vector cells are the most often used honeycomb cell types in engineering application (Figure 1.2).

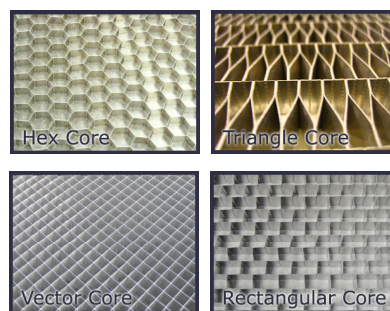


Figure 1.2 Classical cell types of honeycomb core thin layer

Taking the hexagonal cell type as an example, we look into the manufacturing method and process of honeycomb thin layer. To produce a honeycomb core thin layer, first is to press plates to be corrugated sheets by using gears. Then the corrugated sheets that contain a certain shape are bonded one by one to make a whole structure. In the mean while the hexagonal cavities will be formed between each two sheets (Figure 1.3). One point needs to be paid attention is that due to this kind of manufacturing process the horizontal cell walls are twice the thickness of other cell walls.

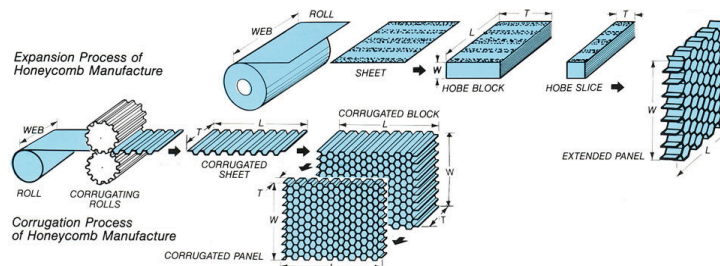


Figure 1.3 Manufacturing processes of hexagonal cell type honeycomb core thin layer

The sandwich shells used in the ACU are composed of carbon skins and an aluminum honeycomb core thin layer. More precisely, the skins are the combination of nine carbon-

fiber-reinforced polymer layers, which are regarded as an orthotropic material. The aluminum honeycomb core thin layer has hexagonal type cells, which shows the inhomogeneous and anisotropic characteristics (Figure 1.4).

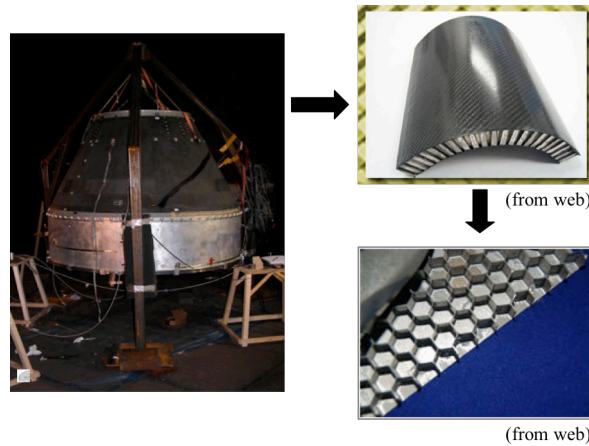


Figure 1.4 Honeycomb core sandwich shells in ACU

Based on our industrial object and requirements, we make numerical modeling of choc wave propagation in the considered sandwich shells. However, we meet a multi-scale problem when doing the numerical simulation. Firstly, the considered sandwich shell has very large shell size, the magnitude order of which is meter, while each honeycomb cell has a very small cell size, the magnitude order of which is millimeter. Especially, if we look into the cellular microstructure, we find that the magnitude order of the cell wall height is centimeter, the one of cell diameter is millimeter and the one of cell wall thickness is micrometer (Figure 1.5). Secondly, the characteristic time of the considered choc wave is about  $10^{-4}$  (s), while this choc wave propagates through the whole shell needs about  $10^{-2}$  (s).

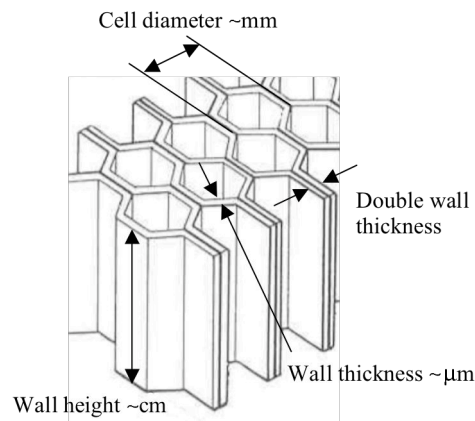


Figure 1.5 Typical geometry characteristics of the honeycomb core thin layer of the sandwich shells used in ACU

Because of the spatial and the time multi-scale problem, we could not use a numerical model that maintains the detailed cellular microstructure, which costs enormous calculation quantities that probably make the calculation prohibitive. Therefore, classical homogenized models, which neglect ‘each real cell’ but look for an equivalent constitutive law with continuous mechanical characteristics instead, has been taken into account, for which, the way to calculate the equivalent mechanical characteristics becomes the key work.

## 1.2 Qualification of the homogenized models

### 1.2.1 Homogenized models

Two classical methods to calculate the equivalent mechanical characteristics of sandwich panels were put forward respectively by Gibson in 1988 and Burton in 1997 and have been applied to numbers of studies under their working conditions [Gibson (1988); Burton (1997)]. In the mean while, other viewpoint of the homogenization have also been looked for in order to make a more general validated method [Dal Maso (1993); Chen (1998); Davini (2011)]. Homogenized models offer an efficient and reliable solution to investigate the static or low frequency dynamic behaviors of honeycomb core sandwich panels and have been validated in various domains, such as viscoelastic honeycomb panel equipped with piezoelectric patches [Florens (2010)].

In our previous work, two types of homogenized models: mono-layered and multi-layered, based on the Burton method, were investigated firstly to model a honeycomb core sandwich plate. The mono-layered homogenized model did not distinguish the skins and the honeycomb core thin layer, so that sandwich plate was homogenized entirely to one orthotropic plate with equivalent mechanical characteristics. Contrarily, the multi-layered homogenized model maintained three layers while only treating the honeycomb core thin layer to an equivalent homogenized orthotropic layer. In the multi-layered homogenized model, the mechanical characteristics of the skins and the homogenized honeycomb core thin layer were distinguished while the continuity of the displacements on the two interfaces was taken into account (Figure 1.6). Both the mono- and the multi-layered model used the Reissner-Mindlin kinematics for thick plate since the shear deformation can be taken into account appropriately [Grédé (2006); Grédé (2009)].

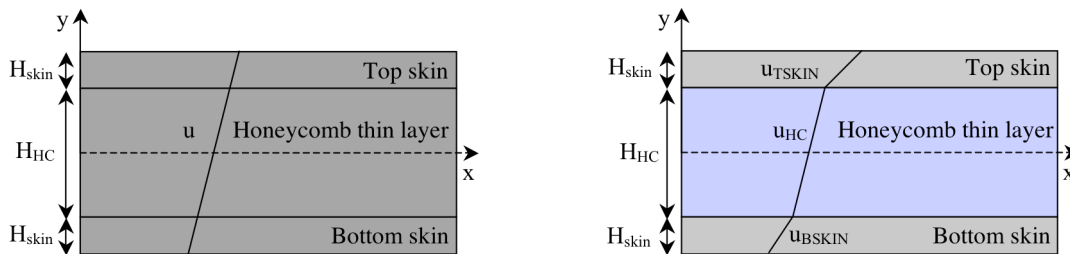


Figure 1.6 Two types of homogenized models (left) Mono-layered homogenized model; (right) Multi-layered homogenized model

### 1.2.2 Theoretical analysis of wave propagation in homogenized model

In order to look into the qualification of the homogenized models, we need to investigate the dynamic behaviors of the homogenized models. Therefore, first of all, we study analytically the wave propagation velocities in the homogenized models, whose results will be numerically compared with the ones obtained by our new numerical approaches that are based on the Bloch wave theory in the chapter 3 and 4.

Consider a mono-layered homogenized orthotropic plate, with  $C_{11}$ ,  $C_{22}$ ,  $C_{12}$ ,  $C_{44}$ ,  $C_{55}$  and  $C_{66}$  the components of orthotropic 2D stiffness matrix,  $\rho$  the mass density and the thickness  $H$ . The homogenized plate is parameterized in its local plate basis  $(\mathbf{e}_1, \mathbf{e}_2, \mathbf{n})$ , where  $(\mathbf{e}_1, \mathbf{e}_2)$  forms an orthonormed basis in the middle plane of the plate and the  $\mathbf{n}$  is a unit vector perpendicular to the plate (Figure 1.7).

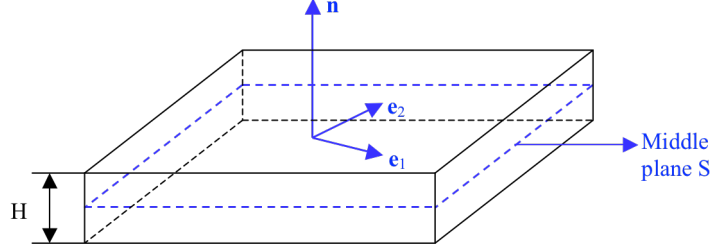


Figure 1.7 Mono-layered homogenized orthotropic plate

Any point  $\mathbf{r}$  of the plate is given in the plate's local basis as:

$$\mathbf{r}(\mathbf{x}_s, \xi) = \mathbf{x}_s + \xi \mathbf{n} \quad (1.1)$$

with  $\mathbf{x}_s = s_1 \mathbf{e}_1 + s_2 \mathbf{e}_2$  the points on the middle plane S and  $\xi$  the coordinate in the thickness of the plate in the range from  $-\frac{H}{2}$  to  $\frac{H}{2}$ . The 5 degrees of freedom (5dofs) Mindlin kinematics is used here, according to which, the displacement  $\mathbf{u}$  reads as:

$$\mathbf{u} = \mathbf{u}_{0s} + u_{0n} \mathbf{n} + \xi \mathbf{u}_{1s} \quad (1.2)$$

with  $\mathbf{u}_{0s} = u_{0s1} \mathbf{e}_1 + u_{0s2} \mathbf{e}_2$  and  $u_{0n}$  respectively the membrane displacement and the deflection of the middle plane and  $\mathbf{u}_{1s} = u_{1s1} \mathbf{e}_1 + u_{1s2} \mathbf{e}_2$  the displacements in the thickness of the plate due to the rotation of the perpendicular fibers. The equilibrium equation of the plate is:

$$\begin{aligned} \mathbf{Q}_s(\xi_s, \xi_s) \cdot \mathbf{U}_{0s} &= \rho \omega^2 \mathbf{U}_{0s} \\ \xi_s \cdot (\mathbf{C}_{st} \cdot \mathbf{U}_{1s}) &= i[\rho \omega^2 - \xi_s \cdot (\mathbf{C}_{st} \cdot \xi_s)] U_{0n} \\ \frac{12}{H^2} i U_{0n} (\mathbf{C}_{st} \cdot \xi_s) &= \left[ \rho \omega^2 \mathbf{I}_{2d} - \mathbf{Q}_s(\xi_s, \xi_s) - \frac{12}{H^2} \mathbf{C}_{st} \right] \cdot \mathbf{U}_{1s} \end{aligned} \quad (1.3)$$

with  $\mathbf{U}_{0s}$ ,  $U_{0n}$  and  $\mathbf{U}_{1s}$  the wave mode of  $\mathbf{u}_{0s}$ ,  $u_{0n}$  and  $\mathbf{u}_{1s}$ ,  $\mathbf{Q}_s(\xi_s, \xi_s)$  the acoustic tensor in the plane S,  $\xi_s = \|\xi_s\| (A \mathbf{e}_1 + B \mathbf{e}_2)$  the wave vector (Figure 1.8),  $\mathbf{C}_{st}$  the transverse shear stiffness tensor and  $\omega$  the angular frequency.

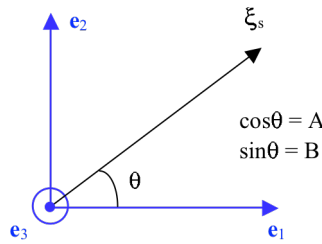


Figure 1.8 Wave vector direction

### (a) Membrane wave propagation

Our previous work [Grédé (2009)] shown that the phase velocity of membrane wave could be obtained as:

$$c_{qp,qS}^2 = \frac{A^2 C_{11} + B^2 C_{22} + C_{66} \pm \sqrt{\Delta}}{2\rho} \quad (1.4)$$

$$\Delta = (A^2 C_{11} + B^2 C_{22} + C_{66})^2 - 4[(A^2 C_{11} + B^2 C_{66})(A^2 C_{66} + B^2 C_{22}) - A^2 B^2 (C_{66} + C_{12})^2]$$

We find that the membrane wave in the homogenized orthotropic plate is neither perpendicular nor parallel to the wave vector. In other words, no pure pressure wave or shear wave exists, while instead, a quasi-pressure wave and a quasi-transverse wave is found in the homogenized orthotropic plate. Second, the wave propagation velocities show anisotropic nature [Tie (2009)].

### (b) Bending and transverse shear wave propagation

In parallel to the study of the membrane wave propagation in the homogenized orthotropic plate, we also study the bending and transverse shear waves propagation in the plate (Appendix A) and get a sixth-degree polynomial of the propagation velocities:

$$A_3 c_f^6 + A_2 c_f^4 + A_1 c_f^2 + A_0 = 0 \quad (1.5)$$

with

$$\begin{aligned} A_3 &= -\left(1 - \frac{12C_{55}}{H^2 \omega^2 \rho}\right) \left(1 - \frac{12C_{44}}{H^2 \omega^2 \rho}\right) \\ A_2 &= \left(1 - \frac{12C_{55}}{H^2 \omega^2 \rho}\right) \left(1 - \frac{12C_{44}}{H^2 \omega^2 \rho}\right) \left(\frac{C_{55}}{\rho} a^2 + \frac{C_{44}}{\rho} b^2\right) + \left(1 - \frac{12C_{55}}{H^2 \omega^2 \rho}\right) \left(\frac{C_{66}}{\rho} a^2 + \frac{C_{22}}{\rho} b^2\right) \\ &\quad + \left(1 - \frac{12C_{44}}{H^2 \omega^2 \rho}\right) \left(\frac{C_{11}}{\rho} a^2 + \frac{C_{66}}{\rho} b^2\right) + \left(1 - \frac{12C_{55}}{H^2 \omega^2 \rho}\right) \frac{12C_{44}^2}{H^2 \omega^2 \rho^2} b^2 + (1 - \kappa_{st2}^2) \frac{12C_{55}^2}{H^2 \omega^2 \rho^2} a^2 \\ A_1 &= -\left(\frac{C_{55}}{\rho} a^2 + \frac{C_{44}}{\rho} b^2\right) \left(\left(1 - \frac{12C_{44}}{H^2 \omega^2 \rho}\right) \left(\frac{C_{11}}{\rho} a^2 + \frac{C_{66}}{\rho} b^2\right) + \left(1 - \frac{12C_{55}}{H^2 \omega^2 \rho}\right) \left(\frac{C_{66}}{\rho} a^2 + \frac{C_{22}}{\rho} b^2\right)\right) \\ &\quad - \left(\frac{C_{66}}{\rho} a^2 + \frac{C_{22}}{\rho} b^2\right) \left(\frac{C_{11}}{\rho} a^2 + \frac{C_{66}}{\rho} b^2\right) \\ &\quad - \frac{12}{H^2 \omega^2 \rho^2} \left(C_{44}^2 b^2 \left(\frac{C_{11}}{\rho} a^2 + \frac{C_{66}}{\rho} b^2\right) - 2C_{55} C_{44} a^2 b^2 \left(\frac{C_{12}}{\rho} + \frac{C_{66}}{\rho}\right) + C_{55}^2 a^2 \left(\frac{C_{66}}{\rho} a^2 + \frac{C_{22}}{\rho} b^2\right)\right) \\ &\quad + a^2 b^2 \left(\frac{C_{12}}{\rho} + \frac{C_{66}}{\rho}\right) \\ A_0 &= \left(\frac{C_{55}}{\rho} a^2 + \frac{C_{44}}{\rho} b^2\right) \left(\left(\frac{C_{66}}{\rho} a^2 + \frac{C_{22}}{\rho} b^2\right) \left(\frac{C_{11}}{\rho} a^2 + \frac{C_{66}}{\rho} b^2\right) - a^2 b^2 \left(\frac{C_{12}}{\rho} + \frac{C_{66}}{\rho}\right)\right) \end{aligned} \quad (1.6)$$

which can be numerically solved.

### 1.2.3 Numerical simulation analysis of homogenized models

Secondly, we investigate numerically the membrane and the bending and transverse shear waves behaviors of the homogenized models. Denote the mono-layered homogenized plate model by HM5 and the multi-layered homogenized plate model by 5/5/5. Furthermore, owing to the skins were much thinner and stiffer when compared to the honeycomb core thin layer, they in fact do not have the same contribution as the honeycomb core thin layer to the transverse shear stiffness of sandwich. Therefore, another adjusted type of mono-layered model, HM5Cs, with neglecting the transverse shear of skins is studied as well.

A 3D reference plate model is set up to exam whether the simulation results of the homogenized models correspond to the behaviors of a real sandwich plate. According to the studied honeycomb core sandwich shells, the reference model plate is constructed. Its skins are composed of nine carbon-fiber-reinforced polymer layers and its aluminum honeycomb core thin layer keeps all the cellular microstructure (Figure 1.9).

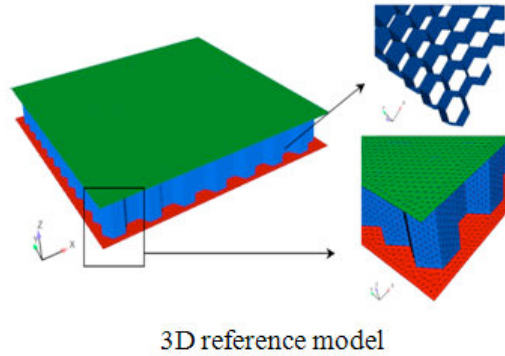


Figure 1.9 3D reference model of honeycomb core sandwich plate

Series of Ricker signal function respectively with the period,  $3\mu\text{s}$ ,  $30\mu\text{s}$  and  $90\mu\text{s}$  are triggered firstly in-plane of the plates to investigate the membrane wave behaviors of the four models. The corresponding frequencies of signal maximal amplitude were 666 KHz, 66 KHz and 22 KHz, which cover a very large frequency range. Then the  $30\mu\text{s}$  and  $90\mu\text{s}$  Ricker signal is trigged separately perpendicular to the plates to study the bending and transverse shear wave behaviors (Figure 1.10).

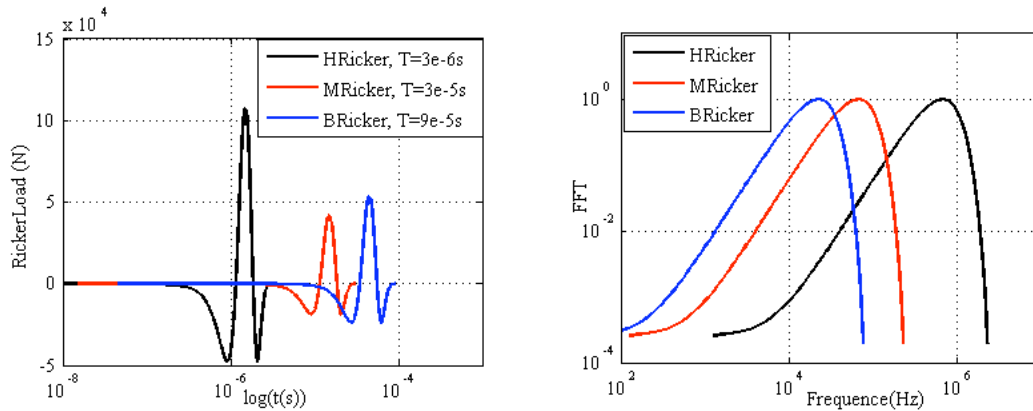


Figure 1.10 External loading: Ricker signal function (left) Time domain; (right) Frequency domain

Two test points, one close to the edge of the model plate and the other in the middle of the plate, are chosen to observe the dynamic behaviors of the mono-layered homogenized model. For the reference model and the multi-layered homogenized model, four points are taken into account since the average results of the top and bottom skin are considered.

**(a) Membrane wave behaviors comparison**

The membrane wave behaviors of the models are investigated at first. The in-plane wave displacement of the four models is compared. It is found that both the mono- and the multi-layered model match well with the reference model (Figure 1.11). Homogenized models could correctly represent the membrane wave behaviors of the sandwich plate.

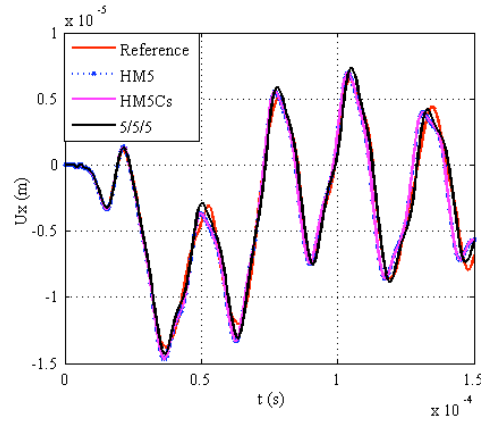


Figure 1.11 In-plane wave displacement of four models on the test points close to the edge of plates

**(b) Bending and transverse shear waves comparison**

Then the bending and transverse shear wave behaviors of the models are considered. The out-of-plane displacement of the four models is compared. First it is noticed that contrary to the membrane wave behaviors, the bending and transverse shear wave behaviors of HM5 model has an evident difference from the reference model, while the adjusted model, HM5Cs, performs an improved simulation result. In other words, the shear stiffness of honeycomb core thin layer plays a main role in the bending and transverse shear wave behaviors of the sandwich plate.

Second it is remarked that the multi-layered homogenized model could mostly correspond to the reference model in the considered frequency range, while its simulation performances become worse with the increase of frequency (Figure 1.12).

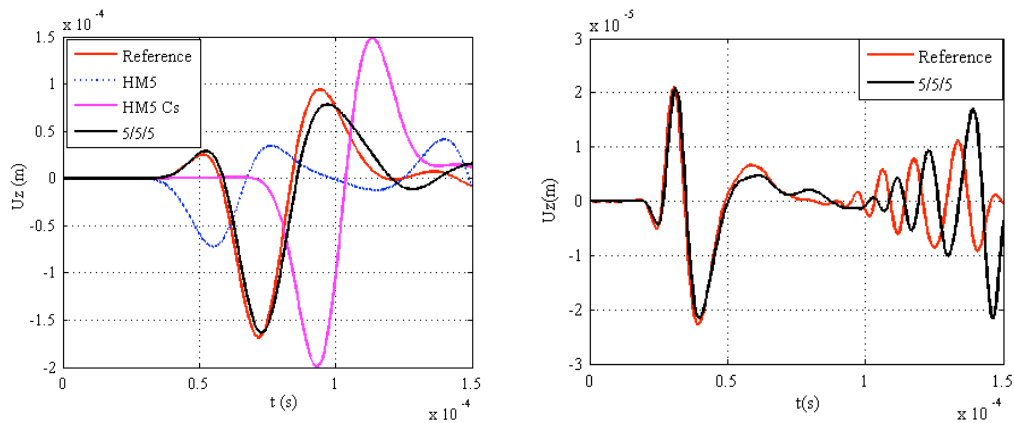


Figure 1.12 Out-of-plane wave displacement of four models at the edge of the plate (left) Ricker loading maximal amplitude frequency 22 KHz; (right) Ricker loading maximal amplitude frequency 66 KHz

Moreover, the bending and transverse shear wave propagation velocity in the four models can be numerically obtained, for which we find that the wave velocity of the multi-layered model can better coincide the one of the reference model (Figure 1.13).

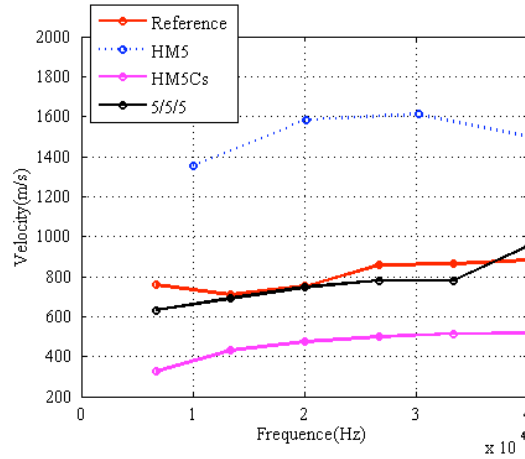


Figure 1.13 Bending and transverse shear wave propagation velocity

Now we know that the homogenized models could describe the membrane wave behaviors of the sandwich in a large frequency range but they fail to describe the bending and transverse shear wave behavior for the same frequency range. The errors come from two main aspects. Firstly, the honeycomb core thin layer plays a very important role in the bending and transverse shear behavior of the sandwich plate. Compared with the skins, the honeycomb core thin layer is a thick and soft structure composed of thin aluminum sheets. It has complex wave propagation situations and deformation modes in cells. It is not easy to find an accurate simulation model that is allowed to including all the complicated deformation information. For instance, the transverse shear warping was not taken into account by the Mindlin thick plate kinematics (Figure 1.14).

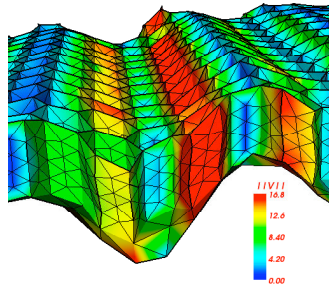


Figure 1.14 Transverse shear warping in cells

Second, in HF range, the involved wavelength is close to the honeycomb cellular size. In other words, HF wave is able to distinguish each honeycomb cell. Therefore it is not feasible to still use the homogenized models for HF wave simulation since they ignore the cells as well as the effects coming from the periodicity of the sandwich.

To make a new numerical modeling of honeycomb sandwich that allows introducing the HF wave propagation phenomenon within honeycomb cells but not increasing the calculation efforts, we propose to take advantage of the periodicity of the honeycomb, thanks to which the analysis and study of wave propagation can be reduced to a primitive cell instead of a entire honeycomb plate.

### 1.3 Research work on periodic networks

In 1883, the Floquet-Bloch theory that was first put forward by Floquet to study a 1D Mathieu's equation in periodic media and then developed by Bloch to solve for a more general 3D problem of electrons in crystal lattices in 1928 [Floquet (1883); Bloch (1928)]. Nowadays, the Floquet-Bloch has become the foundation theory for the research on periodic networks. In 1946, Brillouin applied the Floquet-Bloch theory to analyze the elastic wave propagation in periodic networks, where the definition of Brillouin zone was first given to explain the wave vector in periodic networks was restricted in the reciprocal cell of the network [Brillouin (1946)].

Periodic cellular networks are discontinuous in geometry and material properties. From 1960's, the growing attention has been paid to the study on periodic networks since they have been more and more used in engineering application. It has been firstly paid attention that a special wave phenomenon, wave attenuation, exists in periodic networks, which means when elastic wave propagating in a periodic network, within some frequency intervals, wave can not propagate through the network but is attenuated quickly within the periodic cells [Cremer (1967)]. The corresponding frequency intervals form the frequency bandgaps of the network.

In 1970's, the direction solution of wave propagation was deeply discussed by professor D. J. Mead from Southampton university first to the 1D periodically-supported beams and then to the 2D plates [Mead (1970); Mead (1979)]. The most important relation between the propagation constant  $\mu$  and the system's eigenvalue  $\omega$  has been obtained and analyzed to explain the wave attenuation phenomenon [Mead (1973)], which was due to the creation of the stationary waves resulted from the wave reflection, transmission and conversion when across periodic cells. Other analogical studies were also developed at Southampton during 1970-1996, such as studying the coupled bending-longitudinal wave motion in periodic beams, the free vibration in cylindrical shell and harmonic response of sandwich plates [Mead (1983); Mead (1987); Mead (1991)].

In 1995, the dynamic stiffness matrix representation combined with the skew-symmetric matrix was used to solve for the eigensolutions of a symplectic eigenvalue problem by professor Zhong from Dalian university of Technology [Zhong (1995)]. A more general calculation method was applied to the study of the wave propagation in a periodic wave-guide by Mencik in 2005 [Mencik (2005)].

Since the frequency bandgaps is a most important and interesting characteristics for periodic networks, lots of investigations has already been developed in quantities of types periodic networks [Sigalas (1992); Sigalas (1993); Richards (2003); Tawfik (2004)]. It was found that the frequency bandgaps is anisotropic in the periodic network and depends on the impedance mismatch generated by periodic discontinuities in geometry or material properties within one cell or between adjacent cells [Langley (1997); Ruzzene (2003); Gonella et al. (2008); Tian (2011)]. As an important consequence, periodic cellular networks can be considered as frequency or spatial filters depending on different patterns or network designs.

Generally, recent studies are concentrated on two main aspects: first was to explore the frequency bandgaps of different periodic networks with various types periodic cells [Jeong (2004); Srikantha Phani (2006); Spadoni (2009); Tee (2010);]. Second has been focused on bandgaps design on the viewpoint of vibration control [Jensen (2002); Sigmund (2003); Barbarosie (2004)]. Generally, engineers look for the bandgaps of periodic networks, take advantage of which the network can attenuate the vibration in the corresponding frequency ranges. Therefore, numbers of research has been developed on creating the bandgaps

artificially by adding a sub-network in the primitive cell, with which a locally resonant system can be formed and results in bandgaps [Liu (2000); Ho (2003)]. It is said that the bandgaps created by the locally resonant system are allowed to locate in a lower frequency range but with a narrower gap width when compared with natural bandgaps. Moreover, other emphases have also been paid to study the effects of boundary layer, the disordered periodic networks, the influence of damping and defects on bandgaps, and the HF vibration analysis on periodic networks under fluid loadings [Srikantha Phani (2008); Langley (1995); Bouzit (1995); Sorokin (2004); Zhang (2005); Collet (2011)]. Especially for the influence of defects on bandgaps, it has been studied that the imperfection of periodic networks effectively affects the structure of bandgaps and can create defect bandgaps [Sigalas (1998); Wu (2002); Martinsson (2003)].

Most part of the work on periodic networks was done with the finite element method (FEM). In 1997, the periodic network theory combining with the statistic energy analysis method (SEA) on study of the modal density and energy flow was developed by Langley and in 2000 the periodic network theory combining with the Boundary element method (BEM) was applied to study a large embedded network by Clouteau [(Langley (1997); Cotoni (2008); Clouteau (2000)].

In the present work, the Floquet-Bloch theory with FEM will be developed and applied to study periodic networks and finally the honeycomb core sandwich plates. The special emphasis will be put on figuring out the frequency bandgaps, the influence of mechanic/geometric parameters on the bandgaps networks and the wave propagation and the energy flow situation.

## **Conclusion**

Honeycomb core sandwich panels are a kind of composite materials that have been widely used in aeronautic engineering. The honeycomb core sandwich plate considered in present work is composed of two orthotropic carbon skins and an aluminum honeycomb core thin layer. The skins are thin and stiff but the honeycomb core thin layer is thick and soft.

Based on the industrial requirement, a numerical modeling of HF frequency choc wave propagating in honeycomb sandwich plate by using mono- and multi-layered homogenized models was developed previously for the homogenized models neglected the honeycomb microstructure and offered an efficient numerical simulation. In the mean while, a 3D reference sandwich model with a small sample plate size was also been set up to compare with the mono- and multi-layered homogenized models. However, our studies indicated that the homogenized models failed to give reasonable simulation results for the HF bending and transverse shear waves behaviors of sandwich.

By looking at the wave propagation in orthotropic plates, we found that the bending and transverse shear waves were mostly controlled by the honeycomb core thin layer, in which case the homogenized models were too simplified to considering all the complicated deformations, especially in HF range, much more interactions occurred between the wave and the periodic cells. In addition, because the mono-layered homogenized model did not distinguish the transverse shear between the skins and the honeycomb, it gave an even worse result.

Therefore, we looked for a more precise numerical model but without augmenting the calculation efforts. As the honeycomb sandwich can be treated as a kind of periodic structure, we considered developing a model by only calculating the wave propagation situation in a

primitive cell of sandwich instead of the whole structure by means of using the Floquet-Bloch theory. A brief view was given to the recent researches that were based the Floquet-Bloch theory on analyzing the wave propagation in periodic structures.

# Bloch wave analysis on periodic networks

*In the chapter, the Bloch wave theory is introduced at first, so its application to analyzing elastic wave propagation in periodic networks composed of elastic thin structures, by virtue of which we can take advantage of the periodicity of the networks in order to save calculation efforts. The definition of the first Brillouin zone, uniquely defined primitive cell in the reciprocal phase space of Bloch wave vectors is illustrated briefly as well. Then the way to analyze the dispersion relation between the Bloch wave vector and the eigenfrequency is presented in a one dimensional (1D) periodic beam network, for which analytic solutions are available and result in a straightforward investigation of the existence of frequency bandgaps. Then the relative first Brillouin zone of each periodic network is built and illustrated. Finally, analytic models based on the Bloch wave theory for two dimensional (2D) periodic hexagonal and rectangular beam networks and three dimensional (3D) periodic networks: a honeycomb thin layer and a honeycomb core sandwich plate, are defined.*

## Summary

---

<b>2.1 Bloch wave approach</b> .....	<b>20</b>
2.1.1 Direct and inverse Bloch wave transforms.....	21
2.1.2 Bloch wave analysis of elastic wave propagation in periodic networks.....	22
2.1.3 Brillouin zone .....	22
<b>2.2 Explicit analysis on dispersion relation in 1D periodic beam network</b> .....	<b>24</b>
2.2.1 Longitudinal wave propagation .....	25
2.2.2 Bending and transverse shear wave propagation.....	30
<b>2.3 Bloch wave eigenvalue model of 2D periodic beam networks</b> .....	<b>32</b>
2.3.1 Periodic hexagonal network .....	32
2.3.2 Periodic rectangular network.....	38
<b>2.4 Bloch wave eigenvalue model of 3D periodic plate networks</b> .....	<b>39</b>
2.4.1 Honeycomb thin layer .....	39
2.4.2 Honeycomb core sandwich plate .....	42
<b>Conclusion</b> .....	<b>44</b>

---

## 2.1 Bloch wave approach

Bloch wave or Bloch state is first discovered and applied to the quantum mechanics of electrons in crystal lattice by Felix Bloch [Bloch (1928)]. It describes the wave function of a particle, usually an electron, placed in a periodic potential. The simplest example is the Kronig-Penney model, an infinite 1D periodic lattice composed of the same type of atoms (Figure 2.1) [Atkins (2005)]. Suppose there exists an electron in the lattice. The aim is to solve the following time-independent Schrödinger equation of the model as:

$$-\frac{\hbar^2}{2m_e} \frac{d^2\psi(r)}{dr^2} + V(r)\psi(r) = E\psi(r) \quad (2.1)$$

where  $r$  is the coordinate of any point in the lattice and  $V(r)$  is the periodic potential of the electron, which is described as the "potential well" spreading along the periodic lattice of atoms. The period of the model under consideration is denoted by  $a$ :  $V(r) = V(r+a)$ .  $E$  and  $\psi(r)$  are respectively the electron energy and the electron solution of the Schrödinger equation (2.1).

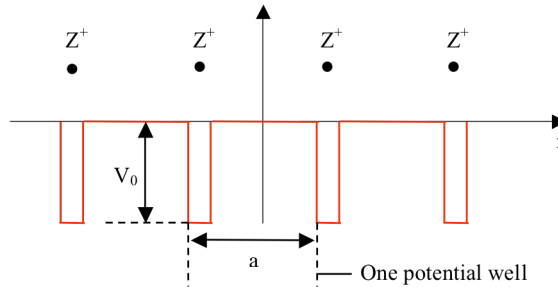


Figure 2.1 1D Kronig-Penney model

The Bloch wave theory states in fact that the electron solution,  $\psi(r)$ , to the Schrödinger equation for such a system may be written as the product of a plane wave envelope function and a periodic Bloch wave function  $\psi^B(r, k)$  as:

$$\psi_k(r) = \psi^B(r, k)e^{-ikr} \quad (2.2)$$

with  $k$  the Bloch wave vector. In the 1D Kronig-Penney model,  $k$  is scalar. Actually, for each  $k$ , it corresponds to one Bloch wave function,  $\psi^B(r, k)$ , which has the same periodicity as the model:

$$\psi^B(r, k) = \psi^B(r + a, k) \quad (2.3)$$

By substituting (2.2) into (2.1), the Schrödinger equation can be in fact rewritten and regarded as an eigenvalue problem with the eigenvalue  $E(k)$  and the Bloch wave eigenmode  $\psi^B(r, k)$  as:

$$\frac{d^2 \psi^B(r, k)}{dr^2} + 2ik \frac{d\psi^B(r, k)}{dr} - \left( \frac{2m_e}{\hbar^2} V(r) + k^2 \right) \psi^B(r, k) = -\frac{2m_e}{\hbar^2} E \psi^B(r, k) \quad (2.4)$$

Because  $\psi^B(r, k)$  is periodic along the lattice, it gives the same results whether we solve it within one potential well or in the whole lattice. Consequently, it is enough to solve the equation (2.4) within one potential well, with which we can investigate the electronic waves in the whole lattice.

More generally, a Bloch-wave description has been extended to any wave-like phenomenon in a periodic medium. It can be expressed in several forms according to different application domains and requirements. For example, a periodic dielectric in electromagnetism leads to photonic crystals and a periodic acoustic medium leads to phononic crystals [Yeh (1977); Jones (2007)]. In mechanics, the Bloch wave theory is often used to study different periodic networks to look for periodic wave modes.

### 2.1.1 Direct and inverse Bloch wave transforms

Given a  $N$ -dimensional periodic cellular network  $\Omega$ , with a primitive cell  $Q_0$ , then any point  $\mathbf{r}$  of  $\Omega$  can be parameterized with respect to a point  $\mathbf{p}$  of  $Q_0$  in the following way:

$$\mathbf{r} = \mathbf{p} + n_j \mathbf{g}_j \quad (2.5)$$

with  $n_j \in \mathbb{Z}$  and  $\{\mathbf{g}_j\}_{j=1,\dots,N}$  the periodicity vectors basis of  $\Omega$ , which is also called direct cell basis.  $\{\mathbf{g}_j\}$  is generally not orthonormal and its choice is not unique. The Einstein summation convention is used here:  $n_j \mathbf{g}_j = \sum_{j=1}^N n_j \mathbf{g}_j$ .

The Bloch wave theory [Kittel (1962); Sanchez-Palencia (1989); Sjöberg (2005)] states that a non-periodic function  $\mathbf{u}(\mathbf{r})$  defined on  $\Omega$  can be transformed or decomposed into its Bloch wave mode  $\mathbf{U}^B(\mathbf{r}, \mathbf{k})$ :

$$\mathbf{U}^B(\mathbf{r}, \mathbf{k}) = \sum_{\{n_j\} \in \mathbb{Z}^N} \mathbf{u}(\mathbf{r} + n_j \mathbf{g}_j) \cdot e^{i\mathbf{k} \cdot (\mathbf{r} + n_j \mathbf{g}_j)} \quad (2.6)$$

where  $\mathbf{k}$  denotes the Bloch wave vector belonging to the reciprocal phase space to the periodic network  $\Omega$ . Based on (2.6), it is straightforward that  $\mathbf{U}^B(\mathbf{r}, \mathbf{k})$  is periodic and has the same periods as  $\Omega$  as:

$$\mathbf{U}^B(\mathbf{p} + n_j \mathbf{g}_j, \mathbf{k}) = \mathbf{U}^B(\mathbf{p}, \mathbf{k}) \quad (2.7)$$

Inversely, the inverse Bloch wave transform reconstitute the original function  $\mathbf{u}(\mathbf{r})$  in the following way:

$$\mathbf{u}(\mathbf{r}) = \frac{1}{\text{vol}(Q^0)} \int_{Q^0} \mathbf{U}^B(\mathbf{r}, \mathbf{k}) e^{-i\mathbf{k} \cdot \mathbf{r}} d\mathbf{k} \quad (2.8)$$

with  $Q^0$  the reciprocal cell dual to the primitive cell  $Q_0$ .  $Q^0$  is also known as the first Brillouin zone and has the following relationship with  $Q_0$  as:

$$\text{vol}(Q_0) \text{vol}(Q^0) = (2\pi)^N \quad (2.9)$$

Taking  $Q^0$  as a primitive cell, a reciprocal periodic network can be formed along another periodicity vectors basis,  $\{\mathbf{g}^l\}_{l=1,\dots,N}$ , which satisfies the following relationship with  $\{\mathbf{g}_j\}$  as:

$$\mathbf{g}_j \cdot \mathbf{g}^l = 2\pi \delta_{jl} \quad (2.10)$$

with  $\delta_{jl}$  the Kronecker delta.  $\{\mathbf{g}^l\}$  is in fact the contravariant basis of the direct covariant basis  $\{\mathbf{g}_j\}$  and called the reciprocal cell basis.

As a simple example, Figure 2.2 shows that a direct Bloch wave transform, with  $k = 5$ , of a Gauss function defined on a periodic network composed of rods with the period equal to 1.

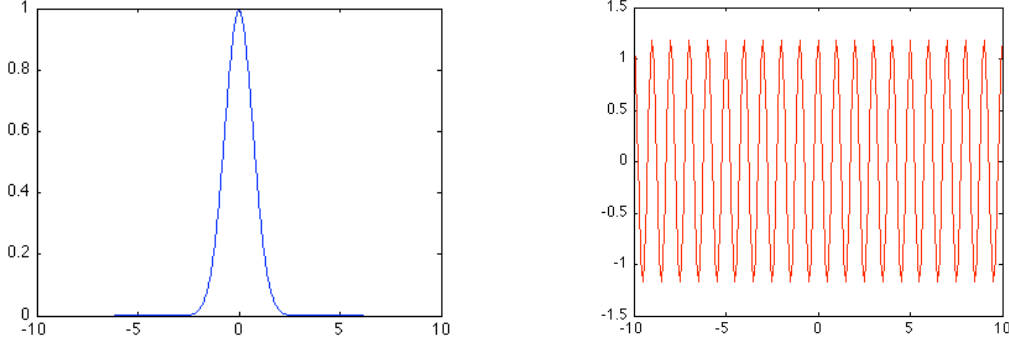


Figure 2.2 (left) Gauss function; (right) Its bloch wave transform with the wave vector  $k = 5$

### 2.1.2 Bloch wave analysis of elastic wave propagation in periodic networks

To analyze the elastic wave propagation in the periodic network  $\Omega$  using the Bloch wave theory, we search for plane waves propagating at angular frequency  $\omega$  with a Bloch wave mode  $\mathbf{U}^B(\mathbf{r}, \mathbf{k})$  as wave mode defined as follows:

$$\mathbf{u}_k(\mathbf{r}, t) = \mathbf{U}^B(\mathbf{r}, \mathbf{k})e^{-i(\mathbf{k}\cdot\mathbf{r}-\omega t)} \quad (2.11)$$

where  $t$  denotes the time variable. It is straightforward that for  $\mathbf{r} = \mathbf{p} + n_j\mathbf{g}_j$ , we have:

$$\mathbf{u}_k(\mathbf{r}, t) = \mathbf{u}_k(\mathbf{p}, t)e^{-i\mathbf{k}\cdot(n_j\mathbf{g}_j)} \quad (2.12)$$

Therefore, the wave propagation phenomena,  $\mathbf{u}_k(\mathbf{r}, t)$ , in the whole periodic network  $\Omega$  can be fully understood through their Bloch wave mode analysis,  $\mathbf{U}^B(\mathbf{p}, \mathbf{k})$ , within the primitive cell  $Q_0$ . In addition, it has been also proven that, if  $\mathbf{k}' = \mathbf{k} + n_j\mathbf{g}_j^1$ , for  $\forall \{n_j\} \in \mathbb{Z}^N$ , then we have:

$$\mathbf{u}_{k'}(\mathbf{r}, t) = \mathbf{u}_k(\mathbf{r}, t) \quad (2.13)$$

Hence, the wave vector  $\mathbf{k}$  is also periodic on the reciprocal network with  $\{\mathbf{g}_j^1\}_{j=1,\dots,N}$  as basis of periodicity vectors [Jones (2007); Spadoni (2009); Tie (2012)]. It means that the solutions can be completely characterized by their behavior in a single period in the reciprocal network, which is in fact the first Brillouin zone  $Q^0$ , since it gives the limitation of all the possible wave propagation directions for  $\Omega$ . Full dispersion relation between the wave vector  $\mathbf{k}$  and the angular frequency  $\omega$  can be obtained by only evaluating it over  $Q^0$ .

It is known that the honeycomb sandwich plate that we are interested in is a periodic network with hexagonal cells of plates, so it is reasonable for us to apply the Bloch wave analysis on the wave propagation in honeycomb sandwich. Therefore lots of numerical efforts can be saved so that the numerical modeling and analysis taking into account the cellular microstructure of the honeycomb becomes feasible.

### 2.1.3 Brillouin zone

The first Brillouin zone is an essential concept of the Bloch wave analysis and so its identification constitutes a very important step of the application of the Bloch wave theory. In fact, the first Brillouin zone,  $Q^0$  is defined as the set of the points in the reciprocal network that can be reached from the origin without crossing any Bragg plane, which bisects the reciprocal cell basis [Kittel (1962)].

For a first example, we consider a 1D periodic network with the primitive cell  $Q_0$ , the period  $\lambda$  and the direct cell basis  $\mathbf{g}_1$ . Point O is the origin and  $\mathbf{e}_x$  is the Cartesian basis (Figure 2.3).

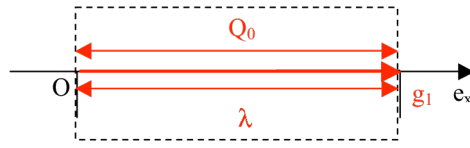


Figure 2.3 1D periodic network

According to (2.10), we can obtain the reciprocal cell basis in the same direction as  $\mathbf{g}_1$  with the norm,  $\|\mathbf{g}^1\| = 2\pi/\lambda$ . Placing the origin, O, as the center of the first Brillouin zone, we then draw the perpendicular bisector of  $\mathbf{g}^1$  as well as its symmetric line in the other side of origin. The interval delimited by those two lines is the first Brillouin zone  $Q^0$  of the 1D periodic network (Figure 2.4).

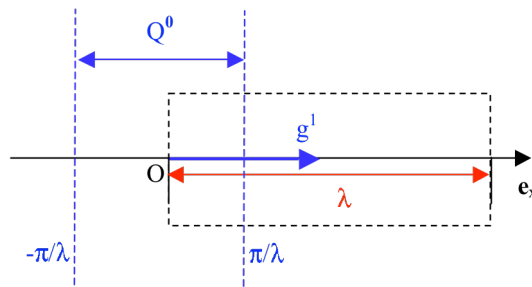


Figure 2.4 The first Brillouin zone of the 1D periodic network

As a second example, we consider a 2D periodic network built from a rectangular primitive cell  $Q_0$ , with the horizontal period denoted by  $\lambda_1$  and the vertical one by  $\lambda_2$ . Figure 2.5 shows  $(\mathbf{g}_1, \mathbf{g}_2)$  the direct cell basis vectors,  $(\mathbf{g}^1, \mathbf{g}^2)$  the reciprocal cell basis vectors and  $(\mathbf{e}_x, \mathbf{e}_y)$  the Cartesian basis vectors. Accordingly, the direct and reciprocal cell basis can be respectively expressed in the Cartesian basis as:

$$\begin{aligned} \mathbf{g}_1 &= \lambda_1 \mathbf{e}_x, \quad \mathbf{g}_2 = \lambda_2 \mathbf{e}_y \\ \mathbf{g}^1 &= \frac{2\pi}{\lambda_1} \mathbf{e}_x, \quad \mathbf{g}^2 = \frac{2\pi}{\lambda_2} \mathbf{e}_y \end{aligned} \quad (2.14)$$

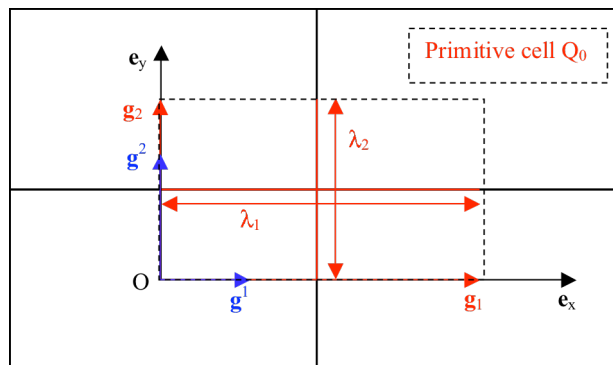


Figure 2.5 2D periodic cellular network with rectangular primitive cell

Place O as the center of the first Brillouin zone and draw the perpendicular bisectors of  $\mathbf{g}^1$  and  $\mathbf{g}^2$  as well as the symmetric lines. The closed polygon,  $Z_1Z_2Z_3Z_4$ , contoured by these perpendicular bisectors is taken as the first Brillouin zone of the network (Figure 2.6).

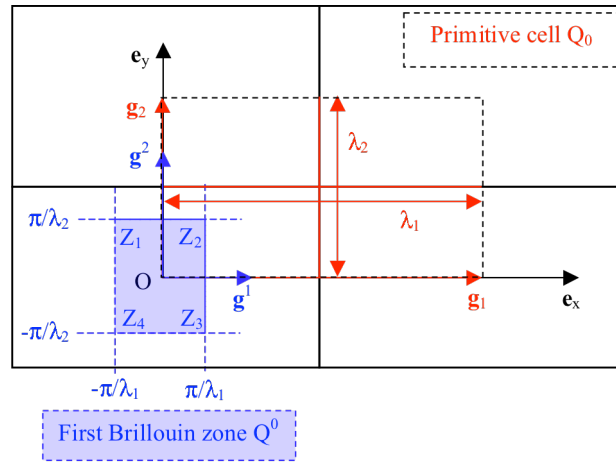


Figure 2.6 The first Brillouin zone of the 2D periodic rectangular network

After introducing the essential concepts of the Bloch wave theory, now we can start applying it to study the wave propagation in periodic networks step by step. Our final objective is to analyze the phenomena of elastic wave propagation in the honeycomb core sandwich plate.

## 2.2 Explicit analysis of dispersion relation in 1D periodic beam network

First of all, the study of the elastic wave propagation in periodic cellular networks using the Bloch wave theory begins with a 1D infinite periodic network composed of elastic beams. For in this simple 1D case, analytical solutions are available, with the help of which we can explain the basic principles in a clear and easy way and we can explain the wave phenomena observed in the network mathematically as well as physically. Therefore, the 1D case constitutes in fact a valuable help to understand and analyze the wave propagation situations in 2D or 3D periodic networks.

The 1D infinite periodic network considered here is described in Figure 2.7: It is composed of two types of elastic beams with different geometrical and mechanical characteristics displaying periodicity along the network. As for the primitive cell of the network we can use the substructure composed of two rigidly-jointed beams,  $B_1$  and  $B_2$ , respectively of length  $l_1$  and  $l_2$ , therefore the period is  $\lambda = l_1 + l_2$ . The Lamé coefficients and the density are respectively  $(\lambda_1, \mu_1, \rho_1)$  and  $(\lambda_2, \mu_2, \rho_2)$ . The whole network is considered under the Cartesian basis  $(\mathbf{e}_x, \mathbf{e}_y)$ . The thickness of both beams in the direction  $\mathbf{e}_y$  is  $H$ .

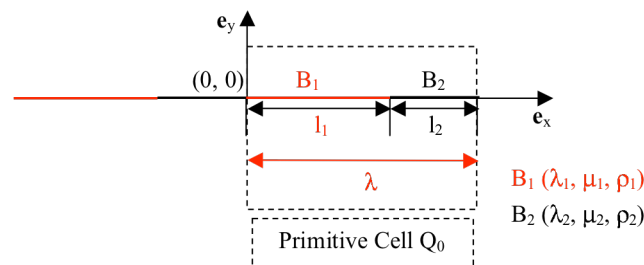


Figure 2.7 1D periodic beam network and its primitive cell

Then any point  $\mathbf{r}$  of the 1D network is given by the components of Cartesian coordinate system as:

$$\mathbf{r}(x, \xi) = x \mathbf{e}_x + \xi \mathbf{e}_y \quad (2.15)$$

where  $\xi$  is the variable in the transverse section of beams. The Timoshenko kinematics for thick beams is used here for it takes into account the transverse shear deformation and the rotational inertia effects of beams. As only the displacements in the plane Oxy are considered herein, the displacement  $\mathbf{u}$  in each beam reads as:

$$\mathbf{u}(x, \xi, t) = u_{0x}(x, t)\mathbf{e}_x + u_{0y}(x, t)\mathbf{e}_y + \xi u_1(x, t)\mathbf{e}_x \quad (2.16)$$

where  $u_{0x}(x, t)$  and  $u_{0y}(x, t)$  are respectively the longitudinal displacement and the deflection of the neutral axis of beam in the plane Oxy and  $u_1(x, t)$  the displacement in the thickness due to the rotation of its transverse sections. Consequently, both  $u_{0y}(x, t)$  and  $u_1(x, t)$  describe the transverse shear and the bending behaviors of the beam in the plane Oxy. Within the classical plane stresses assumption, then the dynamic equilibrium equations of the  $i$ -th beam read as:

$$\begin{cases} E_j \frac{d^2 u_{0x}(x, t)}{dx^2} = \rho_j \frac{d^2 u_{0x}(x, t)}{dt^2} \\ \mu_j \left( \frac{d^2 u_{0y}(x, t)}{dx^2} + \frac{du_1(x, t)}{dx} \right) = \rho_j \frac{d^2 u_{0y}(x, t)}{dt^2}, \quad (j=1, 2) \\ E_j \frac{d^2 u_1(x, t)}{dx^2} - \frac{12\mu_j}{H^2} \left( \frac{du_{0y}(x, t)}{dx} + u_1(x, t) \right) = \rho_j \frac{d^2 u_1(x, t)}{dt^2} \end{cases} \quad (2.17)$$

with  $E_j$  the Young's modulus. More precisely, in (2.17), the first single equation of  $u_{0x}$  refers to the longitudinal wave along the beam axis and the other two refer to the bending and transverse shear waves in the plane Oxy. The two parts are completely uncoupled and so can be analyzed independently.

## 2.2.1 Longitudinal wave propagation

### a) Dispersion relation analysis

First of all, we are interested in studying the longitudinal wave propagation in the 1D periodic network. For simplicity concern, the subscript "0x" will be omitted hereafter  $u(x, t) = u_{0x}(x, t)$ , so the equilibrium equation of the  $j$ -th beam ( $j = 1, 2$ ) reads simply as:

$$E_j \frac{d^2 u(x, t)}{dx^2} = \rho_j \frac{d^2 u(x, t)}{dt^2} \quad (2.18)$$

According to (2.11), we look for the plane waves propagating defined as the following:

$$u(x, t) = U^B(x, k) e^{-i(kx - \omega t)} \quad (2.19)$$

where  $\omega$  denotes the anagular frequency,  $U^B(x, k)$  the Bloch wave mode and  $k$  the Bloch wave vector. Substituting (2.19) to (2.18), we get the following Bloch wave transform of the equilibrium equation:

$$E_j \frac{d^2 U^B(x, k)}{dx^2} - 2ikE_j \frac{dU^B(x, k)}{dx} - E_j k^2 U^B(x, k) = -\rho_j \omega^2 U^B(x, k) \quad (2.20)$$

The equation (2.20) defines in fact an eigenvalue problem with the eigenvalue  $\omega = 2\pi f$ ,  $f$  the eigenfrequency, and the eigenmode  $U^B(x, k)$ . Consequently, from now on we look for the eigenvalue as well as the eigenmode of (2.20) within the primitive cell instead of the longitudinal wave propagation solutions in the whole 1D periodic network.

It is straightforward that the general solution of (2.20) has the following analytical form:

$$U_j^B(x, k) = a_j e^{i\left(k + \frac{\omega}{c_j}\right)x} + b_j e^{i\left(k - \frac{\omega}{c_j}\right)x} \quad (2.21)$$

where  $c_j = \sqrt{E_j/\rho_j}$  is the longitudinal wave velocity in the  $j$ -th beam and  $(a_j, b_j)$  are two unknown constants for the  $j$ -th beam, which can be entirely determined when the following interface conditions between the two beams at their junction point and the periodic boundary conditions at the ends of the primitive cell are considered (Figure 2.8).

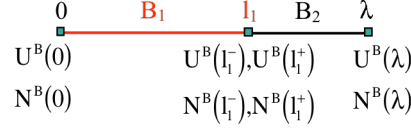


Figure 2.8 Displacement and force components to be considered in the interface and boundary conditions within the primitive cell

$$\begin{aligned} U^B(l_1^-) &= U^B(l_1^+), \quad N^B(l_1^-) = N^B(l_1^+) \\ U^B(0) &= U^B(\lambda), \quad N^B(0) = N^B(\lambda) \end{aligned} \quad (2.22)$$

where  $N^B$  is the Bloch wave transform of the generalized longitudinal force reading as:

$$N^B = HE \left( \frac{dU^B}{dx} - ikU^B \right) \quad (2.23)$$

By substituting (2.21) into (2.22), we get the following system of four linear equations:

$$\mathbf{A}(\omega, k; c_1, c_2) \begin{Bmatrix} a_1 \\ b_1 \\ a_2 \\ b_2 \end{Bmatrix} = 0 \quad (2.24)$$

with a coefficient matrix  $\mathbf{A}$  depending on the Bloch wave vector and the eigenvalue, which is defined as following:

$$\mathbf{A}(\omega, k; c_1, c_2) = \begin{bmatrix} 1 & 1 & 1 & 1 \\ ik_{1p} & ik_{1m} & -ik_{2p} & -ik_{2m} \\ e^{-ik_{1p}l_1} & e^{-ik_{1m}l_1} & -e^{ik_{2p}l_2} & -e^{ik_{2m}l_2} \\ ik_{1p}e^{-ik_{1p}l_1} & ik_{1m}e^{-ik_{1m}l_1} & -ik_{2p}e^{ik_{2p}l_2} & -ik_{2m}e^{ik_{2m}l_2} \end{bmatrix} \quad (2.25)$$

with  $k_{1p} = k + \frac{\omega}{c_1}$ ,  $k_{1m} = k - \frac{\omega}{c_1}$ ,  $k_{2p} = k - \frac{\omega}{c_2}$ ,  $k_{2m} = k + \frac{\omega}{c_2}$ .

To ensure that the system (2.24) admits nontrivial solutions, the determinant of matrix  $\mathbf{A}$  should vanish:  $\det(\mathbf{A}) = 0$ , which gives rise to a dispersion relation between  $k$  and  $\omega$ . For the longitudinal wave in the 1D periodic network, the dispersion relation can be written in the following analytical form:

$$\begin{aligned}\cos(\lambda k) &= \cos(\omega T_1) \cos(\omega T_2) - \left( \frac{Z_1}{2Z_2} + \frac{Z_2}{2Z_1} \right) \sin(\omega T_1) \sin(\omega T_2) \\ &= \frac{Z_m^2}{Z_1 Z_2} \cos(\omega T_m) - \frac{Z_d^2}{Z_1 Z_2} \cos(\omega T_d)\end{aligned}\quad (2.26)$$

where  $Z_m = (Z_1 + Z_2)/2$ ,  $Z_d = (Z_1 - Z_2)/2$ ,  $T_m = T_1 + T_2$  and  $T_d = T_1 - T_2$  with  $Z_j = \rho_j c_j$  the characteristic acoustic impedance of the  $j$ -th beam and  $T_j = l_j/c_j$  the time for the longitudinal waves to pass through it. Based on the equation (2.26), for each given  $\omega$ , two kinds of solutions of the Bloch wave vector  $k = k_r + i k_{im}$  can be obtained. Either  $k$  is a real number:

$$\begin{aligned}k_{im} &= 0 \\ k_r &= \frac{1}{\lambda} \arccos \left( \frac{Z_m^2}{Z_1 Z_2} \cos(\omega T_m) - \frac{Z_d^2}{Z_1 Z_2} \cos(\omega T_d) \right) \\ \text{or } k_r &= \frac{1}{\lambda} \left( 2\pi - \arccos \left( \frac{Z_m^2}{Z_1 Z_2} \cos(\omega T_m) - \frac{Z_d^2}{Z_1 Z_2} \cos(\omega T_d) \right) \right)\end{aligned}\quad (2.27)$$

or  $k$  is a complex value:

$$\begin{aligned}k_r &= 0 \text{ or } \frac{\pi}{\lambda} \\ k_{im} &= \frac{1}{\lambda} \operatorname{arccosh} \left( \frac{Z_m^2}{Z_1 Z_2} \cos(\omega T_m) - \frac{Z_d^2}{Z_1 Z_2} \cos(\omega T_d) \right) \\ \text{or } k_{im} &= \frac{1}{\lambda} \operatorname{arccosh} \left( -\frac{Z_m^2}{Z_1 Z_2} \cos(\omega T_m) + \frac{Z_d^2}{Z_1 Z_2} \cos(\omega T_d) \right)\end{aligned}\quad (2.28)$$

and result in the following Bloch wave eigenmode in the  $i$ -th beam as:

$$U_j^B(x, k) = a_j e^{i \left( k_r + \frac{\omega}{c_j} \right) x} e^{-k_{im} x} + b_j e^{i \left( k_r - \frac{\omega}{c_j} \right) x} e^{-k_{im} x}\quad (2.29)$$

Therefore, when  $k$  is real ( $k_{im} = 0$ ), the Bloch wave eigenmode  $U_j^B$  is a propagating mode: It is transmitted to the adjacent cells with the same amplitude and there is no energy loss when propagating through the periodic network. Otherwise, when  $k$  is complex or purely imaginary ( $k_{im} \neq 0$ ),  $U_j^B$  is an evanescent mode: It vanishes rapidly when propagating to the adjacent cells and the energy exchange between periodic cells is equal to zero [Mead (1973)].

The above analytical results explain a special wave phenomenon, the frequency bandgaps, which exists when elastic wave are propagating in the periodic cellular networks. We call the intervals of eigenvalues that correspond to the real values of  $k$  as frequency pass band, for the waves can pass through the network. On the contrary, the intervals correspond to the complex or pure imaginary values of  $k$  as frequency stop band or bandgaps, for the waves are rapidly attenuated and cannot propagate through the network (Figure 2.9).

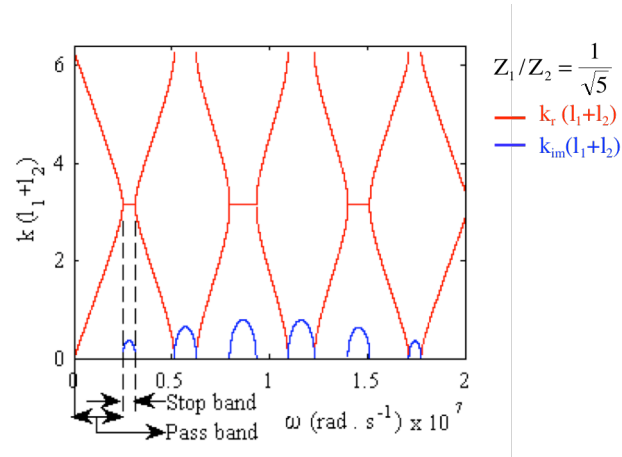


Figure 2.9 Frequency pass and stop bands of longitudinal wave in the 1D periodic network

More studies indicate that this wave phenomenon is due to the creation of stationary waves resulting from the wave reflection, transmission and conversion when propagating across the cells. Physically, when an elastic wave propagates in a periodic network, reflected waves occur when the elastic wave crossing every cell. Generally, the reflected waves will be counteracted finally. However, for some particular wave lengths, due to reflected waves from each cell with the same phase, they will interfere between them and then form much more stronger reflected waves. In physics, we call this phenomenon as the Bragg reflection. The new reflected waves attenuate the propagation of elastic wave. Therefore, in the corresponding frequency ranges, we can observe the bandgaps. The waves lengths and their corresponding frequency ranges can be referred to the Bragg's law [Sigalas (2005)].

According to the equation (2.26) we find that the frequency bandgaps in the 1D periodic network mainly depends on the impedance mismatch generated by periodic discontinuities in geometry or material properties. For instance, in the special case where  $Z_1/Z_2 = 1$ , we can get (2.26) as:  $\cos(\lambda k) = \cos(\omega T_m)$ , which leads to  $\lambda k = \omega T_m$ . Hence  $k = \omega/c_{avg}$ , with  $c_{avg} = (l_1 + l_2)/(T_1 + T_2)$  the average longitudinal wave propagation velocity in the primitive cell. Since  $\omega$  and  $c_{avg}$  are both real values, there exists no imaginary value for the Bloch wave vector. In other words, all the  $U_j^B$  are propagating in the network (Figure 2.10).

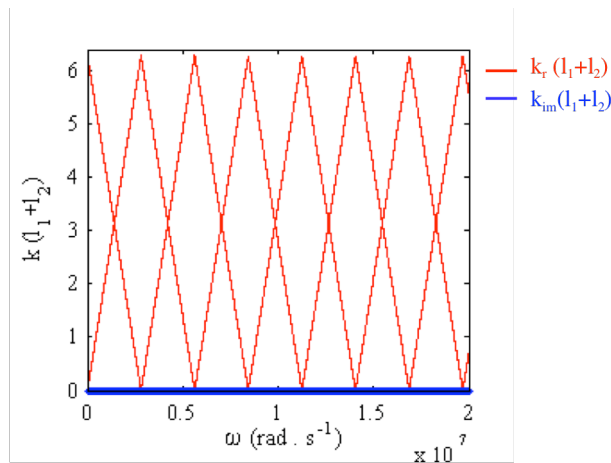


Figure 2.10  $Z_1/Z_2 = 1$ , no stop band of longitudinal wave existing in the 1D periodic network

Otherwise, these analytical results are used as the first reference to validate the numerical tools that we developed and used to obtain the numerical analyses presented in the next chapter.

### ***b) Diffracted wave analysis***

Now we consider an incident plane wave  $u_1(x, t) = e^{i(k_1x - \omega_1t)}$ , with the amplitude equal to 1, the incident wave vector  $k_1$  and the incident wave angular frequency  $\omega_1$ . We are interested in investigating how it propagates through the 1D periodic network and how it is perturbed by the periodic cells. To do this, the wave solution  $u(x, t)$  in the 1D periodic network is decomposed into two parts in the following way:

$$u(x, t) = u_1(x, t) + u_d(x, t) \quad (2.30)$$

where  $u_d(x, t)$  denotes the diffracted wave caused by the periodic cells and indicates in fact the difference between the wave motion in a periodic network and in a homogenous one.

Substituting (2.30) into the equilibrium equation (2.18), we get:

$$E_i \frac{d^2 u_d(x, t)}{dx^2} + \left\{ E_i \frac{d^2 u_1(x, t)}{dx^2} - \rho_i \frac{d^2 u_1(x, t)}{dt^2} \right\} = \rho_i \frac{d^2 u_d(x, t)}{dt^2} \quad (2.31)$$

where the second term of the left hand member can be considered as an external loading  $f_e$  due to the incident wave. In order to fully exploit the advantages of the Bloch wave analysis, we write the Bloch wave transform  $U_d^B$  of the diffracted wave as a linear combination of the Bloch wave eigenmodes (2.29) already calculated:

$$U_d^B(x, k) = \sum_m \alpha_m(k) U_m^B(x, k) \quad (2.32)$$

with the coefficient  $\alpha_m(k)$ , which can be finally calculated in the following way:

$$\alpha_m(k) = \frac{F_m(k)}{\rho_i(\omega^2 - \omega_1^2)} \quad (2.33)$$

where  $F_m(k)$  is the coefficient of the linear combination of  $U_m^B$  for the Bloch wave transform of  $f_e$  as:

$$f_e^B(x, k) = \sum_m F_m(k) U_m^B(x, k) \quad (2.34)$$

Finally, the diffracted wave  $u_d$  is obtained by means of the inverse Bloch wave transformation in the primitive cell as well as in the  $n^{\text{th}}$  cell of the network:

$$u_d(x + n\lambda, t) = \frac{1}{\text{vol}(Q^0)} \int_{Q^0} U_d^B(x, k) e^{-ik(x+n\lambda)} e^{-i\omega_1 t} dk, \quad (n \in Z) \quad (2.35)$$

Moreover, based on the analytical studies we can know that the diffracted wave is characterized certainly by the eigenmodes, the eigenvalues and but also the incident wave angular.

For example, two incident waves with respectively two different wavelengths in the first beam,  $\lambda_0$ , equal to 0.3 and 0.075 times of a given primitive cell's size are considered. For these two incident waves, the involved frequencies, are respectively  $f_1 = 2.5\text{kHz}$  and  $f_1 = 10\text{kHz}$ . Figure 2.11 presents the ratio of amplitude between the incident wave  $u_1$  and the diffracted wave  $u_d$  in the both cases. We observe firstly an important amplification

phenomenon of wave amplitude due to the diffraction caused by the periodic cellular structure. Secondly, we remark that the amplification level does not seem to be significantly affected by the incident wave's frequency  $f_i$ .

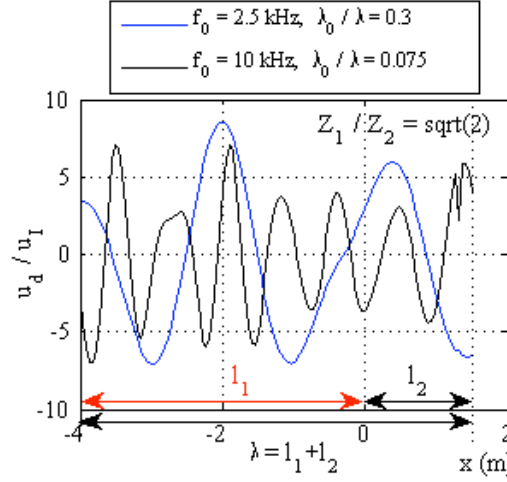


Figure 2.11 Wave amplification inside the primitive cell

## 2.2.2 Bending and transverse shear wave propagation

Now we consider the bending and transverse shear waves in the plane Oxy propagating in the 1D periodic network. For the  $j$ -th beam, the Bloch wave transform of the dynamic equilibrium eigen-equations are obtained:

$$\begin{aligned} \frac{d^2 U_{0y}^B(x, k)}{dx^2} - 2ik \frac{dU_{0y}^B(x, k)}{dx} - k^2 U_{0y}^B(x, k) + \frac{dU_1^B(x, k)}{dx} - ikU_1^B(x, k) &= -\frac{\rho_j \omega^2}{\mu_j} U_{0y}^B(x, k), \quad (j=1, 2) \\ \frac{d^2 U_1^B(x, k)}{dx^2} - 2ik \frac{dU_1^B(x, k)}{dx} - \left[ k^2 + \frac{12\mu_j}{E_j H^2} \right] U_1^B(x, k) - \frac{12\mu_j}{E_j H^2} \left( \frac{dU_{0y}^B(x, k)}{dx} - ikU_{0y}^B(x, k) \right) &= -\frac{\rho_j \omega^2}{E_j} U_1^B(x, k) \end{aligned} \quad (2.36)$$

with  $\omega$  the eigenvalue and  $(U_{0y}^B(x, k), U_1^B(x, k))$  the Bloch wave modes of  $(u_{0y}(x, t), u_1(x, t))$ .

Contrary to the case of the longitudinal wave, we do not have analytical general solutions of the bending and transverse shear waves. Therefore, in this case, we solve (2.36) numerically by searching for  $(\omega, (U_{0y}^B(x, k), U_1^B(x, k)))$  within the frequency range of interest for each

discretized Bloch wave vector  $k$  in the first Brillouin zone  $Q^0 = \left[ -\frac{\pi}{\lambda}, \frac{\pi}{\lambda} \right]$ .

The numerical simulation of bending and transverse shear waves is performed using Lagrange quadratic three nodes elements whose size is about 0.1mm a quarter of the wavelength of the bending waves at 100 kHz. The considered beam length  $l_1+l_2$ , which will be given in the next chapter, is about 55 times the element size. Besides, the first Brillouin zone  $Q^0$  is discretized into 114 elements.

In parallel, we have compared two beam models respectively of the Timoshenko kinematics with Lagrange quadratic three nodes elements and of the Euler-Bernoulli kinematics with cubic Hermitian elements in order to check whether numerical locking phenomena take place when the Timoshenko kinematics is used to model thin beams. The size of the two kinds of elements is about 0.1mm. The considered geometric and mechanical characteristics that will be given in the next chapter, in which the period  $l_1+l_2$  is about 300 times the thickness  $H$  of

beams. We find that the no numerical locking phenomena occur if we use the Timoshenko kinematics with the three nodes elements in the simulation.

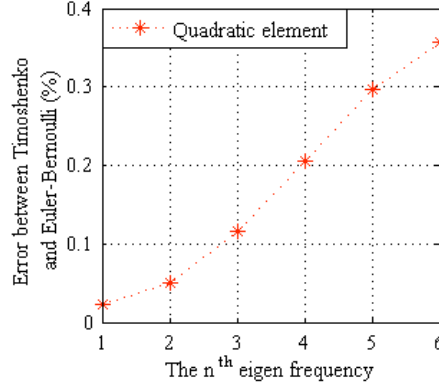


Figure 2.12 (left) Eigenfrequencies errors between the Timoshenko kinematics and the Euler-Bernoulli kinematics for the considered thin beam

To get the dispersion relation as well as the Bloch wave eigenmodes, the internal interface and the periodic boundary conditions for the bending and transverse shear waves should be probably imposed, constituting in the continuity of the displacement and the rotation, and in the equilibrium of the generalized beam forces and moments at both the junction point and the two ends of the primitive cell (Figure 2.13)

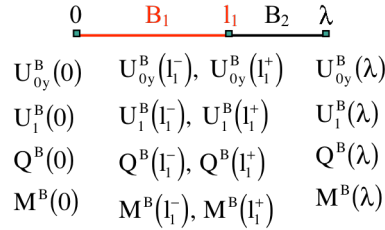


Figure 2.13 Displacement, rotation, generalized beam force and moment at the junction point and the two ends of the primitive cell

So, the interface internal conditions between the two beams at their junction point read as:

$$\begin{aligned} U_{0y}^B(I_1^-) &= U_{0y}^B(I_1^+), \quad Q^B(I_1^-) = Q^B(I_1^+) \\ U_1^B(I_1^-) &= U_1^B(I_1^+), \quad M^B(I_1^-) = M^B(I_1^+) \end{aligned} \quad (2.37)$$

and also the periodic boundary conditions at the ends of the primitive cell read as:

$$\begin{aligned} U_{0y}^B(0) &= U_{0y}^B(\lambda), \quad Q^B(0) = Q^B(\lambda) \\ U_1^B(0) &= U_1^B(\lambda), \quad M^B(0) = M^B(\lambda) \end{aligned} \quad (2.38)$$

where  $Q^B(x, k)$  is the Bloch wave transform of the generalized transverse shear force and  $M^B(x, k)$  is the Bloch wave transform of the generalized bending moments:

$$\begin{aligned} Q^B &= \mu H \left( \frac{dU_{0y}^B}{dx} - ikU_{0y}^B + U_1^B \right) \\ M^B &= E \frac{H^3}{12} \left( \frac{dU_1^B}{dx} - ikU_1^B \right) \end{aligned} \quad (2.39)$$

Combining (2.36) with all the interface junction conditions and periodic boundary conditions (2.37) and (2.38), then we can get the complete definition of the Bloch wave eigenproblem of the bending and transverse shear waves, whose numerical solving allows obtaining the dispersion relation presented in the next chapter. Not like in the longitudinal wave case, when we solve directly this eigenproblem, we get the eigenvalues  $\omega$  for each wave vector  $k$  of real value discretized in the first Brillouin zone. Hence by plotting the dispersion curves  $k - \omega$ , we can remark easily the stop bands, but we have no idea of the values of  $k_{im}$  (see the next chapter).

## 2.3 2D periodic beam networks

In this section, the Bloch wave theory is applied to the analysis of the elastic wave propagation in 2D periodic beam networks. The focus is first given to the hexagonal cell type network. On the one hand, since the honeycomb sandwich plate is a periodic hexagonal network made of plates, it is interesting for us to study a network with the same cellular shape but composed of beams. Although the beam network has similar difficulties as those of plates, as the wave phenomena in the plane and out of the plane of the 2D network are completely uncoupled, so it is easier to discuss both the membrane and bending waves and have a better understanding, useful then for the honeycomb thin layer made of plates. On the other hand, some studies have already been done on looking for the dispersion relation of hexagonal or hexagonal chiral cell type beam networks, especially for the in-plane membrane waves [Srikantha Phani (2006); Spadoni (2009)], we can therefore, with the reference to those results, validate our approach and consider further the out-of-plane bending waves. Finally, as mentioned in chapter 1, rectangular cell type sandwich panels are also commonly used in engineering application, hence we investigate a periodic rectangular beam network as well.

### 2.3.1 Hexagonal network

The choice of the primitive cell is not unique. In the case of the periodic hexagonal network, we can choose, for example, either a primitive cell composed of three beams, used for example by Gonella et al. [Gonella (2008)], or another one composed of five beams primitive cell (Figure 2.14). In the present work, we propose to use the second one, for which the periodic conditions can be more easily imposed by COMSOL software.

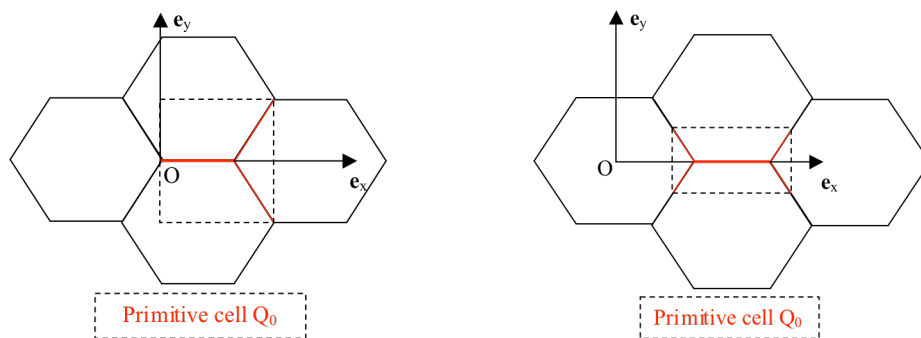


Figure 2.14 Two possible primitive cells in the case of 2D periodic beam hexagonal network

To discretize  $\mathbf{k}$ , we need to consider the first Brillouin zone of the hexagonal primitive cell. For the 2D hexagonal periodic network, we notice that there are three possible direct cell bases and so three corresponding reciprocal cell bases (Figure 2.15). By translating the primitive cell along any group of the three bases, we can obtain the tiling of the whole hexagonal periodic network.

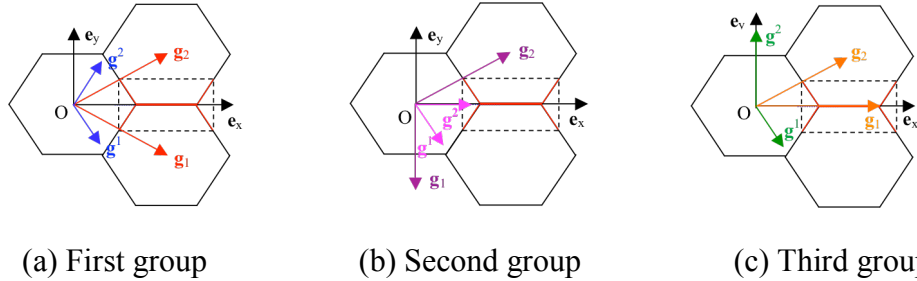


Figure 2.15 Three possible direct cell bases and the corresponding reciprocal cell bases

For each reciprocal cell basis, we can have a relevant reciprocal primitive cell. The minimal intersection of the three cells,  $Z_1Z_2Z_3Z_4Z_5Z_6$ , is the first Brillouin zone of the hexagonal periodic network. It is found that  $Q^0$  is also a hexagonal cell (Figure 2.16).

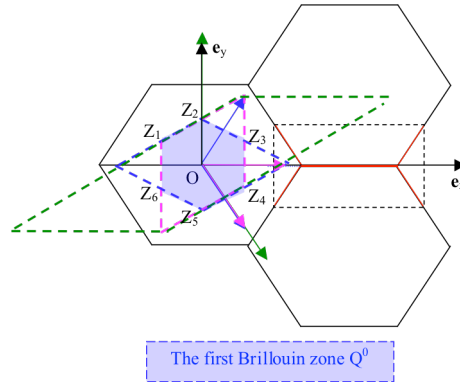


Figure 2.16 First Brillouin zone of the periodic hexagonal network

Instead of considering the whole first Brillouin zone, we adopt another method, which consist in looking for the eigenvalues of the Bloch eigenproblem only for the  $\mathbf{k}$  locating on the contour of a subdomain of the first Brillouin zone, called irreducible zone (Figure 2.17). Indeed, without rigorous proof, this method has been widely accepted in the related literatures and seems to offer an efficient solution and provides furthermore a clearer view on dispersion relation of periodic structures [Kittel 1962; Srikantha Phani 2006;]. Owing to the symmetry of the first Brillouin zone, it is believed that the maximal and minimal values of  $\omega$  occur along the irreducible zone's contour, so the dispersion relation obtained between those phase vectors  $\mathbf{k}$  and the eigenvalues for the study of the frequency bandgaps estimated to be sufficient.

For the numerical simulations presented in the present work, both the first Brillouin zone and the contour of the irreducible zone are discretized to obtain respectively 3D dispersion surfaces and 2D dispersion curves.

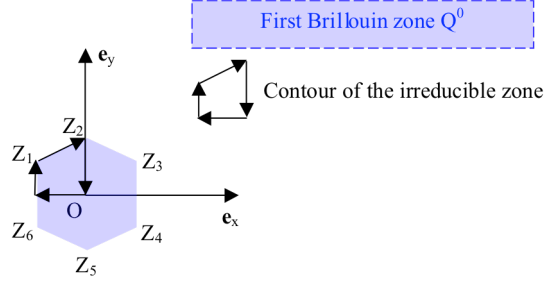


Figure 2.17 First Brillouin zone and irreducible zone of the hexagonal network

Now back on the primitive cell, each beam is parameterized from its local beam basis ( $\mathbf{e}_1$ ,  $\mathbf{e}_2$ ,  $\mathbf{e}_3$ ) first, where the axis  $\mathbf{e}_3$  is the neutral axis of the beam, the axis  $\mathbf{e}_2$  is perpendicular to the beam and located in the plane Oxy of 2D network and the axis  $\mathbf{e}_1$  is perpendicular to the plane of the 2D network. The whole network is then considered in the global Cartesian basis ( $\mathbf{e}_x$ ,  $\mathbf{e}_y$ ,  $\mathbf{e}_z$ ) (Figure 2.18). As for the geometric and mechanical characteristics of the primitive cell, they are defined as the following: the Lamé coefficients and the density of all the beams are  $(\lambda, \mu, \rho)$ , the length  $s$  of the horizontal beam  $B_{CEN}$  is twice the length of the other four beams. The thickness (in the local direction  $\mathbf{e}_2$ ) and the width (in the local direction  $\mathbf{e}_1$ ) of  $B_{CEN}$  are  $(H_1, T)$  and of the others are  $(H_0, T)$ . Due to the manufacturing process of the periodic hexagonal network,  $H_1$  usually could be twice  $H_0$ .

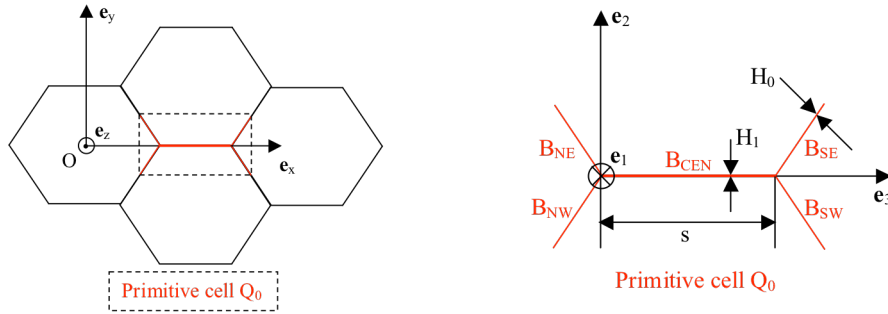


Figure 2.18 (left) 2D periodic hexagonal beam network in the global Cartesian basis ( $\mathbf{e}_x$ ,  $\mathbf{e}_y$ ,  $\mathbf{e}_z$ ); (right) Primitive cell of the hexagonal network in the local beam basis ( $\mathbf{e}_1$ ,  $\mathbf{e}_2$ ,  $\mathbf{e}_3$ ) draw here only for the center beam  $B_{CEN}$

Any point  $\mathbf{r}$  in each beam is given by its local coordinates in each beam local basis in the classical way:

$$\mathbf{r}(x_\alpha, x_3) = \sum_{\alpha=1,2} x_\alpha \mathbf{e}_\alpha + x_3 \mathbf{e}_3 \quad (2.40)$$

where  $x_\alpha$  denotes the coordinates in the transverse sections with  $\alpha = 1, 2$ . The Timoshenko kinematics decomposes the displacement  $\mathbf{u}$  of each beam as:

$$\mathbf{u} = u_{01} \mathbf{e}_1 + u_{02} \mathbf{e}_2 + u_{03} \mathbf{e}_3 - x_2 u_{13} \mathbf{e}_1 + x_1 u_{13} \mathbf{e}_2 + (x_2 u_{11} - x_1 u_{12}) \mathbf{e}_3 \quad (2.41)$$

with  $u_{03}$  the displacements of the beam's neutral axis along this axis,  $u_{0\alpha}$  the deflection of the neutral axis in the directions  $\mathbf{e}_\alpha$ ,  $u_{11}$  and  $u_{12}$  the rotation of the transverse sections due to the bending of the beam and  $u_{13}$  the rotation of the transverse sections due to the twisting.

Now we are interested in analyzing the wave phenomena in the plane of the 2D network, defined by Oxy, and out of this same plane, as fortunately, the equilibrium equations of the 2D network allows a complete uncoupling of these two phenomena:

$$\begin{cases}
E \frac{d^2 u_{03}}{dx_3^2} = \rho \frac{d^2 u_{03}}{dt^2} \\
\mu \left( \frac{d^2 u_{02}}{dx_3^2} + \frac{du_{11}}{dx_3} \right) = \rho \frac{d^2 u_{02}}{dt^2} \\
E \frac{d^2 u_{11}}{dx_3^2} - \frac{12\mu}{H_m^2} \left( \frac{du_{02}}{dx_3} + u_{11} \right) = \rho \frac{d^2 u_{11}}{dt^2} \\
\mu \left( \frac{d^2 u_{01}}{dx_3^2} - \frac{du_{12}}{dx_3} \right) = \rho \frac{d^2 u_{01}}{dt^2} \\
\frac{ET^2}{12} \frac{d^2 u_{12}}{dx_3^2} + \mu \left( \frac{du_{01}}{dx_3} - u_{12} \right) = \frac{\rho T^2}{12} \frac{d^2 u_{12}}{dt^2}, \quad (m=0, 1) \\
\mu \frac{d^2 u_{13}}{dx_3^2} = \rho \frac{d^2 u_{13}}{dt^2}
\end{cases} \quad (2.42)$$

Hence, similar to the analysis of 1D periodic network, the in-plane membrane waves and the out-of-plane bending waves of the 2D periodic beam network can be considered independently.

#### a) In-plane membrane wave propagation

The Bloch wave transform of the equilibrium equations of the in-plane membrane waves are:

$$\begin{aligned}
\frac{d^2 U_{03}^B}{dx_3^2} - 2i(\mathbf{k} \cdot x_3 \mathbf{e}_3) \frac{dU_{03}^B}{dx_3} - (\mathbf{k} \cdot x_3 \mathbf{e}_3)^2 U_{03}^B &= -\frac{\rho \omega^2}{E} U_{03}^B \quad (m=0, 1) \\
\frac{d^2 U_{02}^B}{dx_3^2} - 2i(\mathbf{k} \cdot x_3 \mathbf{e}_3) \frac{dU_{02}^B}{dx_3} - (\mathbf{k} \cdot x_3 \mathbf{e}_3)^2 U_{02}^B + \frac{dU_{11}^B}{dx_3} - i(\mathbf{k} \cdot x_3 \mathbf{e}_3) U_{11}^B &= -\frac{\rho \omega^2}{\mu} U_{02}^B \\
\frac{d^2 U_{11}^B}{dx_3^2} - 2i(\mathbf{k} \cdot x_3 \mathbf{e}_3) \frac{dU_{11}^B}{dx_3} - \left[ (\mathbf{k} \cdot x_3 \mathbf{e}_3)^2 + \frac{12\mu}{EH_m^2} \right] U_{11}^B - \frac{12\mu}{EH_m^2} \left[ \frac{dU_{02}^B}{dx_3} - i(\mathbf{k} \cdot x_3 \mathbf{e}_3) U_{02}^B \right] &= -\frac{\rho \omega^2}{E} U_{11}^B
\end{aligned} \quad (2.43)$$

with  $\omega$  the eigenvalue,  $\mathbf{k}$  the Bloch wave vector, which is also a in plane vector and  $U^B$  the Bloch wave modes. The analytical solutions of (2.43) are generally unavailable, so we numerically search for the eigenvalue and the corresponding Bloch wave eigenmodes in the primitive cell for each given discretized  $\mathbf{k}$  within the first Brillouin zone  $Q^0$  of the 2D periodic hexagonal network.

As for the finite element discretization of the 2D network, Lagrange quadratic three nodes elements with size about 0.09mm are used. We note that the wavelength of the bending waves in the present case at 0.6 MHz contains about 19 elements and the considered horizontal beam whose geometric characteristics will be given in the chapter contains about 34 elements. For discretizing the first Brillouin zone  $Q^0$ , it is first discretized into 501 elements along the axis  $\mathbf{e}_y$  from  $Z_2$  to  $Z_5$  and then for each discretized element along  $Z_2 \rightarrow Z_5$ , it is discretized into 602 elements. The corresponding irreducible zone's contour is discretized into 200 elements.

To complete the definition of the Bloch eigenproblem (2.43), the following interface conditions between the five beams at the interior junction points, A and B, and the periodic boundary conditions at the ends, (C, D, E, F), of the primitive cell are considered (Figure 2.19).

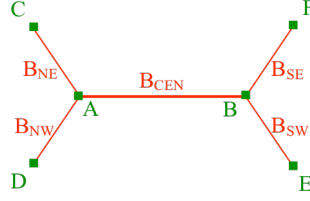


Figure 2.19 Junction points and boundary ends of the hexagonal primitive cell

More precisely, we write, for example at the point A, the continuity of the displacement and the rotation, and the equilibrium of the generalized beam forces and moments:

$$\begin{aligned}
U_{03}^B \mathbf{e}_3(\mathbf{B}_{NE}) + U_{02}^B \mathbf{e}_2(\mathbf{B}_{NE}) &= U_{03}^B \mathbf{e}_3(\mathbf{B}_{NW}) + U_{02}^B \mathbf{e}_2(\mathbf{B}_{NW}) = U_{03}^B \mathbf{e}_3(\mathbf{B}_{CEN}) + U_{02}^B \mathbf{e}_2(\mathbf{B}_{CEN}) \\
U_{11}^B \mathbf{e}_1(\mathbf{B}_{NE}) &= U_{11}^B \mathbf{e}_1(\mathbf{B}_{NW}) = U_{11}^B \mathbf{e}_1(\mathbf{B}_{CEN}) \\
N^B \mathbf{e}_3(\mathbf{B}_{NE}) + Q_2^B \mathbf{e}_2(\mathbf{B}_{NE}) + N^B \mathbf{e}_3(\mathbf{B}_{NW}) + Q_2^B \mathbf{e}_2(\mathbf{B}_{NW}) + N^B \mathbf{e}_3(\mathbf{B}_{CEN}) + Q_2^B \mathbf{e}_2(\mathbf{B}_{CEN}) &= 0 \\
M_2^B \mathbf{e}_1(\mathbf{B}_{NE}) + M_2^B \mathbf{e}_1(\mathbf{B}_{NW}) + M_2^B \mathbf{e}_1(\mathbf{B}_{CEN}) &= 0
\end{aligned} \tag{2.44}$$

where  $N^B$ ,  $Q_2^B$  and  $M_2^B$  are the Bloch wave transform of respectively the generalized longitudinal force, the generalized transverse shear force and the generalized bending moment. Their expressions read as:

$$\begin{aligned}
N^B &= ETH \left[ \frac{dU_{03}^B}{dx_3} - i(\mathbf{k} \cdot x_3 \mathbf{e}_3) U_{03}^B \right] \\
Q_2^B &= \mu TH \left[ \frac{dU_{02}^B}{dx_3} - i(\mathbf{k} \cdot x_3 \mathbf{e}_3) U_{02}^B + U_{11}^B \right] \\
M_2^B &= ET \frac{H^3}{12} \left[ \frac{dU_{11}^B}{dx_3} - i(\mathbf{k} \cdot x_3 \mathbf{e}_3) U_{11}^B \right]
\end{aligned} \tag{2.45}$$

Similar junction conditions are also written at point B. As for the boundary periodic conditions, they consist also in the continuity of the displacement and the rotation, and the equilibrium of the generalized beam forces and moments. More precisely, we write, for example for the pair of points C and E:

$$\begin{aligned}
U_{03}^B \mathbf{e}_3(\mathbf{B}_{NE}) + U_{02}^B \mathbf{e}_2(\mathbf{B}_{NE}) &= U_{03}^B \mathbf{e}_3(\mathbf{B}_{SW}) + U_{02}^B \mathbf{e}_2(\mathbf{B}_{SW}) \\
U_{11}^B \mathbf{e}_1(\mathbf{B}_{NE}) &= U_{11}^B \mathbf{e}_1(\mathbf{B}_{SW}) \\
N^B \mathbf{e}_3(\mathbf{B}_{NE}) + Q_2^B \mathbf{e}_2(\mathbf{B}_{NE}) + N^B \mathbf{e}_3(\mathbf{B}_{SW}) + Q_2^B \mathbf{e}_2(\mathbf{B}_{SW}) &= 0 \\
M_2^B \mathbf{e}_1(\mathbf{B}_{NE}) + M_2^B \mathbf{e}_1(\mathbf{B}_{SW}) &= 0
\end{aligned} \tag{2.46}$$

Similar boundary periodic conditions should also be written for the pair of the points D and F. Combining (2.43) with all the interface conditions and periodic conditions, then we can get the complete definition of the Bloch wave eigenproblem, whose numerical solving allows obtaining the dispersion relation presented in the next chapter.

### b) Out-of-plane bending wave propagation

For the out-of-plane bending waves propagation in the 2D periodic hexagonal network, the Bloch wave transform of the out-of-plane equilibrium equations are as the following:

$$\begin{aligned}
\frac{d^2 U_{13}^B}{dx_3^2} - 2i(\mathbf{k} \cdot x_3 \mathbf{e}_3) \frac{dU_{13}^B}{dx_3} - (\mathbf{k} \cdot x_3 \mathbf{e}_3)^2 U_{13}^B &= -\frac{\rho\omega^2}{\mu} U_{13}^B \\
\frac{d^2 U_{01}^B}{dx_3^2} - 2i(\mathbf{k} \cdot x_3 \mathbf{e}_3) \frac{dU_{01}^B}{dx_3} - (\mathbf{k} \cdot x_3 \mathbf{e}_3)^2 U_{01}^B - \frac{dU_{12}^B}{dx_3} + i(\mathbf{k} \cdot x_3 \mathbf{e}_3) U_{12}^B &= -\frac{\rho\omega^2}{\mu} U_{01}^B \\
\frac{d^2 U_{12}^B}{dx_3^2} - 2i(\mathbf{k} \cdot x_3 \mathbf{e}_3) \frac{dU_{12}^B}{dx_3} - \left[ (\mathbf{k} \cdot x_3 \mathbf{e}_3)^2 + \frac{12\mu}{ET^2} \right] U_{12}^B + \frac{12\mu}{ET^2} \left[ \frac{dU_{01}^B}{dx_3} - i(\mathbf{k} \cdot x_3 \mathbf{e}_3) U_{01}^B \right] &= -\frac{\rho\omega^2}{E} U_{12}^B
\end{aligned} \tag{2.47}$$

with  $(U_{01}^B, U_{12}^B, U_{13}^B)$  the Bloch wave eigenmodes.

For the numerical simulation of the out-of-plane bending waves, we still use Lagrange quadratic three nodes elements of about 0.09 mm size, for which the wavelength of the bending waves of 0.4 MHz contains about 19 elements.

The continuity of the displacement and the rotation, and the equilibrium of the generalized beam forces and moments between the five beams at point A for the out-of-plane waves read as:

$$\begin{aligned}
U_{01}^B \mathbf{e}_1(\mathbf{B}_{NE}) &= U_{01}^B \mathbf{e}_1(\mathbf{B}_{NW}) = U_{01}^B \mathbf{e}_1(\mathbf{B}_{CEN}) \\
U_{13}^B \mathbf{e}_3(\mathbf{B}_{NE}) + U_{12}^B \mathbf{e}_2(\mathbf{B}_{NE}) &= U_{13}^B \mathbf{e}_3(\mathbf{B}_{NW}) + U_{12}^B \mathbf{e}_2(\mathbf{B}_{NW}) = U_{13}^B \mathbf{e}_3(\mathbf{B}_{CEN}) + U_{12}^B \mathbf{e}_2(\mathbf{B}_{CEN}) \\
Q_1^B \mathbf{e}_1(\mathbf{B}_{NE}) + Q_1^B \mathbf{e}_1(\mathbf{B}_{NW}) + Q_1^B \mathbf{e}_1(\mathbf{B}_{CEN}) &= 0 \\
M_3^B \mathbf{e}_3(\mathbf{B}_{NE}) + M_1^B \mathbf{e}_2(\mathbf{B}_{NE}) + M_3^B \mathbf{e}_3(\mathbf{B}_{NW}) + M_1^B \mathbf{e}_2(\mathbf{B}_{NW}) + M_3^B \mathbf{e}_3(\mathbf{B}_{CEN}) + M_1^B \mathbf{e}_2(\mathbf{B}_{CEN}) &= 0
\end{aligned} \tag{2.48}$$

where  $Q_1^B, M_1^B$  and  $M_3^B$  denote the Bloch wave transform of respectively the generalized transverse shear force, the generalized bending moment and the generalized twist moment:

$$\begin{aligned}
Q_1^B &= \mu TH \left[ \frac{dU_{01}^B}{ds} - i(\mathbf{k} \cdot x_3 \mathbf{e}_3) U_{01}^B - U_{12}^B \right] \\
M_1^B &= \mu \frac{T^3 + H^3}{12} \left[ \frac{dU_{13}^B}{ds} - i(\mathbf{k} \cdot x_3 \mathbf{e}_3) U_{13}^B \right] \\
M_3^B &= EH \frac{T^3}{12} \left[ \frac{dU_{12}^B}{ds} - i(\mathbf{k} \cdot x_3 \mathbf{e}_3) U_{12}^B \right]
\end{aligned} \tag{2.49}$$

Similar junction conditions are also imposed at point B. Besides, the boundary periodic conditions between the pair of the points C and E:

$$\begin{aligned}
U_{01}^B \mathbf{e}_1(\mathbf{B}_{NE}) &= U_{01}^B \mathbf{e}_1(\mathbf{B}_{SW}) \\
U_{13}^B \mathbf{e}_3(\mathbf{B}_{NE}) + U_{12}^B \mathbf{e}_2(\mathbf{B}_{NE}) &= U_{13}^B \mathbf{e}_3(\mathbf{B}_{SW}) + U_{12}^B \mathbf{e}_2(\mathbf{B}_{SW}) \\
Q_1^B \mathbf{e}_1(\mathbf{B}_{NE}) + Q_1^B \mathbf{e}_1(\mathbf{B}_{SW}) &= 0 \\
M_3^B \mathbf{e}_3(\mathbf{B}_{NE}) + M_1^B \mathbf{e}_2(\mathbf{B}_{NE}) + M_3^B \mathbf{e}_3(\mathbf{B}_{SW}) + M_1^B \mathbf{e}_2(\mathbf{B}_{SW}) &= 0
\end{aligned} \tag{2.50}$$

and the same kind of boundary periodic conditions are also imposed for the pair of the points D and F. These interior interface conditions and boundary periodic conditions complete the definition of the Bloch eigenproblem (2.47) for the bending wave case of the 2D periodic network.

### 2.3.2 Periodic rectangular network

In parallel to the 2D periodic hexagonal beam network, we consider a 2D periodic rectangular beam network. Rectangular cell has a more simple structure as all the beams in the network perpendicular to each other. Therefore, both the direct cell basis and the reciprocal cell basis are coincide with the Cartesian basis, which makes the definition of its first Brillouin zone as well as the discretization of the latter easier than for the hexagonal network.

The primitive cell  $Q_0$  of the network is composed of four rigidly-jointed elastic beams,  $B_W$ ,  $B_E$ ,  $B_N$  and  $B_S$ . The period in horizontal and vertical directions is respectively  $\lambda_1$  and  $\lambda_2$ . The thickness and the width of the two horizontal beams,  $B_W$  and  $B_E$ , are denoted by  $(H_1, T)$  and the ones of the two vertical beams,  $B_N$  and  $B_S$ , by  $(H_0, T)$ . The mechanical characteristics of the four beams are still  $(\lambda, \mu, \rho)$  (Figure 2.20).

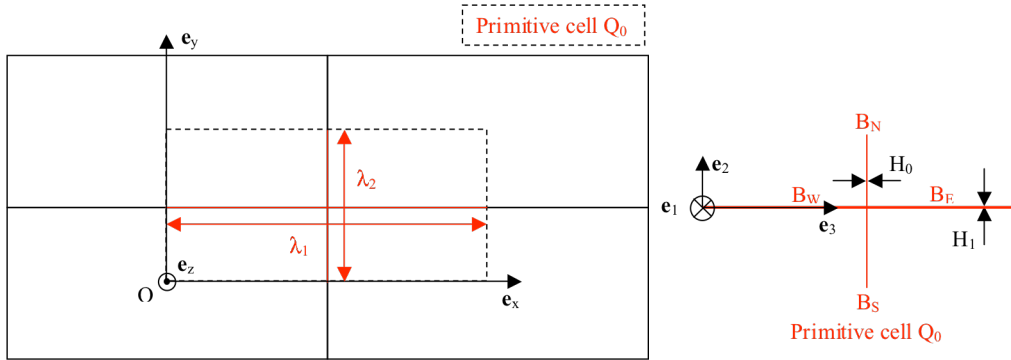


Figure 2.20 (left) periodic rectangular network; (Right) Its primitive cell

The Bloch wave transform of the equilibrium equations for in-plane membrane and out-of-plane bending waves are always governed respectively by (2.43) and (2.47). For all the  $\mathbf{k}$  belonging to the first Brillouin zone as well as those locating on the irreducible zone's contour, the corresponding eigenvalue and Bloch wave eigenmode can be searched numerically by taking into account the interface conditions on the point E and the periodic conditions between the points B and D on the one hand and between the points A and C on the other hand (Figure 2.21)

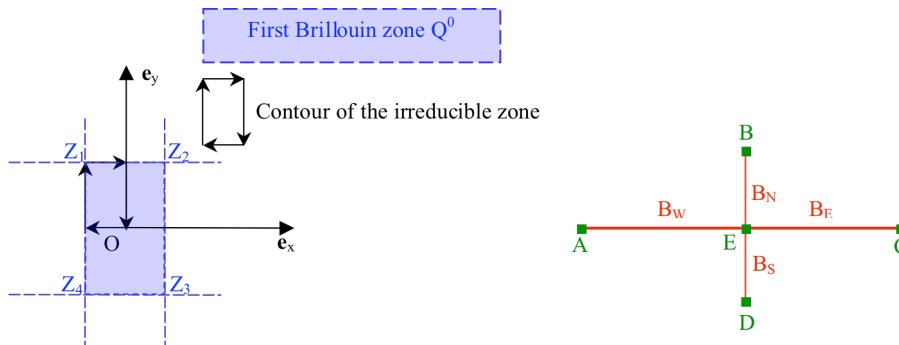


Figure 2.21 (left) First Brillouin zone and irreducible zone of the rectangular network; (right) Junction point and boundary points of the rectangular primitive cell

For the numerical simulation of the rectangular network, we use Lagrange quadratic three nodes elements with size 0.03 mm, where the wavelength of the in-plane membrane waves in the present case at 0.6 MHz can contain about 56 elements and the one of the out-of-plane bending waves contains about 44 elements. The considered horizontal period  $\lambda_1$  that will be

given in the next chapter contains 100 elements. For discretizing the first Brillouin zone  $Q^0$ , it is first discretized into 201 elements along the axis  $\mathbf{e}_y$  from  $Z_2$  to  $Z_3$  and then for each discretized element along  $Z_2 \rightarrow Z_3$ , it is discretized into 201 elements. The corresponding irreducible zone's contour is discretized into 200 elements.

## 2.4 3D periodic plate networks

Finally, the Bloch wave theory is applied for the analysis of the wave propagation in the honeycomb thin layer and then in the honeycomb core sandwich plate. The honeycomb thin layer is a periodic hexagonal network made of plates, so the way to select a primitive cell and build the first Brillouin zone is much similar to the hexagonal beam network.

### 2.4.1 Honeycomb thin layer

The primitive cell  $Q_0$  of the honeycomb thin layer is composed of five rigidly-jointed elastic plates. The mechanic characteristics of all the plates are  $(\lambda, \mu, \rho)$ . The length of the horizontal plate  $P_{CEN}$ ,  $s$ , is twice the length of the other four plates. The thickness and the width of  $P_{CEN}$  is  $(H_1, T)$  and of the others is  $(H_0, T)$ . Similar to the beam network case, due to the manufactory process of the honeycomb thin layer,  $H_1$  is usually twice  $H_0$ . Each plate is parameterized in its local plate basis  $(\mathbf{e}_1, \mathbf{e}_2, \mathbf{n})$  first, where  $(\mathbf{e}_1, \mathbf{e}_2)$  forms an orthonormed basis in the middle plane of the plate and the  $\mathbf{n}$  is a unit vector perpendicular to the plate, while the whole network is finally considered under the global Cartesian basis  $(\mathbf{e}_x, \mathbf{e}_y, \mathbf{e}_z)$  (Figure 2.22).

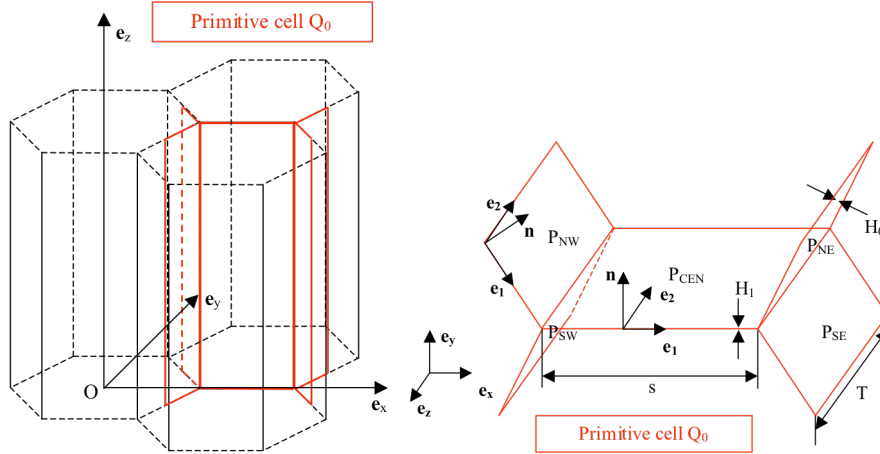


Figure 2.22 (left) Honeycomb thin layer under Cartesian basis  $(\mathbf{e}_x, \mathbf{e}_y, \mathbf{e}_z)$ ; (right) Primitive cell of honeycomb thin layer under local plate basis  $(\mathbf{e}_1, \mathbf{e}_2, \mathbf{n})$

Any point  $\mathbf{r}$  of each plate is given in each plate's local basis as:

$$\mathbf{r}(\mathbf{x}_s, \xi) = \mathbf{x}_s + \xi \mathbf{n} \quad (2.51)$$

with  $\mathbf{x}_s = s_1 \mathbf{e}_1 + s_2 \mathbf{e}_2$  the points on the middle plane  $S$  and  $\xi$  the coordinate in the thickness of the plate in the range from  $-\frac{H_m}{2}$  to  $\frac{H_m}{2}$  for  $m = 0$  or  $1$ . The 5 degrees of freedom (5dofs)

Mindlin kinematics for the thick plate is used here for the shear deformation can be taken into account appropriately. According to the Mindlin model, the displacement  $\mathbf{u}$  in the each plate reads as:

$$\mathbf{u} = \mathbf{u}_{0s} + u_{0n} \mathbf{n} + \xi \mathbf{u}_{1s} \quad (2.52)$$

with  $\mathbf{u}_{0s} = u_{0s1}\mathbf{e}_1 + u_{0s2}\mathbf{e}_2$  and  $u_{0n}$  respectively the membrane displacement and the deflection of the middle plane and  $\mathbf{u}_{1s} = u_{1s1}\mathbf{e}_1 + u_{1s2}\mathbf{e}_2$  the displacements in the thickness of the plate due to the rotation of the perpendicular fibers.

The equilibrium equations of the plates read as:

$$\begin{aligned}\mathbf{Div}\mathbf{N}_s &= \rho H_m \ddot{\mathbf{u}}_{0s} \\ \text{div}\mathbf{Q} &= \rho H_m \ddot{u}_{0n} \\ \mathbf{Div}\mathbf{M}_s - \mathbf{Q} &= \rho \frac{H_m^3}{12} \ddot{\mathbf{u}}_{1s}, \quad (m=0, 1)\end{aligned}\quad (2.53)$$

with  $\mathbf{N}_s$  the generalized membrane force tensor,  $\mathbf{Q}$  the generalized transverse shear force vector and  $\mathbf{M}_s$  the generalized bending moment tensor. They have the following forms:

$$\begin{aligned}\mathbf{N} &= H_m \lambda^* \left( \frac{\partial \mathbf{u}_{0s}}{\partial x_s} \cdot \mathbf{e}_{xs} \right) \mathbf{e}_{xs} \otimes \mathbf{e}_{xs} + H_m 2\mu \frac{\partial \mathbf{u}_{0s}}{\partial x_s} \otimes_s \mathbf{e}_{xs} \\ \mathbf{Q} &= H_m \mu \left( \frac{\partial u_{0n}}{\partial x_s} \mathbf{e}_{xs} + \mathbf{u}_{1s} \right) \\ \mathbf{M}_s &= \frac{H_m^3}{12} \lambda^* \left( \frac{\partial \mathbf{u}_{1s}}{\partial x_s} \cdot \mathbf{e}_{xs} \right) \mathbf{e}_{xs} \otimes \mathbf{e}_{xs} + \frac{H_m^3}{6} \mu \frac{\partial \mathbf{u}_{1s}}{\partial x_s} \otimes_s \mathbf{e}_{xs}, \quad (m=0, 1)\end{aligned}\quad (2.54)$$

with  $\mathbf{e}_{xs} = s_1 / \|\mathbf{x}_s\| \mathbf{e}_1 + s_2 / \|\mathbf{x}_s\| \mathbf{e}_2$  the unit vector in the same direction and  $\lambda^* = 2\mu\lambda/(\lambda+2\mu)$  the 2D Lamé constant in plane stress state. Consequently, the Bloch wave transformation of the equilibrium equations reads as:

$$\begin{aligned}-\rho\omega^2 \mathbf{U}_{0s}^B &= \\ \left[ (\lambda + \mu) \left( \frac{\partial^2 \mathbf{U}_{0s}^B}{\partial x_s^2} + (-i\mathbf{k} \cdot \mathbf{e}_1)(1 + (\mathbf{e}_1 \cdot \mathbf{e}_{xs})) \frac{\partial \mathbf{U}_{0s}^B}{\partial x_s} - (\mathbf{e}_1 \cdot \mathbf{e}_{xs})(\mathbf{k} \cdot \mathbf{e}_1)^2 \mathbf{U}_{0s}^B \right) \cdot \mathbf{e}_{xs} \right] \mathbf{e}_{xs} \\ + \mu \left( \frac{\partial^2 \mathbf{U}_{0s}^B}{\partial x_s^2} + (-i\mathbf{k} \cdot \mathbf{e}_1)(1 + (\mathbf{e}_1 \cdot \mathbf{e}_{xs1})) \frac{\partial \mathbf{U}_{0s}^B}{\partial x_s} - (\mathbf{e}_{xs} \cdot \mathbf{e}_1)(\mathbf{k} \cdot \mathbf{e}_1)^2 \mathbf{U}_{0s}^B \right) \\ -\rho\omega^2 U_{0n}^B &= \\ \mu \left( \frac{\partial^2 U_{0n}^B}{\partial x_s^2} + (-i\mathbf{k} \cdot \mathbf{e}_1)(1 + (\mathbf{e}_1 \cdot \mathbf{e}_{xs})) \frac{\partial U_{0n}^B}{\partial x_s} - (\mathbf{e}_1 \cdot \mathbf{e}_{xs})(\mathbf{k} \cdot \mathbf{e}_1)^2 U_{0n}^B + \frac{\partial \mathbf{U}_{1s}^B}{\partial x_s} \cdot \mathbf{e}_{xs} + (-i\mathbf{k} \cdot \mathbf{e}_1)(\mathbf{U}_{1s}^B \cdot \mathbf{e}_1) \right) \\ -\rho\omega^2 \mathbf{U}_{1s}^B &= \\ \left[ (\lambda + \mu) \left( \frac{\partial^2 \mathbf{U}_{1s}^B}{\partial x_s^2} + (-i\mathbf{k} \cdot \mathbf{e}_1)(1 + (\mathbf{e}_1 \cdot \mathbf{e}_{xs})) \frac{\partial \mathbf{U}_{1s}^B}{\partial x_s} - (\mathbf{e}_1 \cdot \mathbf{e}_{xs})(\mathbf{k} \cdot \mathbf{e}_1)^2 \mathbf{U}_{1s}^B \right) \cdot \mathbf{e}_{xs} \right] \mathbf{e}_{xs} \\ + \mu \left( \frac{\partial^2 \mathbf{U}_{1s}^B}{\partial x_s^2} + (-i\mathbf{k} \cdot \mathbf{e}_1)(1 + (\mathbf{e}_1 \cdot \mathbf{e}_{xs1})) \frac{\partial \mathbf{U}_{1s}^B}{\partial x_s} - (\mathbf{e}_{xs} \cdot \mathbf{e}_1)(\mathbf{k} \cdot \mathbf{e}_1)^2 \mathbf{U}_{1s}^B \right) \\ - \frac{12}{H_m^2} \mu \left[ \left( \frac{\partial U_{0n}^B}{\partial x_s} + (-i\mathbf{k} \cdot \mathbf{e}_1) U_{0n}^B \right) \mathbf{e}_{xs} + \mathbf{U}_{1s}^B \right]\end{aligned}\quad (2.55)$$

with  $\omega$  the eigenvalue,  $\mathbf{k}$  the Bloch wave vector and  $(\mathbf{U}_{0s}^B, U_{0n}^B, \mathbf{U}_{1s}^B)$  the Bloch wave eigenmodes. We notice that, unlike the 2D beam network, no uncoupling is possible between the movement in the plane of the honeycomb thin layer, which is in our case the plane Oxy (Figure 2.22) and the one out of this plane.

For the numerical simulation, Lagrange quadratic triangular elements with size about 0.6 mm

are used, for which the wavelength of bending waves of 13 kHz contains about 6 elements and the considered horizontal plate of the primitive cell whose geometric characteristics will be given in the chapter 4 contains about  $5 \times 20$  elements. Because  $\mathbf{k}$  is only periodic in the plane  $Oxy$ , the first Brillouin zone  $Q^0$  as well as the irreducible zone's contour of the honeycomb thin layer are the same as in the 2D hexagonal beam network. In this case, we discretize first the  $Q^0$  into 201 elements along the axis  $e_y$  from  $Z_2$  to  $Z_5$  and then for each discretized element along  $Z_2 \rightarrow Z_5$ , it is discretized into 201 elements. The corresponding irreducible zone's contour is still discretized into 200 elements.

Besides, we have compared a one-plate model (horizontal plate  $P_{CEN}$ ) and a five-plate (primitive cell) with respectively the Mindlin kinematics with Lagrange quadratic triangular elements and the Kirchhoff-Love kinematics with Argyris shell elements, so that we can check whether numerical locking phenomena take place in the present simulation. The element size in all case is about 0.6mm. The considered geometric and mechanical characteristics that will be given in the chapter 4, in which the length  $s$  of  $P_{CEN}$  is 150 times the thickness  $H_1$ . We find that the considered six eigenfrequencies obtained by the Mindlin kinematics with quadratic triangular elements coincide well with the ones of Kirchhoff model (Figure 2.23).

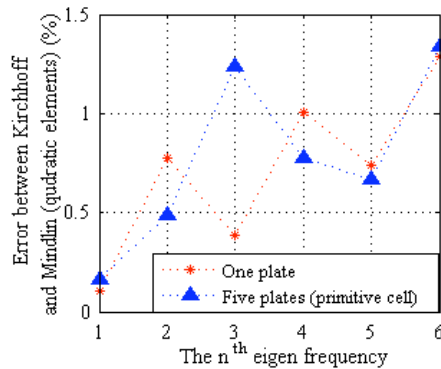


Figure 2.23 Eigenfrequencies errors between the plate models with Mindlin kinematics and the Kirchhoff kinematics

To complete the definition of the Bloch eigenproblem (2.55), the following interface conditions between the five plates at the interior junction edge,  $\Sigma_{IW}$  and  $\Sigma_{IE}$ , and the periodic boundary conditions at the boundary edges,  $(\Sigma_{PNW}, \Sigma_{PSW}, \Sigma_{PNE}, \Sigma_{PSE})$ , of the primitive cell are considered (Figure 2.22).

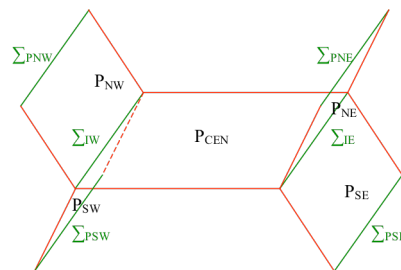


Figure 2.24 Junction edges and boundary edges of the primitive cell of honeycomb thin layer

More precisely, we write, for example on the junction edge  $\Sigma_{IW}$ , the continuity of the displacement and the rotation, and the equilibrium of the generalized force and generalized

beam forces and moments:

$$\begin{aligned}
\mathbf{U}_{0s}^B(\mathbf{P}_{NW}) + \mathbf{U}_{0n}^B \mathbf{n}(\mathbf{P}_{NW}) &= \mathbf{U}_{0s}^B(\mathbf{P}_{CEN}) + \mathbf{U}_{0n}^B \mathbf{n}(\mathbf{P}_{CEN}) = \mathbf{U}_{0s}^B(\mathbf{P}_{SW}) + \mathbf{U}_{0n}^B \mathbf{n}(\mathbf{P}_{SW}) \\
\mathbf{U}_{1sl}^B(\mathbf{P}_{NW}) &= \mathbf{U}_{1sl}^B(\mathbf{P}_{CEN}) = \mathbf{U}_{1sl}^B(\mathbf{P}_{SW}) \\
\mathbf{N}^B \cdot \mathbf{e}_1(\mathbf{P}_{NW}) + (\mathbf{Q}^B \cdot \mathbf{e}_1) \mathbf{n}(\mathbf{P}_{NW}) + \mathbf{N}^B \cdot \mathbf{e}_1(\mathbf{P}_{CEN}) + (\mathbf{Q}^B \cdot \mathbf{e}_1) \mathbf{n}(\mathbf{P}_{CEN}) + \mathbf{N}^B \cdot \mathbf{e}_1(\mathbf{P}_{SW}) + (\mathbf{Q}^B \cdot \mathbf{e}_1) \mathbf{n}(\mathbf{P}_{SW}) &= 0 \\
(\mathbf{M}^B \cdot \mathbf{e}_1) \cdot \mathbf{e}_1(\mathbf{P}_{NW}) + (\mathbf{M}^B \cdot \mathbf{e}_1) \cdot \mathbf{e}_1(\mathbf{P}_{CEN}) + (\mathbf{M}^B \cdot \mathbf{e}_1) \cdot \mathbf{e}_1(\mathbf{P}_{SW}) &= 0
\end{aligned} \tag{2.56}$$

where  $\mathbf{N}^B$ ,  $\mathbf{Q}^B$  and  $\mathbf{M}^B$  denote the Bloch wave transform of respectively the generalized membrane force tensor, the generalized transverse shear force vector and the generalized bending moment tensor. Similar junction conditions are also imposed on the edge  $\sum_{IE}$ . Besides, the boundary periodic conditions between the pair of the edges  $\sum_{PNW}$  and  $\sum_{PSE}$ :

$$\begin{aligned}
\mathbf{U}_{0s}^B(\mathbf{P}_{NW}) + \mathbf{U}_{0n}^B \mathbf{n}(\mathbf{P}_{NW}) &= \mathbf{U}_{0s}^B(\mathbf{P}_{SE}) + \mathbf{U}_{0n}^B \mathbf{n}(\mathbf{P}_{SE}) \\
\mathbf{U}_{1s}^B(\mathbf{P}_{NW}) &= \mathbf{U}_{1s}^B(\mathbf{P}_{SE}) \\
\mathbf{N}^B \cdot \mathbf{e}_1(\mathbf{P}_{NW}) + (\mathbf{Q}^B \cdot \mathbf{e}_1) \mathbf{n}(\mathbf{P}_{NW}) + \mathbf{N}^B \cdot \mathbf{e}_1(\mathbf{P}_{SE}) + (\mathbf{Q}^B \cdot \mathbf{e}_1) \mathbf{n}(\mathbf{P}_{SE}) &= 0 \\
\mathbf{M}^B \cdot \mathbf{e}_1(\mathbf{P}_{NW}) + \mathbf{M}^B \cdot \mathbf{e}_1(\mathbf{P}_{SE}) &= 0
\end{aligned} \tag{2.57}$$

and the same kind of boundary periodic conditions are also imposed for the pair of the edges  $\sum_{PNE}$  and  $\sum_{PSW}$ . These interior interface conditions and boundary periodic conditions complete the definition of the Bloch eigenproblem (2.55) for the honeycomb thin layer and allows obtaining the dispersion relation that will be presented in the chapter 4.

When doing the numerical simulation, we add one more condition for each plate as  $\theta_n = 0$  in its local plate basis, where  $\theta_n$  is the drilling rotation around the axis  $\mathbf{n}$  perpendicular to each plate. It is because the membrane-bending equations (2.55) of the primitive cell do not imply the so-called drilling degree of freedom (dof). For one plate it can simply not be considered at all and eliminated, but here for the primitive cell composed of non-coplanar plates and especially along the junction edges, the bending components of one plate may be converted into the bending modes of another, this drilling degree of freedom should be take into account. To solve this problem and to circumvent the classical problem of singular stiffness matrix, a Lagrange multiplier has been associated with this constraint that is applied only weakly. This is compatible with the interface conditions at the junctions on the two interface edges,  $\sum_{IW}$  and  $\sum_{IE}$ , that only the rotation perpendicular to the plane  $Oxy$  is non-zero. The influence of junction condition on the dispersion characteristics as well as the cellular deformation will be analyzed in the chapter 4.

## 2.4.2 Honeycomb core sandwich plate

The honeycomb core sandwich plate is composed of a honeycomb core thin layer and two skins (Figure 2.23). Therefore, the primitive cell  $Q_0$  of the honeycomb core sandwich plate is composed of seven rigidly-jointed plates,  $\mathbf{P}_{CEN}$ ,  $\mathbf{P}_{NW}$ ,  $\mathbf{P}_{SW}$ ,  $\mathbf{P}_{NE}$ ,  $\mathbf{P}_{SE}$ ,  $\mathbf{P}_{TSKIN}$  and  $\mathbf{P}_{BSKIN}$ , with  $\mathbf{P}_{CEN}$ ,  $\mathbf{P}_{NW}$ ,  $\mathbf{P}_{SW}$ ,  $\mathbf{P}_{NE}$  and  $\mathbf{P}_{SE}$  the primitive cell of the honeycomb thin layer and  $\mathbf{P}_{TSKIN}$  and  $\mathbf{P}_{BSKIN}$  two rhombus plates of the skins. The edge length of  $\mathbf{P}_{TSKIN}$  and  $\mathbf{P}_{BSKIN}$  is  $\sqrt{3}s$ , the thickness is  $H_{skin}$  and the mechanical characteristics are  $(\lambda_{skin}, \mu_{skin}, \rho_{skin})$ . Each plate is parameterized in its local plate basis  $(\mathbf{e}_1, \mathbf{e}_2, \mathbf{n})$  first, while the whole network is finally considered under the global Cartesian basis  $(\mathbf{e}_x, \mathbf{e}_y, \mathbf{e}_z)$  (Figure 2.24).

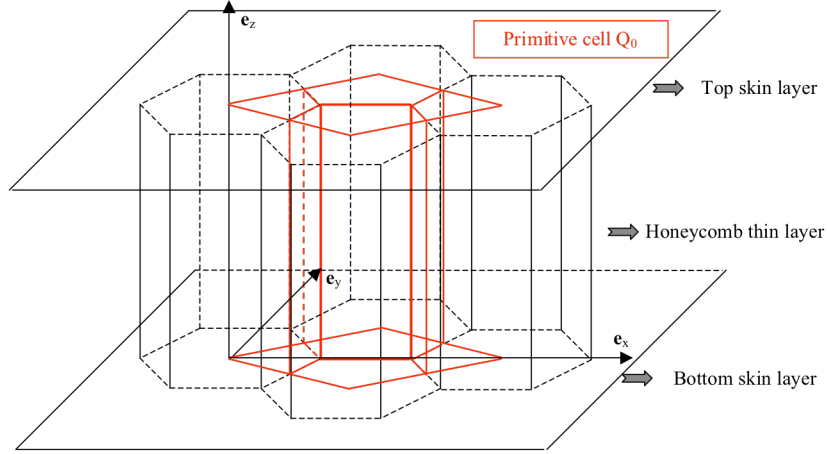


Figure 2.25 Honeycomb core sandwich plate

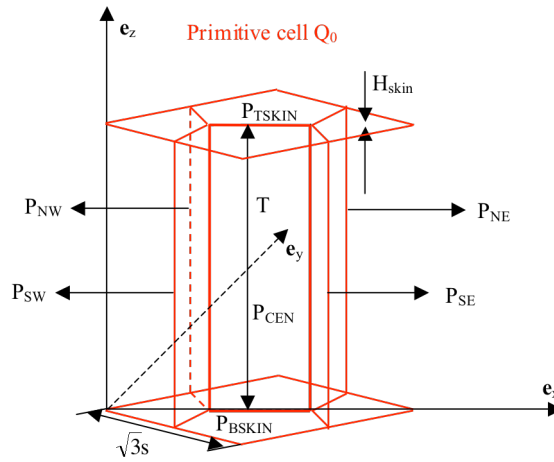


Figure 2.26 Primitive cell of honeycomb core sandwich plate

The Mindlin kinematics for thick plate is still used for the honeycomb core sandwich plate. The Bloch wave transform of the equilibrium equations are always governed by (2.55). The eigenvalue  $\omega$  and its corresponding Bloch wave eigenmodes ( $\mathbf{U}_{0s}^B$ ,  $\mathbf{U}_{0n}^B$ ,  $\mathbf{U}_{1s}^B$ ) are searched for all the Bloch wave vectors in the first Brillouin zone and the irreducible zone's contour (Figure 2.16 and 2.17).

For the numerical simulation of the sandwich plate, we still use Lagrange quadratic triangular elements with size 0.6 mm, for which the wavelength of bending waves of the skins of 13 kHz contains about 61 elements while the one of honeycomb core thin layer contains 6 elements. The considered skins and the horizontal plate of the honeycomb core whose geometric characteristics will be given in the chapter 4 respectively contain about  $9 \times 9$  elements and  $5 \times 20$  elements. The first Brillouin zone  $Q^0$  is discretized into  $201 \times 201$  elements and the corresponding irreducible zone's contour into 200 elements.

To complete the definition of the Bloch eigenproblem of the honeycomb core sandwich plate, besides (2.56) - (2.59), we have the periodic conditions between  $P_{TSKIN}$  and  $P_{BSKIN}$  on the edges of:  $\Sigma_{NW\_TSKIN}$  and  $\Sigma_{SE\_TSKIN}$ ,  $\Sigma_{SW\_TSKIN}$  and  $\Sigma_{NE\_TSKIN}$ ,  $\Sigma_{NW\_BSKIN}$  and  $\Sigma_{SE\_BSKIN}$ ,  $\Sigma_{SW\_BSKIN}$  and  $\Sigma_{NE\_BSKIN}$ .

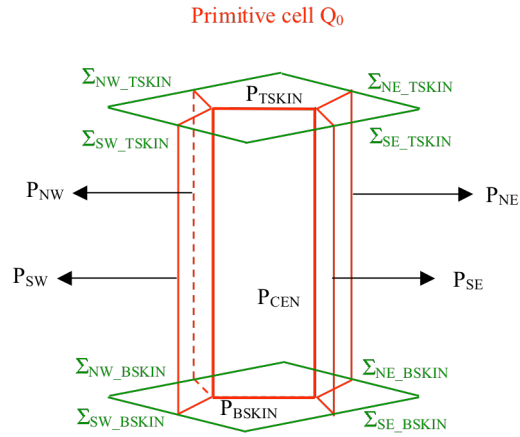


Figure 2.27 Boundary edges of  $P_{\text{TSKIN}}$  and  $P_{\text{BSKIN}}$

## Conclusion

In this chapter, we apply the Bloch wave theory to the study of the elastic wave propagation in the 1D, 2D periodic beam networks and finally the honeycomb thin layer made of plates and honeycomb core sandwich plate.

By combining the Bloch transform of the equilibrium equations with the interface conditions on the junction points/edges inside the primitive cell and also the periodic boundary conditions at the end of the primitive cell, we can obtain the complete definition of the Bloch wave eigenproblem of each periodic network, which allows to getting the dispersion relation between the eigenvalue and the discretized Bloch wave vector restricted in the first Brillouin zone as well as on the irreducible zone's contour. More precisely, in the longitudinal wave propagation case of the 1D periodic beam network, the dispersion relation can be explicated in an analytical way, with which we can prove that the frequency bandgaps are mostly generated by the mismatch of characteristic acoustic impedances in the primitive cell.

# Wave propagation in 1D and 2D periodic networks

*In this chapter, our approach is first applied in the 1D periodic beam network, comparing the dispersion relation and the corresponding Bloch wave eigenmodes calculated numerically to those obtained analytically. Then the influence of acoustic impedance ratio on the bandgaps of the longitudinal wave and the influence of Young's modulus and thickness on the bandgaps of the bending/transverse shear waves is discussed respectively. In the second step, the numerical simulation of elastic wave propagation in the 2D periodic beam networks is presented in detail. The dispersion relation and the Bloch eigenmodes of the in-plane membrane and the out-of-plane bending waves are presented respectively for the hexagonal and rectangular networks. The influence of important material and structural properties, such as the Young's modulus, the thickness and the internal angle, on the bandgaps is analyzed for the hexagonal network. In the end, the wave propagation velocities of several main wave modes are calculated numerically for the hexagonal network, according to which the anisotropic and dispersive nature of the network is highlighted. In parallel, these wave propagation velocities are also compared with a homogenized orthotropic plate model in order to check whether homogenized models can represent the membrane and bending wave behaviors of the network in low frequency (LF) range.*

## Summary

---

<b>3.1 Analysis of the frequency bandgaps in 1D periodic beam network</b> .....	<b>46</b>
3.1.1 Dispersion relation.....	46
3.1.2 Influence of structural and geometric characteristics on frequency bandgaps.....	47
3.1.3 Bloch wave eigenmodes.....	50
<b>3.2 2D periodic hexagonal and rectangular beam networks</b> .....	<b>50</b>
3.2.1 Dispersion relation.....	51
3.2.2 Influence of structural and geometric characteristics on frequency bandgaps of hexagonal network.....	54
3.2.3 Bloch wave eigenmodes.....	62
<b>3.3 Wave propagation velocities analysis in periodic hexagonal beam network</b> .....	<b>65</b>
3.3.1 S-mode and L-mode.....	65
3.3.2 Bending mode.....	67
<b>Conclusion</b> .....	<b>71</b>

---

### 3.1 Analysis of the frequency bandgaps in 1D periodic beam network

According to the Bloch wave analysis on the 1D periodic beam network in chapter 2, now we consider the numerical solving of the Bloch eigenproblem of the elastic wave propagation in the network. The mechanical characteristics of the 1D network considered here are shown in Table 3.1. The study on this kind of periodic network is similar to the one on periodic materials and can be analogized easily to the large amount of results already obtained in other research domains, like periodic materials in quantum mechanics or in photonic research field [Atkins (2005)].

Table 3.1 Geometric and mechanical characteristics of primitive cell of 1D network

	Young's modulus $E_{j(j=1, 2)}$ (GPa)	Poisson's ratio $\nu_{j(j=1, 2)}$	Density $\rho_{j(j=1, 2)}$ ( $\text{kg}\cdot\text{m}^{-3}$ )	Length $l_{j(j=1, 2)}$ (mm)	Thickness H (mm)
Beam1	50	0.33	2700	4	0.02
Beam2	250	0.33	2700	1.5	0.02

#### 3.1.1 Dispersion relation

It has been shown that for the longitudinal wave, the dispersion relation between  $k$  and  $\omega$  can be derived from the linear system (2.24) in an explicit analytical form (2.26), with the help of which for each given  $\omega$ , either real or complex  $k$  can be calculated. Contrarily, for the bending and transverse shear waves numerical solving of the Bloch eigenproblem is necessary, so the first Brillouin zone is discretized and for each discretized  $k$ , we search for the eigenvalues and the eigenmodes. Hence, by this approach, it is not possible to obtain the complex values of  $k$ .

First of all, we have calculated numerically the dispersion curves for the longitudinal wave and compared them to the theoretical dispersion curves. We find that the curves obtained by two methods match well (Figure 3.1).

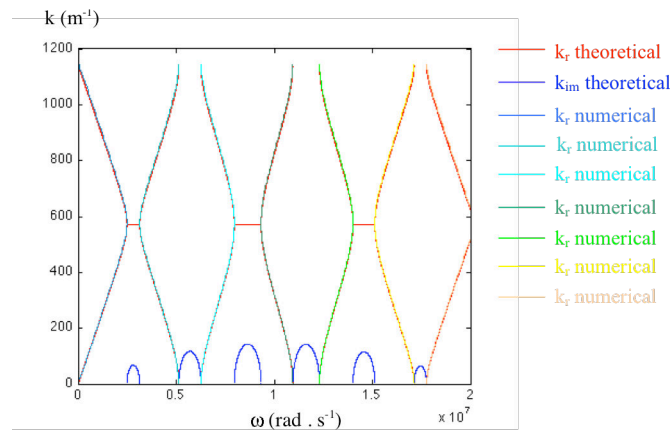


Figure 3.1 Dispersion curves of longitudinal wave obtained by theoretical and numerical analyses

Then the dispersion curves of the bending and transverse shear waves are numerically obtained as well (Figure 3.2(right)). Compared with the longitudinal wave, we find that the bandgaps of bending and transverse shear waves occur in a much lower eigenvalue range. In other words, the first stop band takes place in lower frequency range for the bending and transverse shear waves (Figure 3.3).

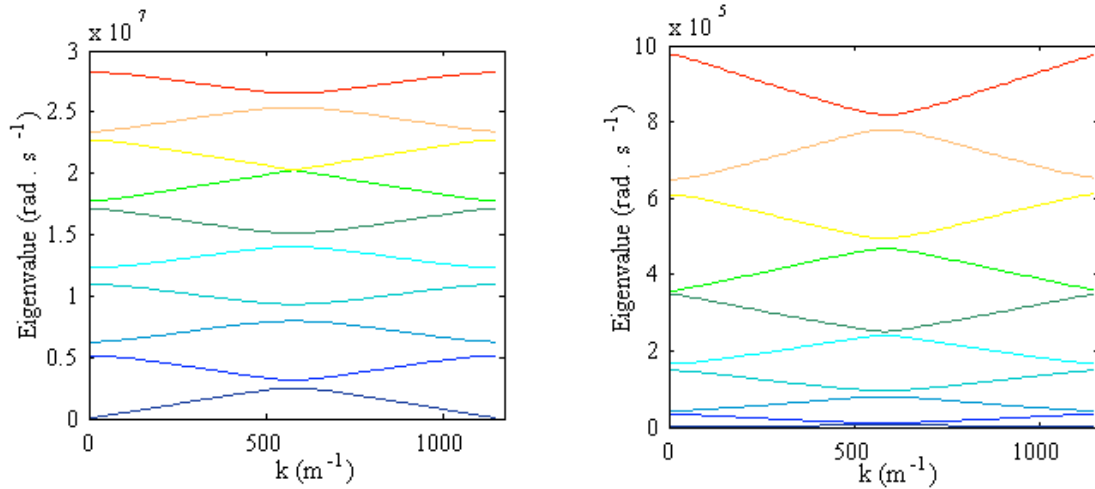


Figure 3.2 (left) Dispersion curves of longitudinal wave; (right) Dispersion curves of bending and transverse shear waves

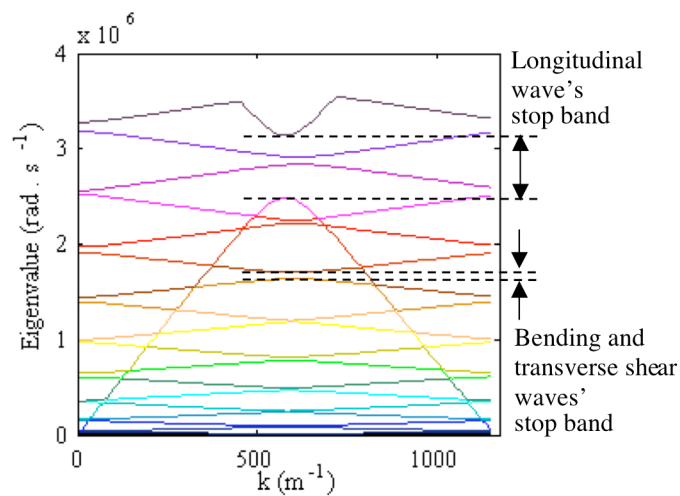


Figure 3.3 Dispersion curves of coupled longitudinal and bending/transverse shear waves of 1D periodic network

### 3.1.2 Influence of structural and geometric characteristics on frequency bandgaps

The parametric study is performed in the 1D periodic network in order to investigate the influence of material and structural properties on the frequency bandgaps.

#### (a) Influence of acoustic impedance on the longitudinal wave

In the case of the longitudinal wave, the analytical dispersion equation (2.26) shows a strong dependence upon the characteristic acoustic impedance ratio,  $Z_1/Z_2$ , between the two beams, so our first investigation concerns the influence of this ratio on the frequency bandgaps. The

special case with  $Z_1/Z_2 = 1$  is considered at first, and as indicated by the analytical result, no frequency bandgap is found. Then, the Young's modulus  $E_2$  of the second beam of the primitive cell is changed to get six different values of the characteristic acoustics impedance ratio, to look into its influence on the bandgaps. Among these six ratios, the second one is considered here as the reference value (Table 3.2).

Table 3.2 Six groups of characteristic acoustic impedance ratio

$E_1$ (GPa)	50	50 (Reference)	50	50	50	50
$E_2$ (GPa)	500	250 (Reference)	100	25	10	5
$Z_1/Z_2$	$1/\sqrt{10}$	$1/\sqrt{5}$ (Reference)	$1/\sqrt{2}$	$\sqrt{2}$	$\sqrt{5}$	$\sqrt{10}$
H (mm)	0.02					

In this part, we choose to use theoretical way to calculate the bandgaps of longitudinal wave as with the dispersion equation we can obtain the explicit values of  $k_{im}$ . The first stop bands corresponding to the different acoustic impedance ratios are compared (Figure 3.4). We notice that the more different from one the acoustic impedance ratio, the larger the stop band and the stronger the attenuation. Finally, we note that, as by changing only the parameter  $E_2$ , we change not only the ratio  $Z_1/Z_2$  but also another parameter  $T_2$  of the dispersion equation (2.26), so it is normal that the first stop bands respectively obtained for  $Z_1/Z_2$  equal to  $1/\sqrt{10}$  and  $\sqrt{10}$  do not coincide. We notice that with the decrease of  $E_2$ , the first stop band moves to lower frequency range.

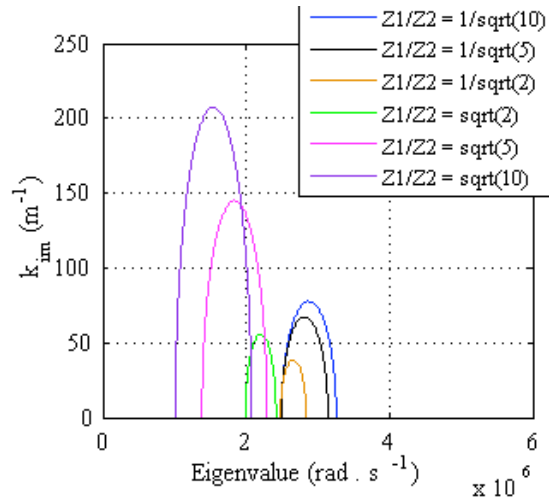


Figure 3.4 Influence of acoustic impedance ratio on longitudinal wave's first stop band

**(b) Influence of Young's modulus ratio on the bending and transverse shear waves**

For the bending and transverse shear waves, as no analytical dispersion equation is available to suggest special choices of the parameters to investigate, so it is natural to consider at first the mismatch of Young's modulus within the primitive cell. Keeping other parameters as the same, six different values of the Young's modulus ratio  $E_1/E_2$  are considered here (Table 3.2). As results, the center location and the width of the six corresponding first stop bands are presented (Figure 3.5).

We obtained the same conclusions as in the case of longitudinal wave. The more the mismatch of Young's modulus, the larger the stop band and with the decrease of  $E_2$ , the first stop band moves to lower frequency range, but the relation is not linear.

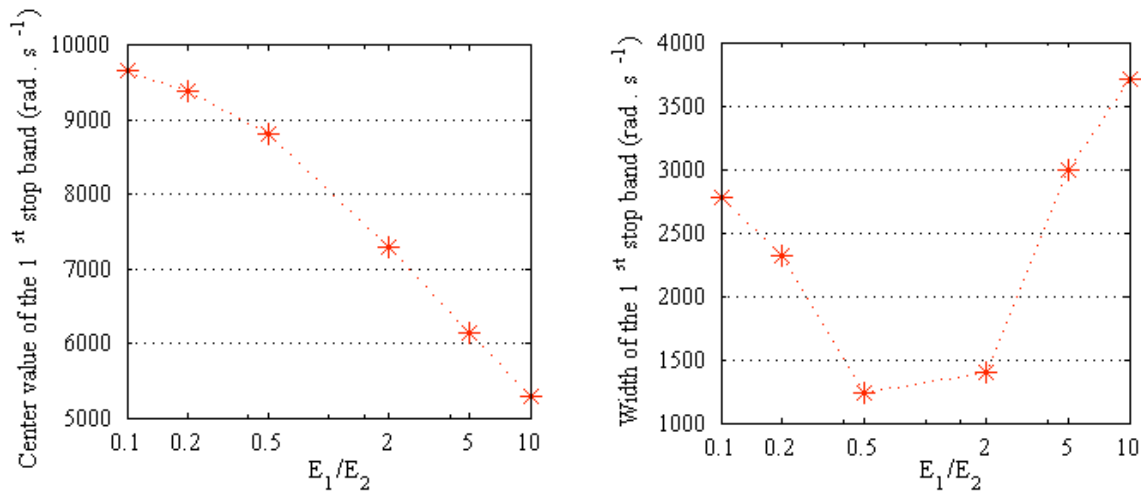


Figure 3.5 Influence of Young's modulus ratio on bending and transverse shear waves' first stop band

**(c) Influence of beam's thickness on the bending and transverse shear waves**

As the thickness is an important parameter for bending wave velocity, we are interested in studying the influence of beam's thickness on the bandgaps of bending and transverse shear waves, with five different values (Table 3.3), while the reference value of Young's modulus is always used for each case.

Table 3.3 Five groups of thickness, H

H (mm)	0.02 (Reference)	0.05	0.2	0.4	0.6
$\lambda/H$	$\approx 300$	$\approx 100$	$\approx 30$	$\approx 14$	$\approx 9$
$E_1$ (GPa)	50				
$E_2$ (GPa)	250				

The center location and the width of the first stop band are still investigated. We remark that with the increase of thickness, the first stop band moves to high range and also becomes larger. Moreover, the order of magnitude of the location and the width links to the order of magnitude of the thickness. In other words, it is believed that the relation between the first stop band and the thickness is linear (Figure 3.6).

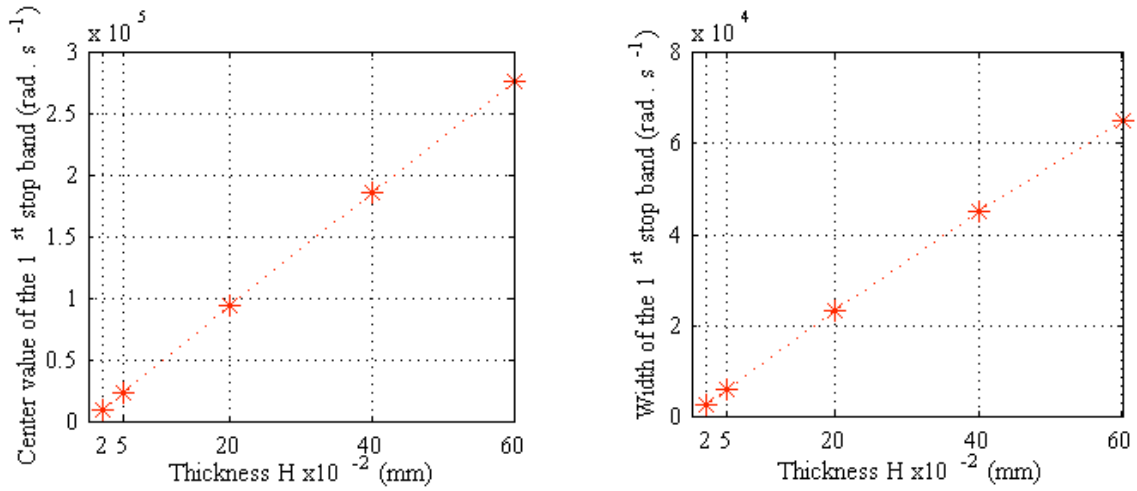


Figure 3.6 Influence of beam's thickness on bending and transverse shear waves' first stop band

### 3.1.3 Bloch wave eigenmodes

Each wave vector  $k$  locating in the first Brillouin zone can correspond to an infinite number of eigenvalues and Bloch eigenmodes. Here, six Bloch wave eigenmodes are presented respectively for the wave vector  $k$  locating at two points of the first Brillouin zone: its center  $k = 0$ , one of its two ends  $k = \pi/\lambda$ . The total displacement is illustrated in color, where the red color represents the maximal value and the blue color means zero. We find that at the end of  $Q^0$ , the first mode of both longitudinal wave and bending and transverse shear wave is a rigid body mode.



Figure 3.7 (left) Six Bloch wave eigenmodes of longitudinal for the  $k$  at the center of  $Q^0$ ; (right) Six Bloch wave eigenmodes of longitudinal wave for the  $k$  at the end of  $Q^0$

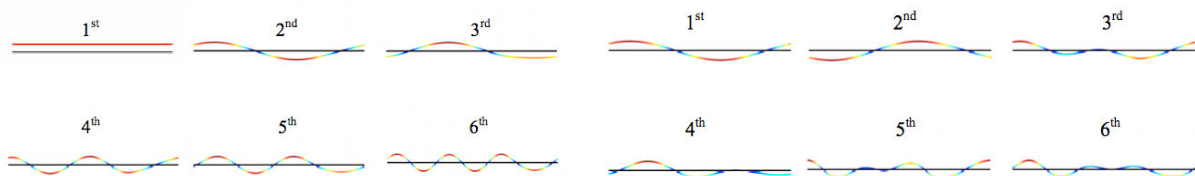


Figure 3.8 (left) Six Bloch wave eigenmodes of bending and transverse shear waves for the  $k$  at the center of  $Q^0$ ; (right) Six Bloch wave eigenmodes of bending and transverse shear waves for the  $k$  at the end of  $Q^0$

## 3.2 2D hexagonal and rectangular beam networks

Based on the Bloch wave analysis on the 2D periodic beam network, the same kind of numerical simulations as in 1D network is also considered for the 2D periodic beam networks. The aim is to obtain important information of the networks with respect to the

elastic wave propagation, for example the dispersion relation, the frequency bandgaps [Spadoni (2009); Tee (2010)], the anisotropy and the Bloch wave eigenmodes.

### 3.2.1 Dispersion relation

#### (a) Periodic hexagonal beam network

First of all, we concentrate with the periodic hexagonal network. The geometric and mechanical characteristics of the primitive cell are presented in Table 3.4.

Table 3.4 Geometric and mechanical characteristics of primitive cell of 2D periodic hexagonal network

	Horizontal beam	Four oblique beams
Young's modulus E (GPa)	70	70
Poisson's ratio $\nu$	0.33	0.33
Density $\rho(\text{kg.m}^{-3})$	2700	2700
Length s (mm)	3	1.5
Width T (mm)	0.12	0.12
Thickness $H_{m(m=0,1)}$ (mm)	0.2	0.2

Both the first Brillouin zone and the irreducible zone's contour are considered here (Figure 3.9), so that we obtain the 3D dispersion surfaces, which contains full information between  $\omega$  and  $\mathbf{k}$ , as well as the 2D curves, which highlight the frequency bandgaps (Figure 3.10).

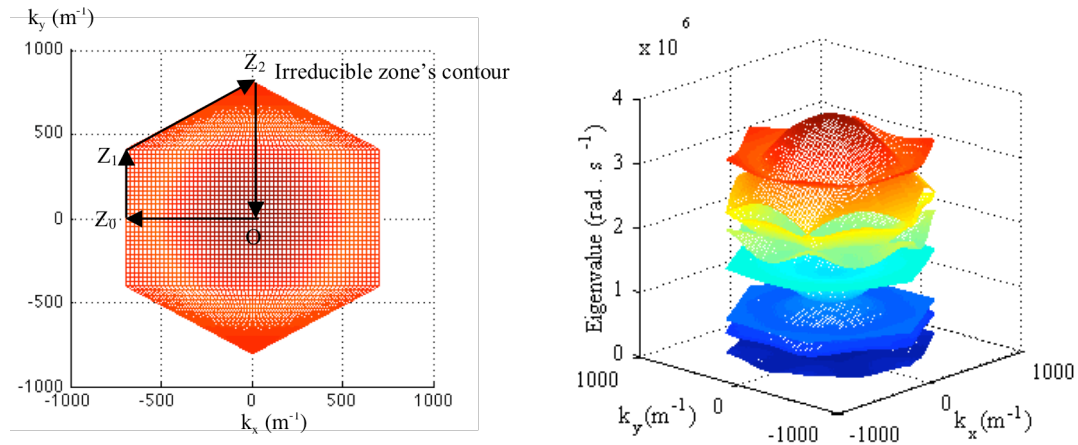


Figure 3.9 (left) First Brillouin zone and irreducible zone's contour; (right) 3D dispersion surfaces of the periodic hexagonal network

Ten first eigenvalues are presented for both the in-plane membrane waves and the out-of-plane bending waves. We find out that for the given geometric and mechanical characteristics, the first stop band of the in-plane membrane waves occurs between the sixth and the seventh eigenvalue, which is at about  $2 \times 10^6 \text{ rad.s}^{-1}$ , correspondingly 0.3 MHz. As for the out-of-plane waves, we remark that no stop band exists within the current eigenvalue range. However, if we search in a higher range, we observe the first stop band for the out-of-plane bending waves appears at about  $6 \times 10^6 \text{ rad.s}^{-1}$ , correspondingly 1 MHz. Compared to the in-plane waves, the first stop of the out-of-plane waves takes place in a much higher frequency range and is narrower. In addition, the common feature that the dispersion curves do not cross but “veer away” when they are to each other is observed [Srikantha Phani (2006)]. Furthermore, we remark that this kind of deflection of curve occurs in the most of the cases at the corner points of the irreducible zone: (O, Z<sub>0</sub>, Z<sub>1</sub>, Z<sub>2</sub>) (Figure 3.10, 3.11 and 3.12).

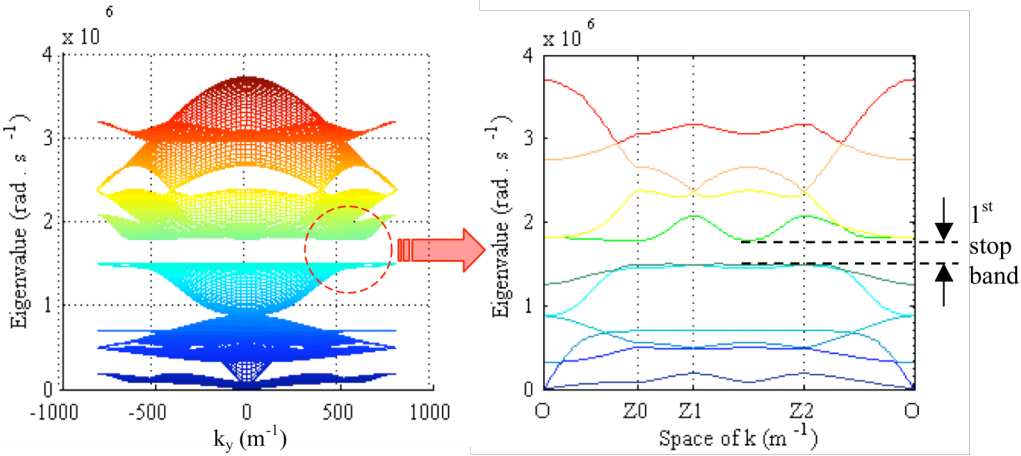


Figure 3.10 (left) 3D dispersion surface; (right) 2D dispersion curve, of in-plane membrane waves

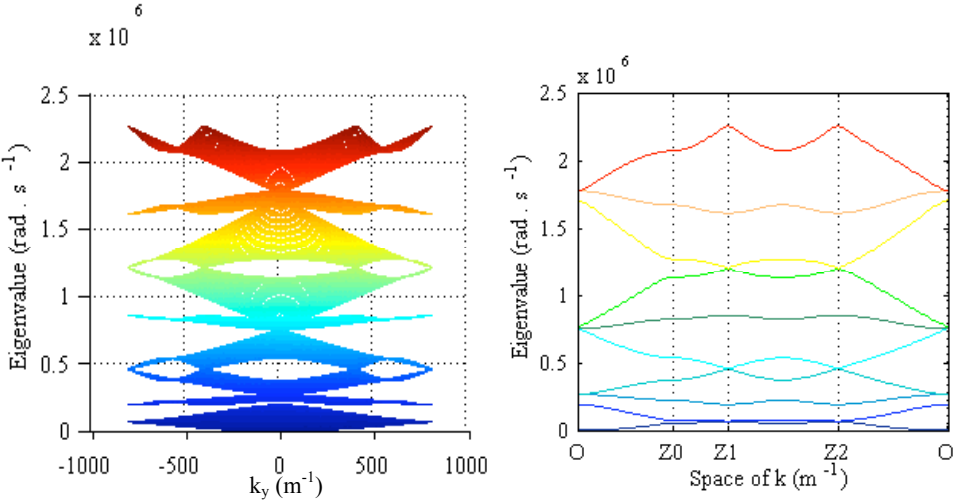


Figure 3.11 (left) 3D dispersion surface; (right) 2D dispersion curve, of out-of-plane bending waves

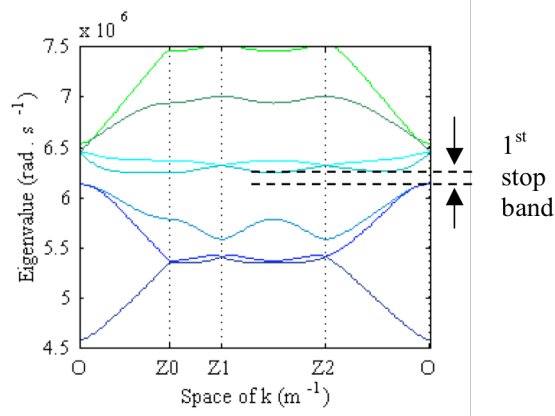


Figure 3.12 1<sup>st</sup> stop band of out-of-plane bending waves

**(b) Periodic rectangular network**

Then, we focus on the rectangular network. The first Brillouin zone and the irreducible zone's contour are considered in order to obtain respectively the dispersion surfaces and curves (Figure 3.13). Table 3.5 lists the geometric and mechanical characteristics of the primitive cell.

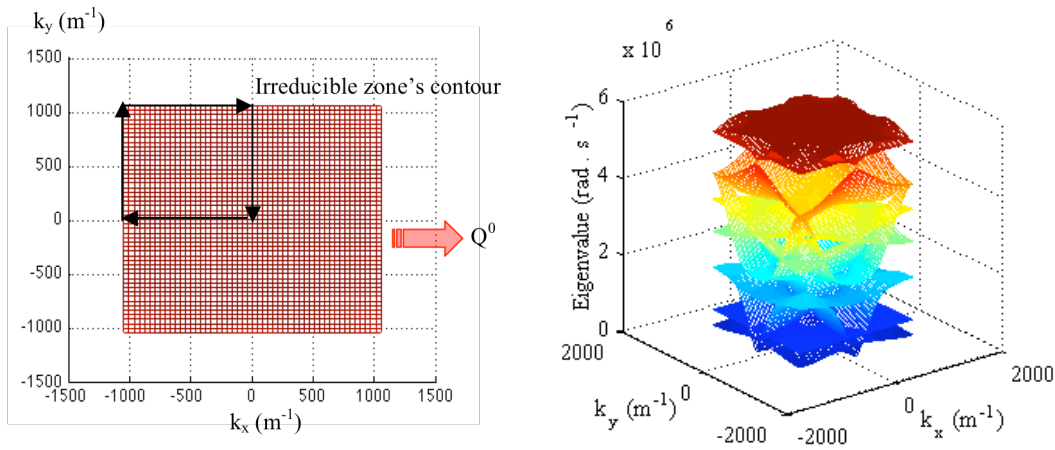


Figure 3.13 (left) First Brillouin zone and irreducible zone's contour; (right) 3D dispersion surfaces of the periodic rectangular network

Table 3.5 Geometric and mechanical characteristics of the primitive cell of 2D periodic rectangular network

	E (GPa)	$\nu$	$\rho$ (kg.m <sup>-3</sup> )	s (mm)	H <sub>m(m=0,1)</sub> (mm)	T (mm)
Horizontal beams	70	0.33	2700	1.5	0.2	0.12
Vertical beams	70	0.33	2700	1.5	0.2	0.12

As an important result, we remark that for the rectangular network, no complete frequency bandgaps exist for neither the in-plane membrane nor the out-of-plane bending waves in the considered frequency range (Figure 3.14 and 3.15), this phenomenon is also reported by

Wang et al. [Wang (2012)]. In other words, for any frequency belonging to the considered frequency range, there is always at least one propagating mode in at least one direction in the rectangular networks. Besides, we find that the dispersion curves of both the in-plane waves and the out-of-plane waves are symmetric, based on which, it is believed that a smaller irreducible zone contour can be chosen for the rectangular network (Figure 3.14 and 3.15).

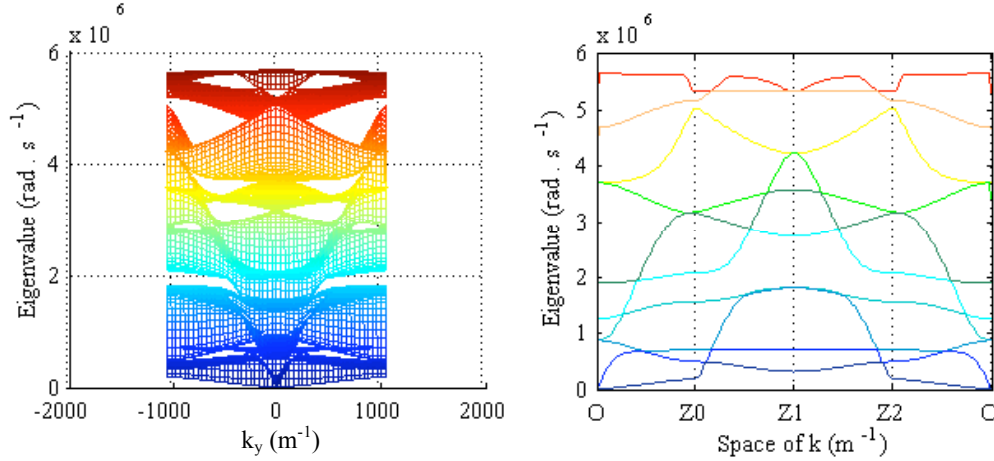


Figure 3.14 (left) 3D dispersion surface; (right) 2D dispersion curve of in-plane membrane waves

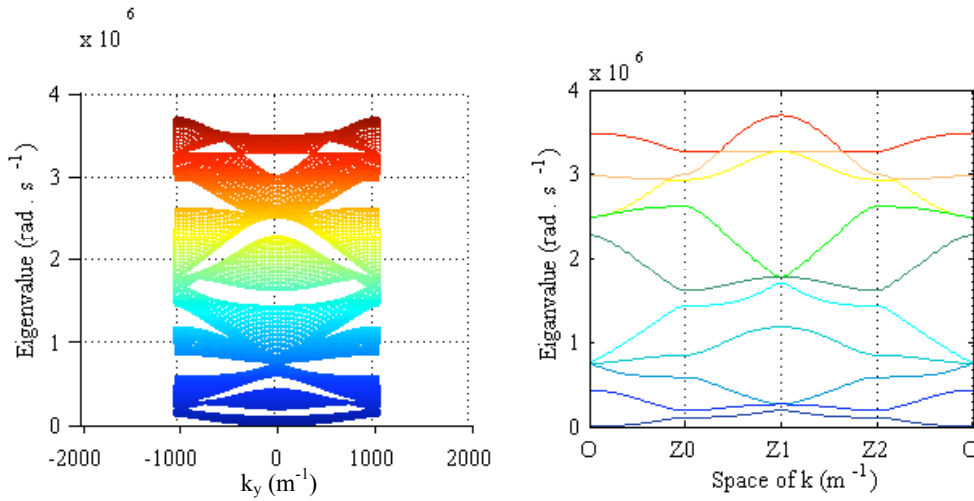


Figure 3.15 (left) 3D dispersion surface; (right) 2D dispersion curve of out-of-plane bending waves

### 3.2.2 Influence of structural and geometric characteristics on frequency bandgaps of hexagonal network

Similarly as for the 1D case, we are interested in the influence on the frequency bandgaps of important structural and geometric parameters, such as the Young's modulus  $E$ , the beam's thickness  $H$  and the internal angle  $\theta$  between the horizontal beam and the oblique one. In the present work, these studies are only performed for the hexagonal network.

#### (a) Influence of Young's modulus

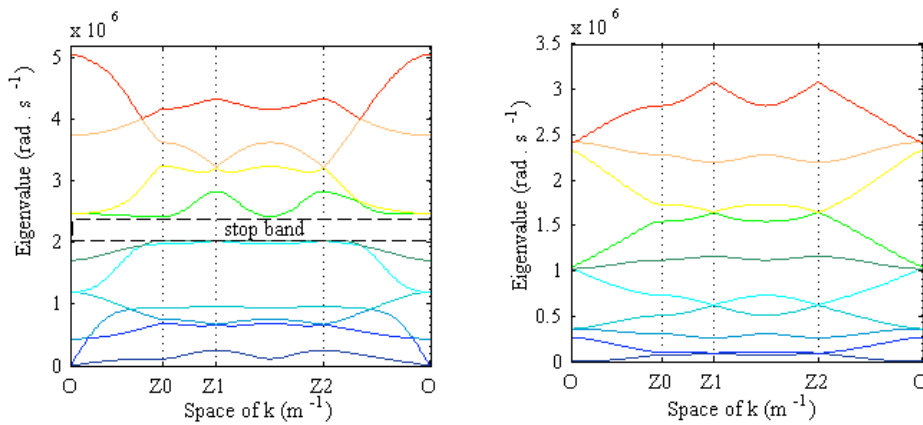
Five different Young's moduli are considered here, among which the value of 70 GPa is taken

as the reference value (Table 3.6).

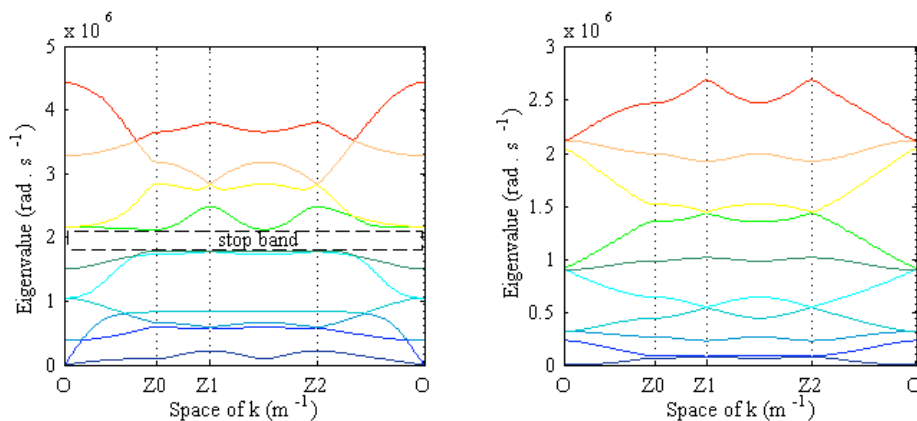
Table 3.6 Young's modulus of five beams in the primitive hexagonal cell

E (GPa)	130	100	70 (Reference)	40	7
$H_0$ (mm)	0.2				
$H_1$ (mm)	0.2				
$\theta$ ( $^\circ$ )	60				

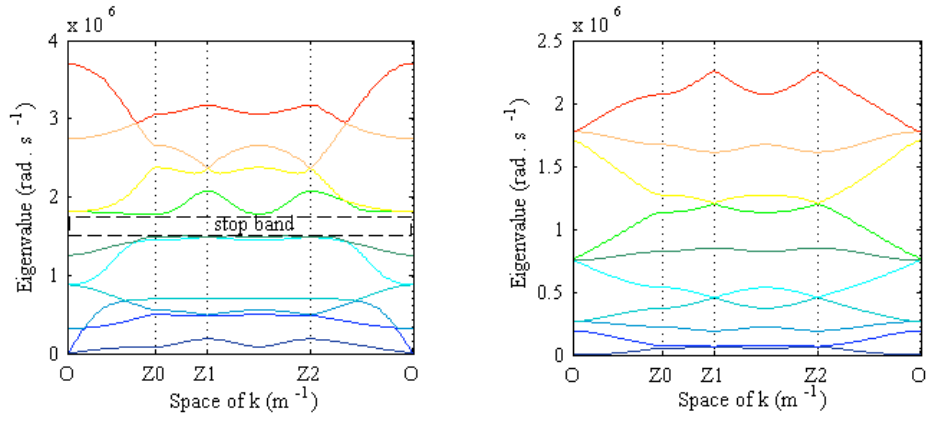
Ten first eigenvalues of both the in-plane membrane and out-of-plane bending waves are obtained for each Young's modulus case. We find that with the decrease of Young's modulus, the eigenvalues of network move down to lower range while the structure of dispersion curves is not affected. Consequently, the first stop band of in-plane waves moves down too. In other words, it is possible to obtain stop bands in LF range if we select "soft" materials for periodic networks (Figure 3.16 and 3.17).



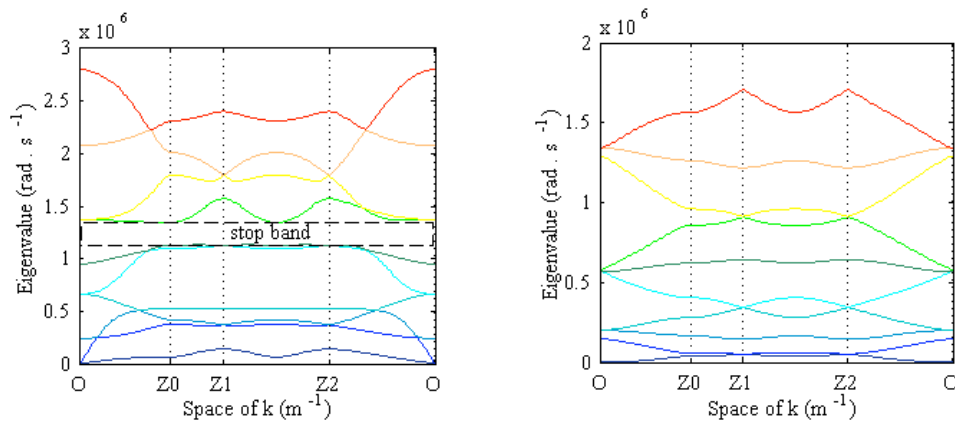
(a) (left) Dispersion curves of in-plane waves; (right) Dispersion curves of out-of-plane waves,  $E = 130$  (GPa)



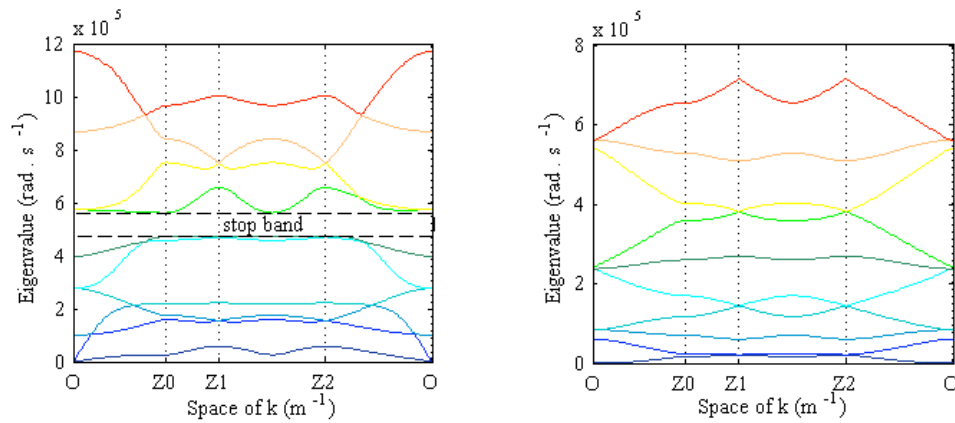
(b) (left) Dispersion curves of in-plane waves; (right) Dispersion curves of out-of-plane waves,  $E = 100$  (GPa)



(c) (left) Dispersion curves of in-plane waves; (right) Dispersion curves of out-of-plane waves,  $E = 70$  (GPa)



(d) (left) Dispersion curves of in-plane waves; (right) Dispersion curves of out-of-plane waves,  $E = 40$  (GPa)



(e) (left) Dispersion curves of in-plane waves; (right) Dispersion curves of out-of-plane waves,  $E = 7$  (GPa)

Figure 3.16 Influence of Young's Modulus on the bandgaps of hexagonal beam network

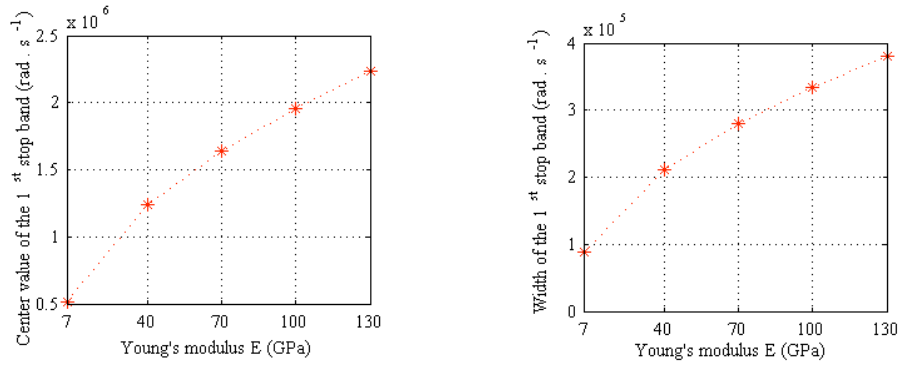


Figure 3.17 Influence of Young's Modulus on the 1<sup>st</sup> stop band of in-plane waves of the hexagonal beam network

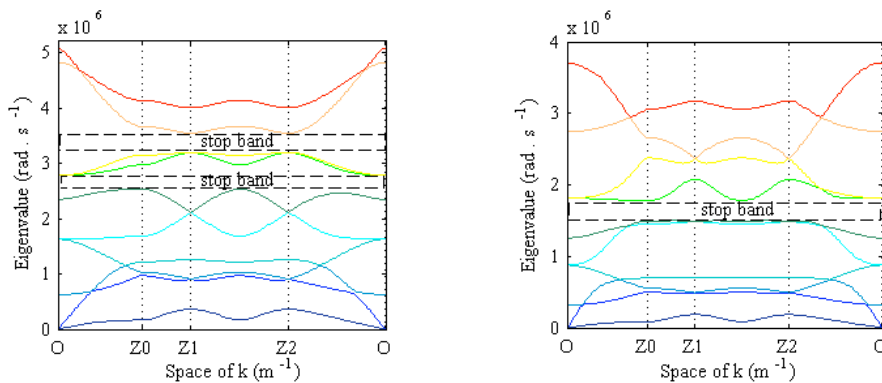
**(b) Influence of beam's thickness**

As for the study of the influence of thickness  $H_m$  with  $m = 0, 1$ , we consider at first the case where the thickness of the oblique beams  $H_0$  is equal to the one of horizontal beam  $H_1$ , but takes respectively four different values, among which 0.2 mm is the reference value (Table 3.7).

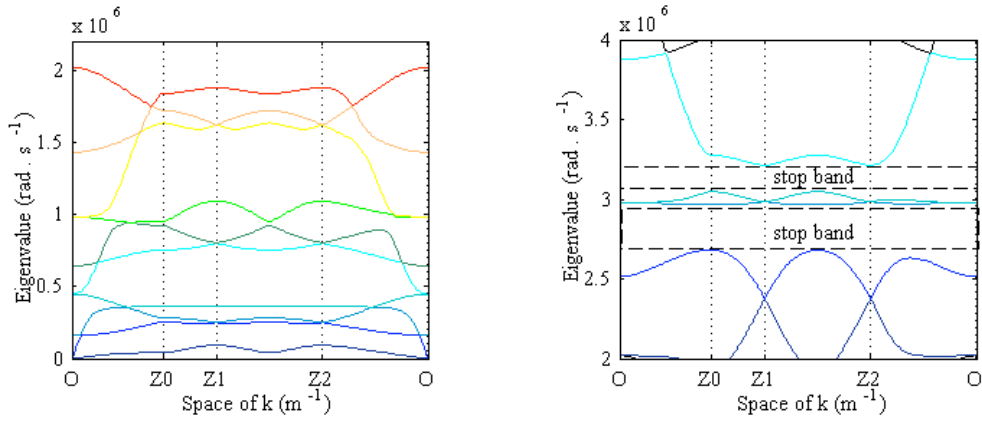
Table 3.7 Thickness,  $H_0 = H_1$

$H_0$ (mm)	0.4	0.2 (Reference)	0.1	0.02
E (GPa)	70			
$\theta$ (°)	60			

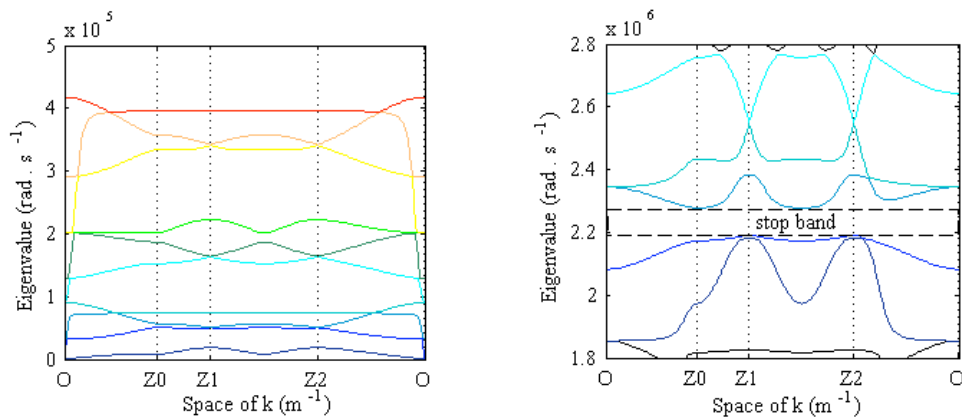
We notice that there are two stop bands of the in-plane waves with  $H_0 = 0.4$  mm and 0.1 mm, while only one stop band exists with  $H_0 = 0.2$  mm and 0.02 mm (Figure 3.18). With the decrease of  $H_0$ , the eigenvalues of the in-plane waves go down to low frequency range but the magnitude order of the center location of the 1<sup>st</sup> stop bands take place, is not significantly affected (Figure 3.19), which is enormously different from the phenomenon we observed in the 1D network. Therefore, it is believed no LF stop bands can be obtained of the in-plane waves of the hexagonal networks no matter what value of  $H$  is chosen. The thickness does not affect the dispersion curves of the bending waves, which are in fact governed by the width  $T$ .



(a) (left) Dispersion curves,  $H_0 = 0.4$ mm; (right) Dispersion curves,  $H_0 = 0.2$ mm



(b) (left) Dispersion curves; (right) First stop band,  $H_0 = 0.1\text{mm}$



(c) (left) Dispersion curves; (right) First stop band,  $H_0 = 0.02\text{mm}$

Figure 3.18 Influence of beam's thickness on the bandgaps of in-plane membrane waves of the hexagonal beam network

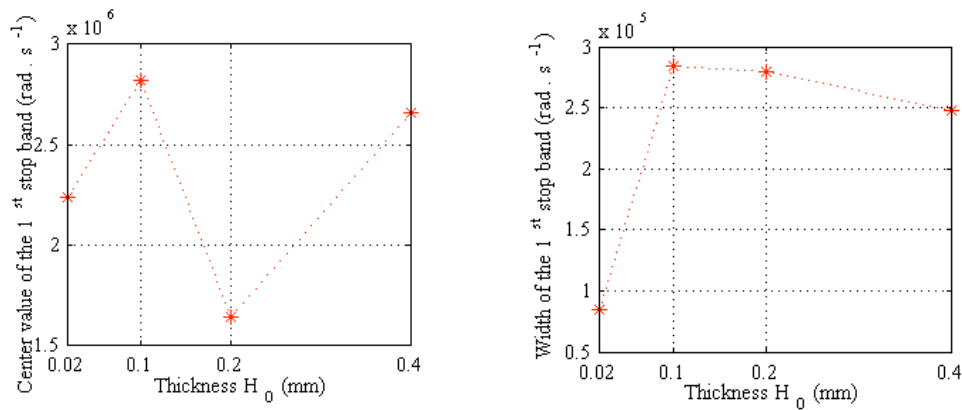


Figure 3.19 Influence of beam's thickness on bending and transverse shear waves' first stop band

**(c) Influence of thickness mismatch**

Due to the manufacturing process of periodic hexagonal networks, usually the horizontal beam is a double-thickness beam. Therefore, two situations,  $H_1 = H_0$  and  $H_1 = 2H_0$ , are investigated in order to take into account the effects of the mismatch between  $H_1$  and  $H_0$  (Figure 3.20 and Table 3.8).

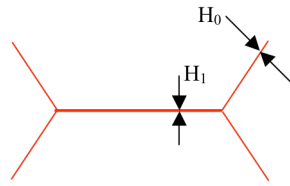


Figure 3.20 Double thickness of the horizontal beam

Table 3.8 Thickness,  $H_0 \neq H_1$

$H_0$ (mm)	$H_1$ (mm)	
0.2	0.2 ( $H_1 = H_0$ )	0.4 ( $H_1 = 2H_0$ )
$E = 70$ (GPa)		
$\theta = 60^\circ$		

Here we only study the in-plane waves. We remark that the double-thickness horizontal beam does change the dispersion curves of the in-plane waves. In the case with  $H_1 = 2H_0$ , there exists no more the first stop that occurs between the 6<sup>th</sup> and 7<sup>th</sup> eigenvalues as privously observed in the case with  $H_1 = H_0$  (Figure 3.21).

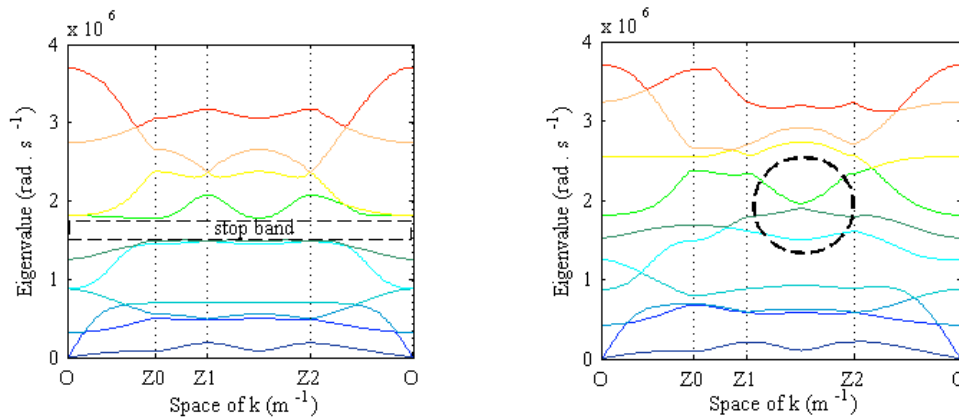


Figure 3.21 (left) Dispersion curves,  $H_1 = H_0$ ; (right) Dispersion curves,  $H_1 = 2H_0$ , Influence of double thickness horizontal beam on the bandgaps of in-plane waves of hexagonal beam network

**(d) Influence of internal angle**

Now let us focus our attention on the influence of internal angle,  $\theta$  (Figure 3.22). The purpose is to know how the different cellular geometry works on the frequency bandgaps of the periodic network and also to validate our numerical tools by comparing our results to the previous research work presented by Gonella et al. [Gonella (2008)]who has already studied the cases of  $\theta$  equal to  $60^\circ$ ,  $80^\circ$  and  $100^\circ$ . Six values of the internal angle  $\theta$  are considered here from  $15^\circ$  to  $90^\circ$  by a sweeping step of  $15^\circ$ . The  $60^\circ$  is our reference angle (Table 3.9).

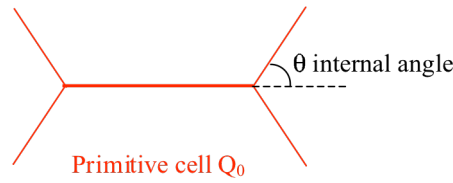


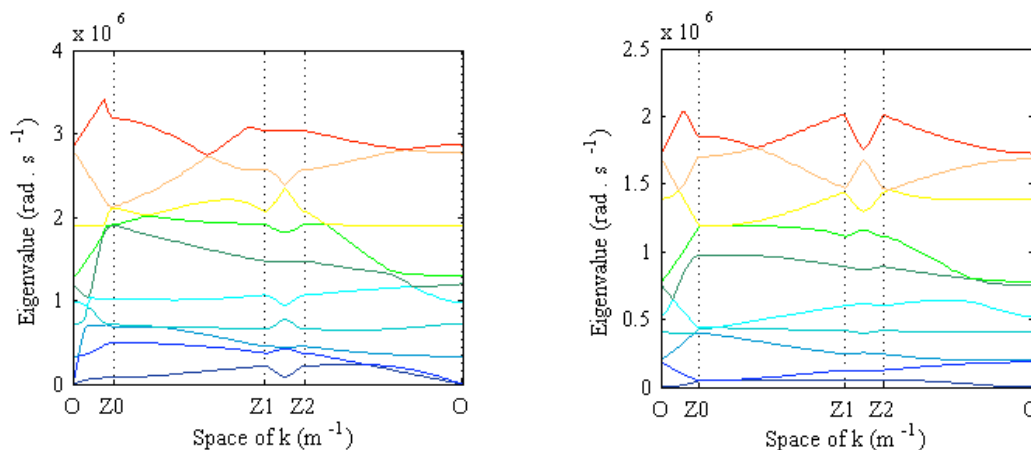
Figure 3.22 Internal angle

Table 3.9 Internal angle,  $\theta$

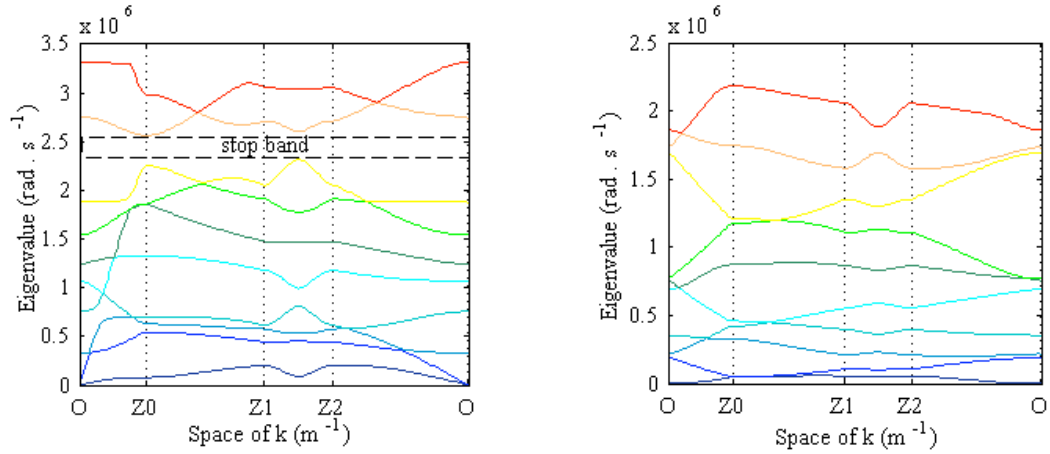
$\theta$	15°	30°	45°	60° (Reference)	75°	90°
$H_0$ (mm)	0.2					
$H_1$ (mm)	0.2					
$E$ (GPa)	70					

We find that the dispersion curves of the six  $\theta$  cases vary from each other but stay in the frequency range nearly of the same order of magnitude. In the cases with  $\theta = 30^\circ, 45^\circ, 60^\circ$  and  $75^\circ$ , the first stop band of the in-plane waves can be observed in the considered eigenvalue range. More precisely, when  $\theta = 30^\circ$  and  $45^\circ$ , the first stop band appears between the 8<sup>th</sup> and 9<sup>th</sup> eigenvalue while it appears between the 6<sup>th</sup> and 7<sup>th</sup> eigenvalue when  $\theta = 60^\circ$  and  $75^\circ$ . No stop band is obtained for the out-of-plane waves in the considered frequency range (Figure 3.23).

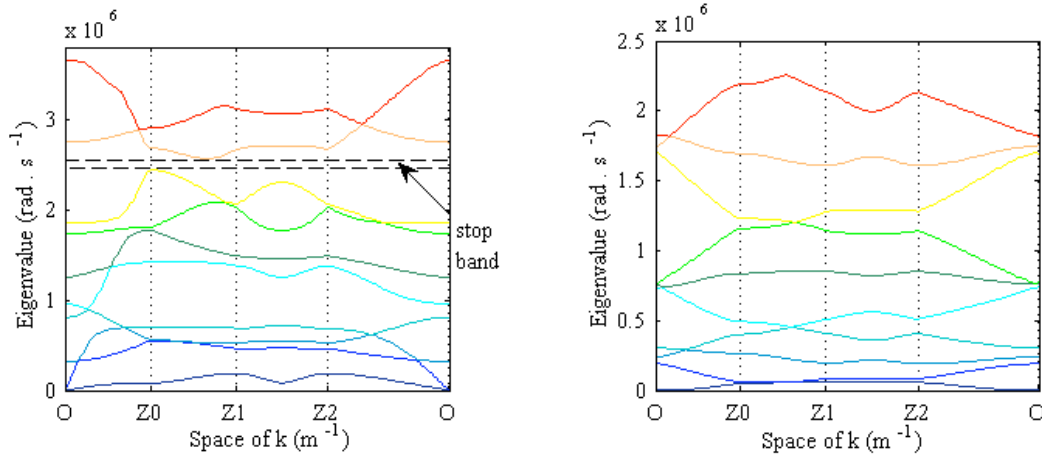
Comparing our results with the work of Gonella, we find that in the case of  $60^\circ$ , the similar dispersion curves have also been obtained by Gonella with the first stop of the in-plane waves takes place between 6<sup>th</sup> and 7<sup>th</sup> eigenvalue. Besides, in their research work, when  $\theta$  changes to  $80^\circ$  and  $100^\circ$ , no stop band can be observed neither.



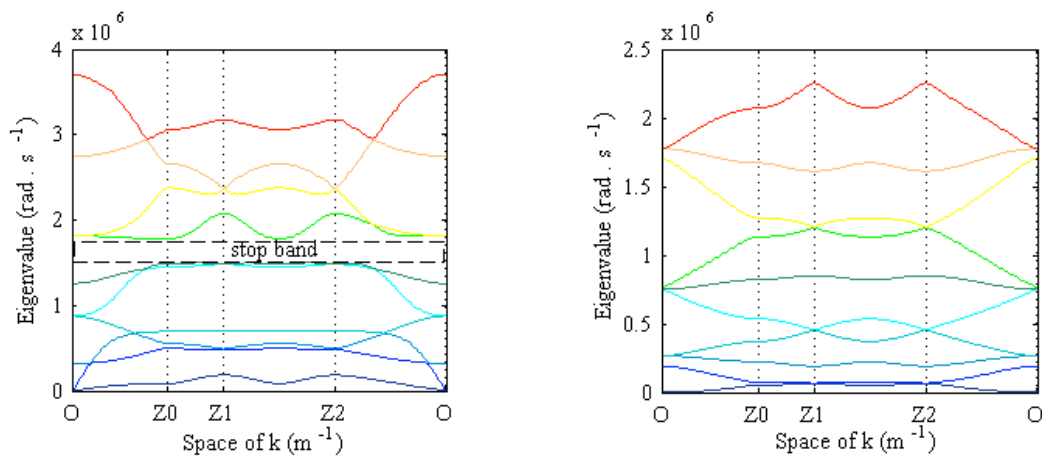
(a) (left) Dispersion curves of in-plane waves; (right) Dispersion curves of out-of-plane waves,  $\theta = 15^\circ$



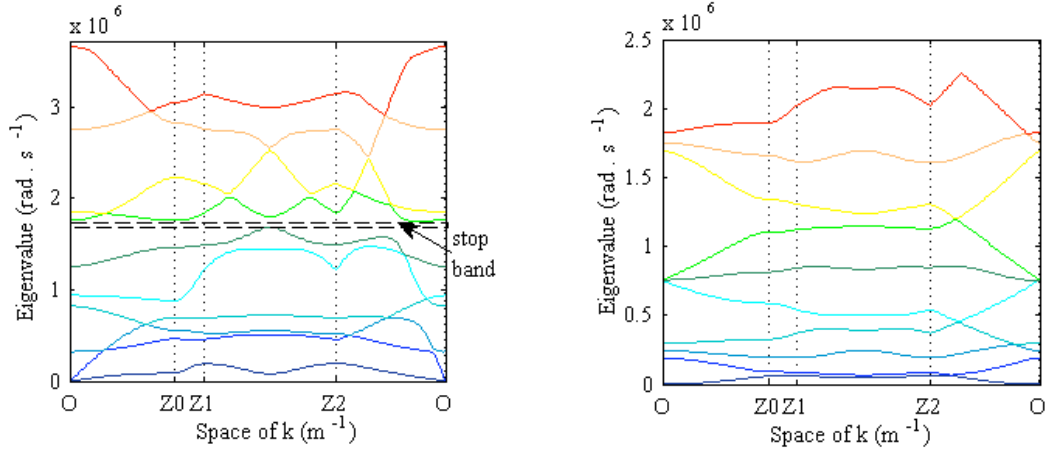
(b) (left) Dispersion curves of in-plane waves; (right) Dispersion curves of out-of-plane waves,  $\theta = 30^\circ$



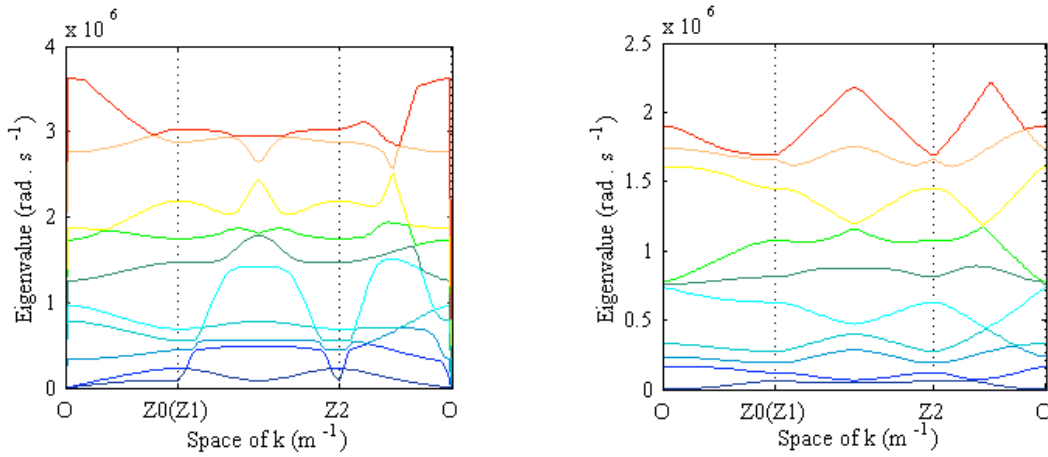
(c) (left) Dispersion curves of in-plane waves; (right) Dispersion curves of out-of-plane waves,  $\theta = 45^\circ$



(d) (left) Dispersion curves of in-plane waves; (right) Dispersion curves of out-of-plane waves,  $\theta = 60^\circ$



(e) (left) Dispersion curves of in-plane waves; (right) Dispersion curves of out-of-plane waves,  $\theta = 75^\circ$



(f) (left) Dispersion curves of in-plane waves; (right) Dispersion curves of out-of-plane waves,  $\theta = 90^\circ$

Figure 3.23 Influence of internal angle on the bandgaps of hexagonal beam network

### 3.2.3 Bloch wave eigenmodes

After having discussed the dispersion relation of the two 2D periodic beam networks in detail, now we look at their Bloch wave eigenmodes.

#### (a) Hexagonal beam network

Six Bloch wave eigenmodes of both the in-plane membrane and out-of-plane bending waves are presented respectively for four angular points, O,  $Z_0$ ,  $Z_1$  and  $Z_2$  on the irreducible zone's contour. The total displacement is displayed in color, where the red color represents the maximal value and the blue color means zero. We notice that on the point O, the first two modes of in-plane waves and the first mode of out-of-plane waves are rigid body modes. Some classical bending and shear modes can be found in low-ordered Bloch modes and other complicated modes are observed in higher order (Figure 3.24, 3.25, 3.26 and 3.27).

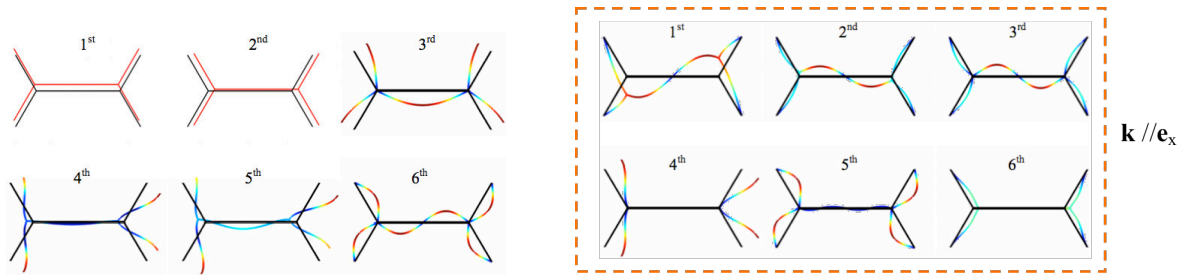


Figure 3.24 (left) Bloch wave eigenmodes of in-plane waves at point O; (right) Bloch wave eigenmodes of in-plane waves at the point  $Z_0$

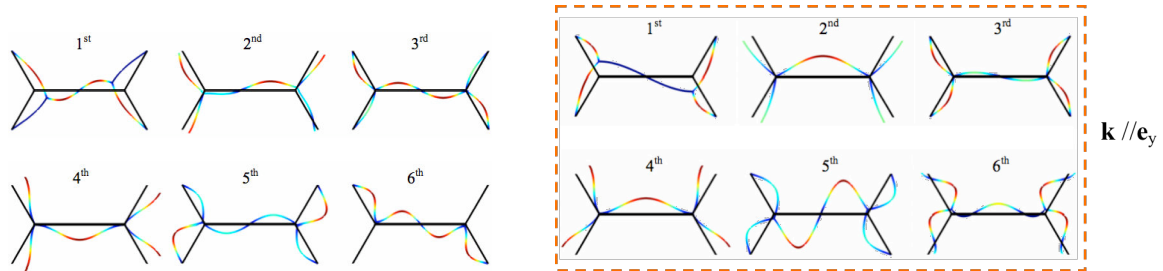


Figure 3.25 (left) Bloch wave eigenmodes of in-plane waves at point  $Z_1$ ; (right) Bloch wave eigenmodes of in-plane waves at point  $Z_2$

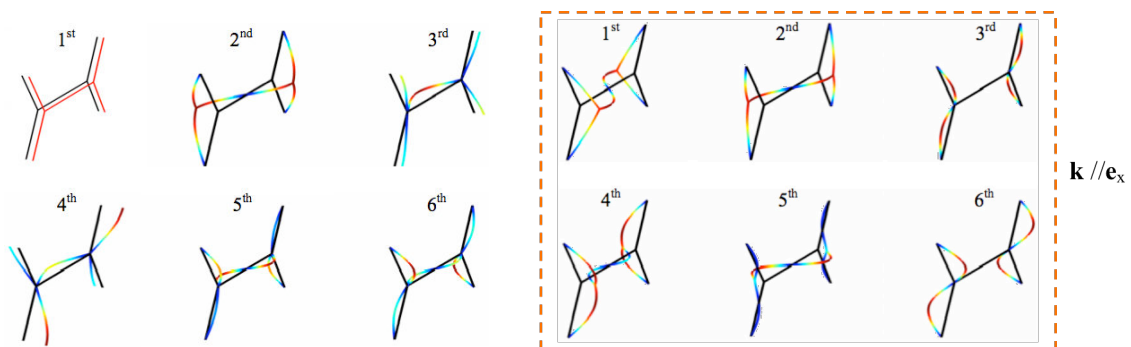


Figure 3.26 (left) Bloch wave eigenmodes of out-of-plane waves at point O; (right) Bloch wave eigenmodes of out-of-plane waves at point  $Z_0$

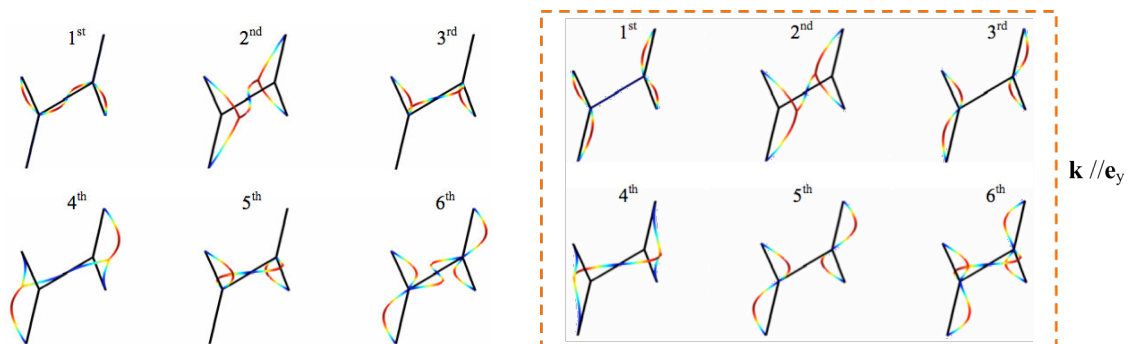


Figure 3.27 (left) Bloch wave eigenmodes of out-of-plane waves at point  $Z_1$ ; (right) Bloch wave eigenmodes of out-of-plane waves at point  $Z_2$

**(b) Rectangular beam network**

Similar to the hexagonal network, six Bloch wave eigenmodes of the in-plane membrane waves and the out-of-plane bending waves are presented respectively for four angular points, O,  $Z_0$ ,  $Z_1$  and  $Z_2$  on the irreducible zone's contour. The total displacement is shown in color, where the red color represents the maximal value and the blue color means zero. As expected, on point O, two rigid body modes are observed for the in-plane waves and one for the out-of-plane waves. The Bloch wave eigenmodes at the point  $Z_0$  are symmetric with the ones at the point  $Z_2$  (Figure 3.28, 3.29, 3.30 and 3.31).

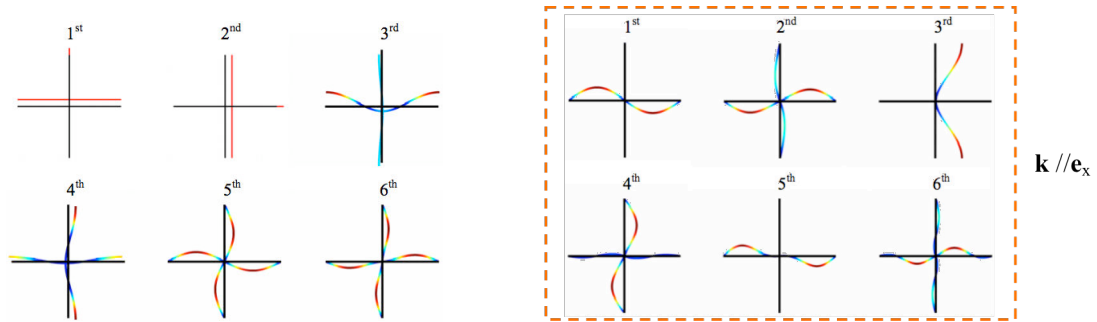


Figure 3.28 (left) Bloch wave eigenmodes of in-plane waves at point O; (right) Bloch wave eigenmodes of in-plane waves at point  $Z_0$

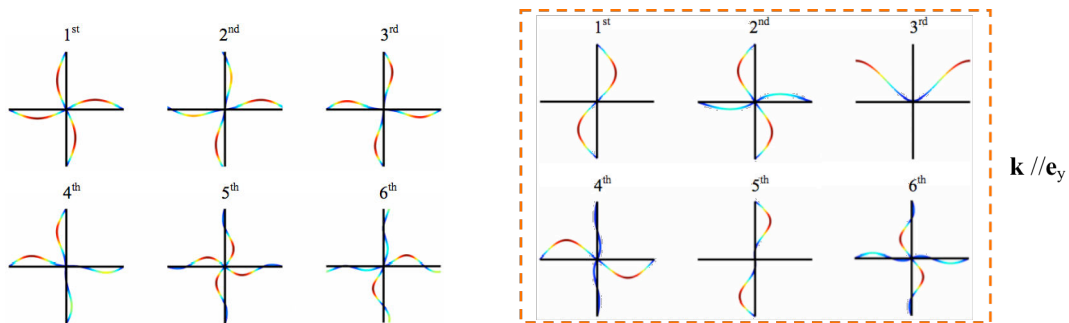


Figure 3.29 (left) Bloch wave eigenmodes of in-plane waves at point  $Z_1$ ; (right) Bloch wave eigenmodes of in-plane waves at point  $Z_2$

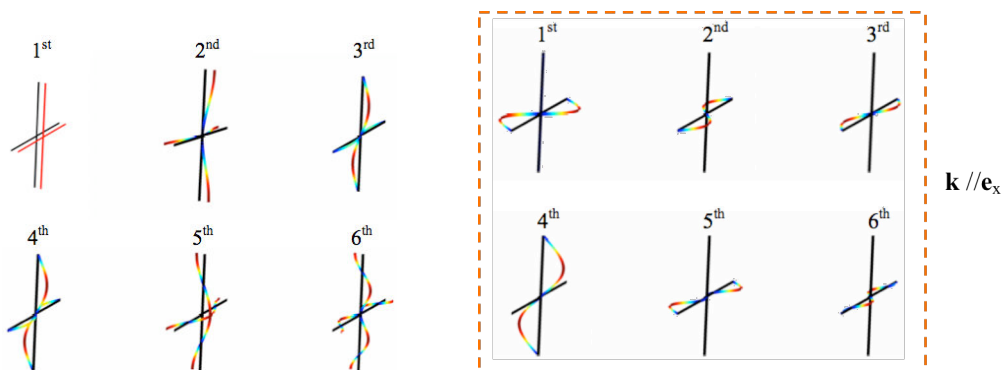


Figure 3.30 (left) Bloch wave eigenmodes of out-of-plane waves at point O; (right) Bloch wave eigenmodes of out-of-plane waves at point  $Z_0$

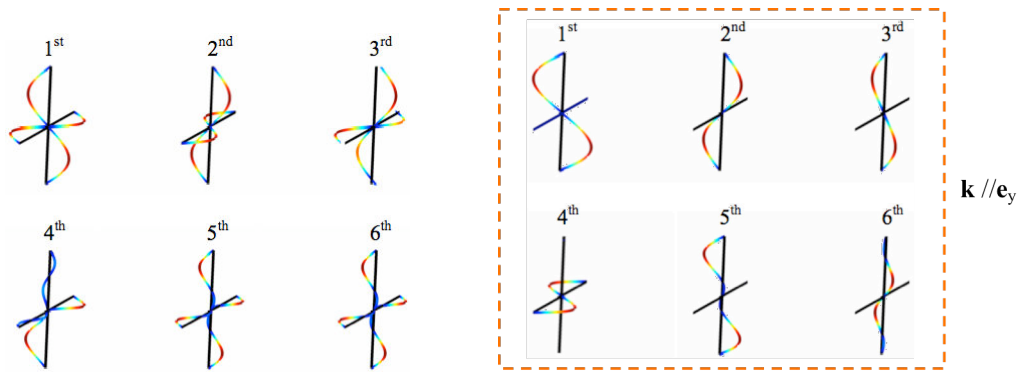


Figure 3.31 (left) Bloch wave eigenmodes of out-of-plane waves at point  $Z_1$ ; (right) Bloch wave eigenmodes of out-of-plane waves at point  $Z_2$

### 3.3 Wave propagation velocities analysis in hexagonal beam network

Using the dispersion surfaces, the phase velocity and the group velocity of each Bloch wave mode can be evaluated and allow considering the anisotropic behavior and the dispersive characteristics of the periodic network [Gonella (2008); Spadoni (2009); Tie (2012)]. More particularly, it is interesting to consider the first two eigenmodes of in-plane waves that emanate from the origin  $O$ , as they can be considered respectively as the membrane shear wave mode (S-mode) and the membrane pressure wave mode (P-mode) [Srikantha Phani (2006)]. Indeed, these modes should coincide, at least in sufficiently LF range, when the wavelength is sufficiently large compared to the primitive cell size, with the classical S and P wave modes of the equivalent homogenous solid. In 2D dispersion curves, the tangent to the first two branches of the curves at any point gives the group velocity of S-mode and P-mode, while the slope of the point on two branches to the origin gives their phase velocities. Therefore, in this section, the dispersion surfaces of the 1<sup>st</sup> and 2<sup>nd</sup> in-plane membrane modes and the 1<sup>st</sup> out-of-plane bending wave mode of the hexagonal network are used to calculate numerically their phase and group velocities, which allow characterizing the periodic network with respect to the wave propagation.

#### 3.3.1 Membrane S-mode and P-mode

First of all, let us consider the S-mode propagation in the hexagonal network, which corresponds to the first dispersion surface of the in-plane Bloch waves modes (Figure 3.32, see also Figure 3.9).

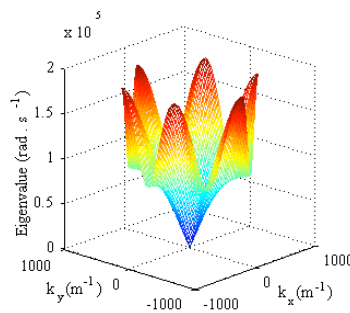


Figure 3.32 Dispersion surface of the 1<sup>st</sup> in-plane Bloch wave mode (S-mode)

We remark firstly that, as expected, in LF range, such as 3.2 kHz, even up to 6 kHz, when the involved wavelength is about ten times the primitive cell size, the network dynamics is more isotropic since the phase and group velocities are approximately independent on directions. The anisotropic characteristics of the network become more pronounced for the two velocities as the frequency increases. Otherwise we notice that the network shows dispersive characteristics varying in the space and remains non-dispersive in precisely six directions corresponding to the hexagonal symmetry of the network. Furthermore, according to the group velocity that in fact represents the wave fronts, it is found that the S-mode has very complex wave fronts in HF range. The velocity caustics phenomena appear for the two modes with the increase of frequency, which has also been observed in anisotropic media [Wolfe 1998] (Figure 3.33).

Thirdly, by comparing the wave velocities of the S-mode obtained by the 1<sup>st</sup> dispersion surface with the theoretical results of an equivalent homogenized orthotropic plate, we find that, in LF range, the wave velocities of the network and the one of the orthotropic plate are in the same order of magnitude, but the orthotropic plate cannot represent the dispersive characteristics of the S-mode of the network. In addition, we find that the S-mode of the orthotropic plate displays anisotropic in horizontal and vertical direction, while the S-mode of the network becomes more and more anisotropic, with the increase of frequency, in the six directions corresponding to the hexagonal symmetry (Figure 3.33).

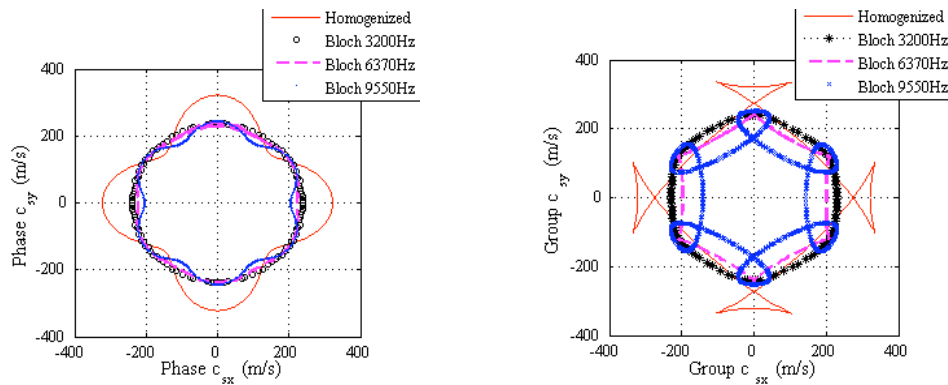


Figure 3.33 Comparison of the wave velocity of the membrane S wave mode between the hexagonal network and its equivalent homogenized plate (left) Phase velocity  $\omega/|\mathbf{k}|$ ; (right) Group velocity  $D_{\mathbf{k}}\omega$

Secondly, let us consider the P-mode propagation in the network. It corresponds to the second dispersion surface of the in-plane Bloch waves modes (Figure 3.34, see also Figure 3.9).

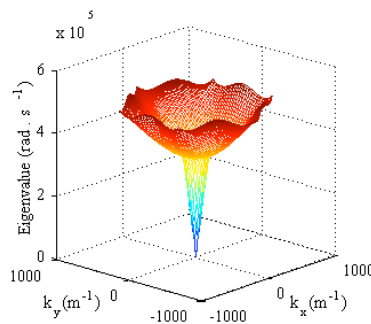


Figure 3.34 Dispersion surface of the 2<sup>nd</sup> in-plane Bloch wave mode (P-mode)

Similar conclusions can also be got for the P-mode propagation in the network. The network

dynamics performed isotropic in LF range, while more anisotropic in high frequency (HF) range. For example at 11 kHz, when the involved wavelength is about 40 times the primitive cell size, the P-mode wave velocities are approximately independent on direction, while at 62 kHz, whose involved wavelength decreases to 3 times the primitive cell size, the P-mode wave velocities shows anisotropy on the six directions corresponding to the hexagonal symmetry. Besides, compared to the S-mode, the P-mode of the network shows much stronger dispersive characteristics, where an enormous velocity caustics phenomenon occurs when the frequency increases (Figure 3.35).

The same, we also compared the wave velocities of the P-mode of the network with the theoretical results of the equivalent homogenized orthotropic plate. As expected, in LF range, the homogenized plate could represent the P-mode of the network as the wave velocities obtained by two models are in the same order of magnitude, but failed when the frequency increases (Figure 3.35).

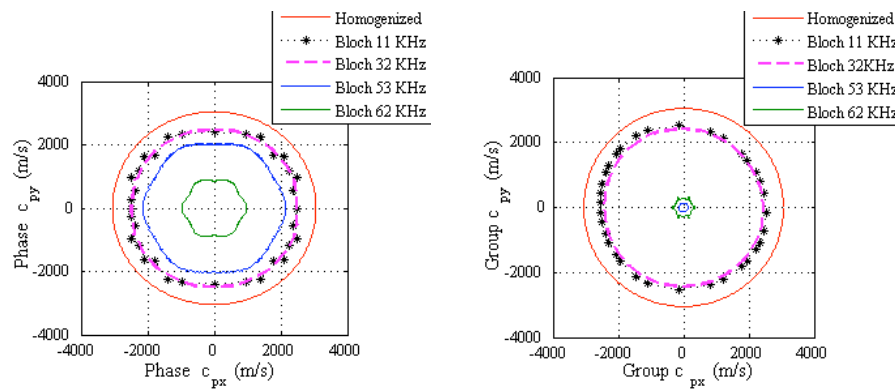


Figure 3.35 Comparison of the wave velocity of the membrane P wave mode between the hexagonal network and its equivalent homogenized plate (left) Phase velocity  $\omega/|\mathbf{k}|$ ; (right) Group velocity  $D_{\mathbf{k}}\omega$

### 3.3.2 Bending mode

Now we consider the 1<sup>st</sup> and 2<sup>nd</sup> dispersion surface of out-of-plane waves (Figure 3.36). We believe that the out-of-plane wave modes should coincide with the bending wave mode of the equivalent homogenized orthotropic plate.

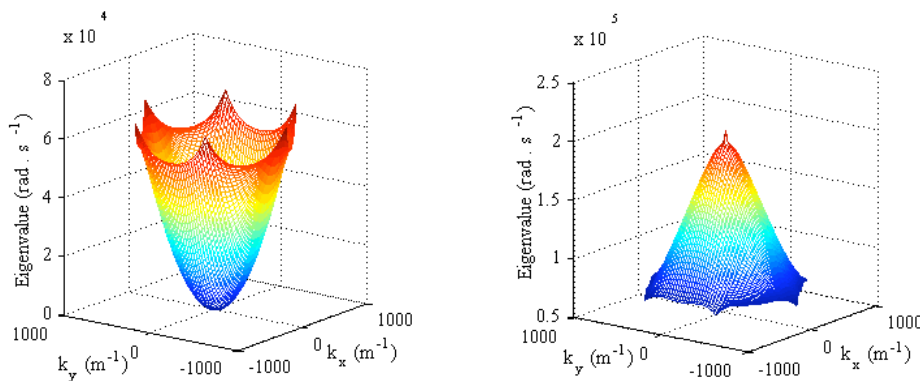


Figure 3.36 (left) Dispersion surface of 1<sup>st</sup> out-of-plane Bloch wave mode; (right) Dispersion surface of 2<sup>nd</sup> out-of-plane Bloch wave mode

Therefore in LF range, where the 1<sup>st</sup> out-of-plane mode is taken into account, generally, the bending mode of the network gives isotropic nature and can be correctly represented by the homogenized plate, but it has a more and more complex wave front with the increase of frequency (Figure 3.37, 3.38 and 3.39).

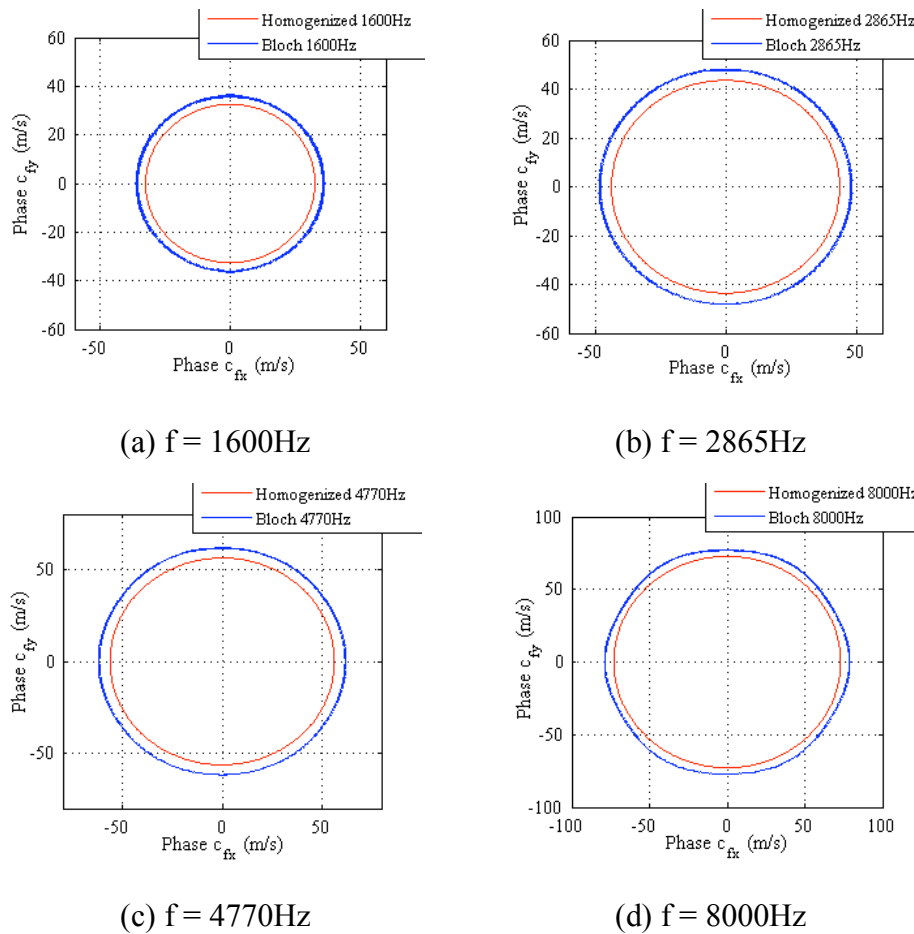


Figure 3.37 Comparison of the phase velocity  $\omega/|\mathbf{k}|$  of the 1<sup>st</sup> out-of-plane bending wave mode of the periodic network and the bending mode of the equivalent homogenized plate

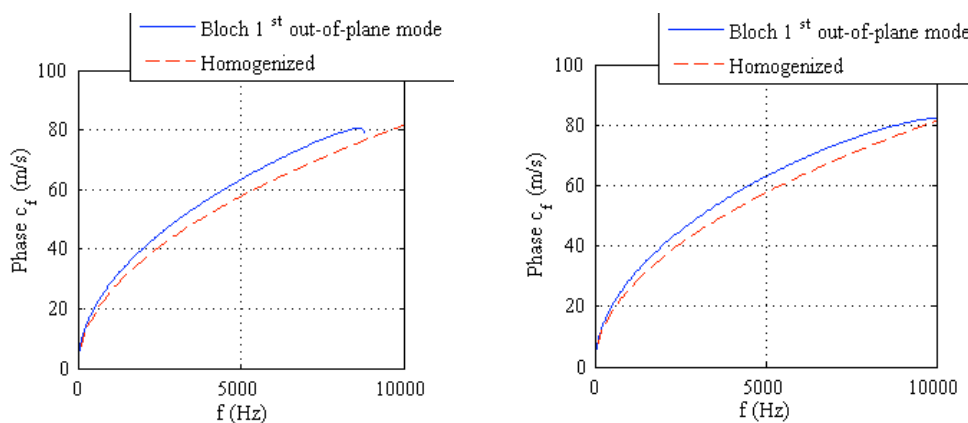


Figure 3.38 Comparison of the phase velocity  $\omega/|\mathbf{k}|$  of the 1<sup>st</sup> out-of-plane bending wave mode of the periodic network and the bending mode of the equivalent homogenized plate (left) Along the axis  $e_x$ ; (right) Along the axis  $e_y$

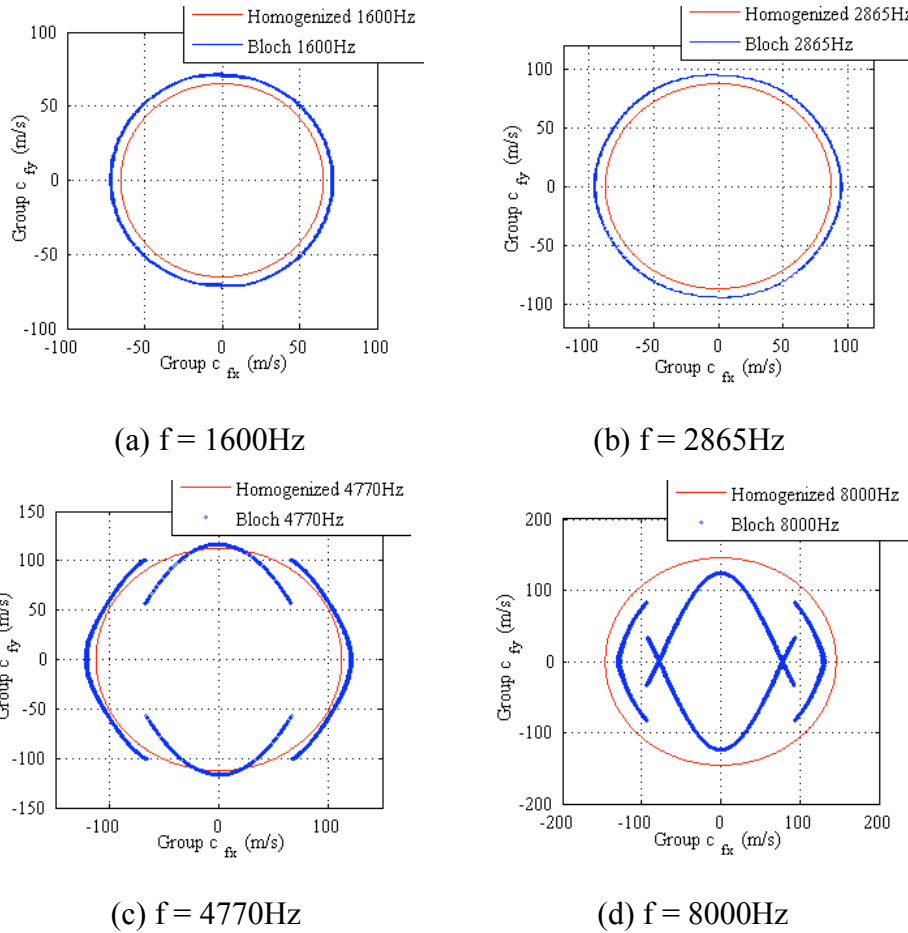
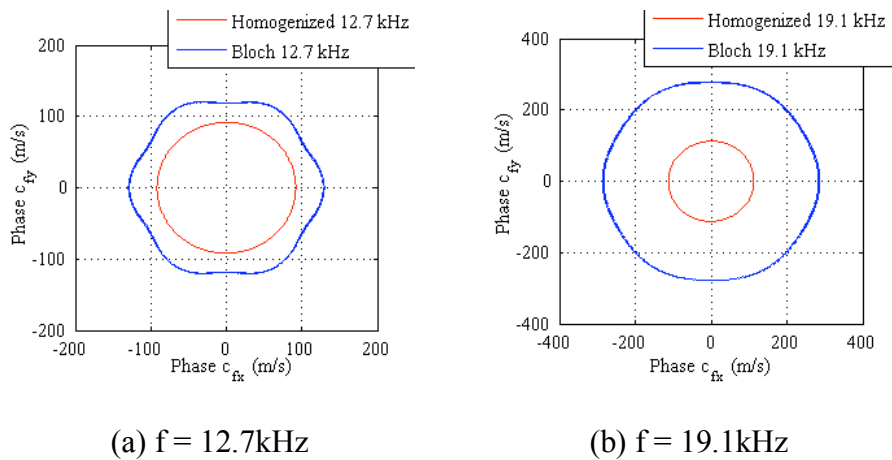
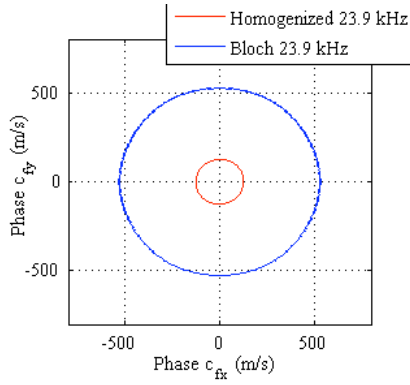


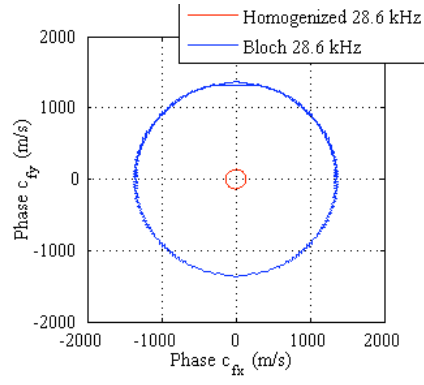
Figure 3.39 Comparison of the group velocity  $D_{\mathbf{k}}\omega$  of the 1<sup>st</sup> out-of-plane bending wave mode of the periodic network and the bending mode of the equivalent homogenized plate

Then in HF range, where the 2<sup>nd</sup> out-of-plane wave mode is taken into account, we notice that the homogenized orthotropic plate cannot give correct simulation result. The 2<sup>nd</sup> out-of-plane wave mode of the network does not show strong anisotropic characteristics but is dispersed much faster than the bending wave in the homogenized plate. Besides, the velocity caustics phenomena occur to the group velocity when the frequency goes up (Figure 3.40, 3.41 and 42).





(c)  $f = 23.9\text{kHz}$



(d)  $f = 28.6\text{kHz}$

Figure 3.40 Comparison of the phase velocity  $\omega/|\mathbf{k}|$  of the 2<sup>nd</sup> out-of-plane bending wave mode of the periodic network and the bending mode of the equivalent homogenized plate

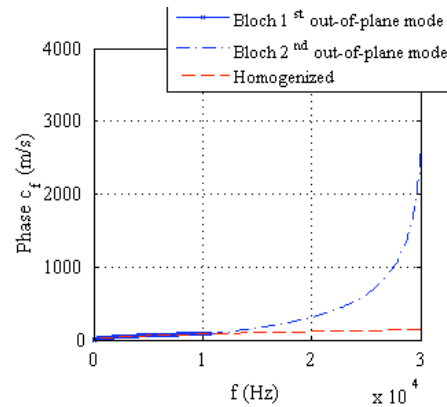
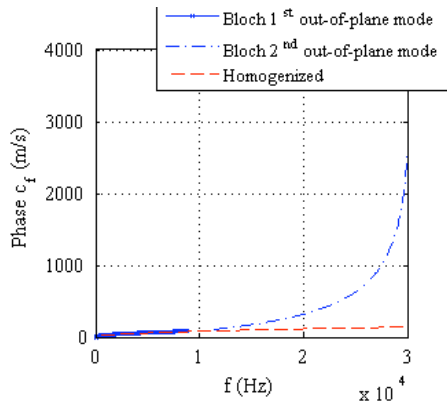
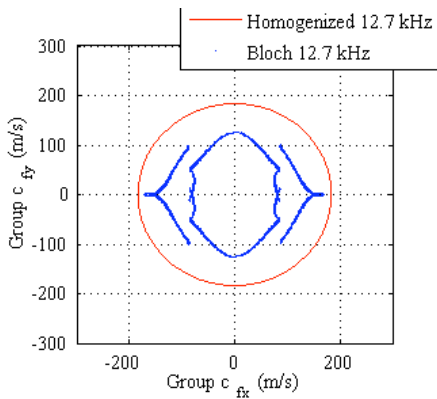
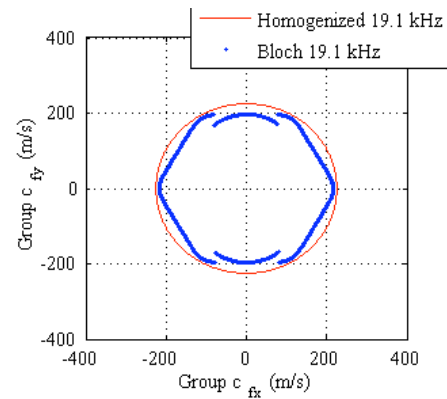


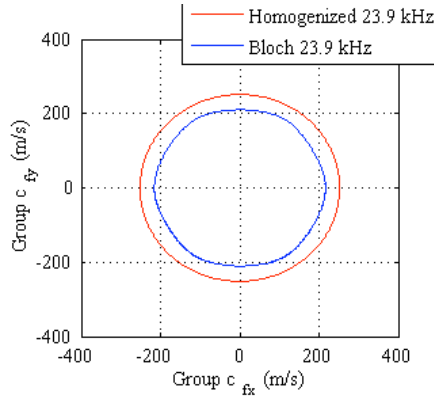
Figure 3.41 Comparison of the phase velocity  $\omega/|\mathbf{k}|$  of the 2<sup>nd</sup> out-of-plane bending wave mode of the periodic network and the bending mode of the equivalent homogenized plate (left) Along the axis  $\mathbf{e}_x$ ; (right) Along the axis  $\mathbf{e}_y$



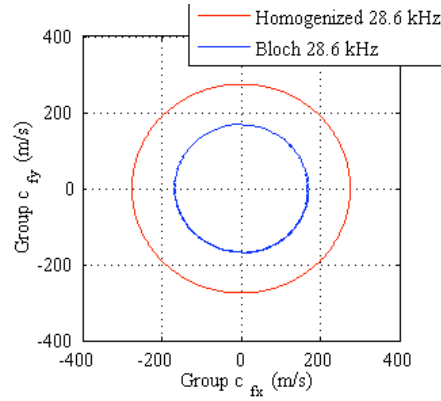
(a)  $f = 12.7\text{kHz}$



(b)  $f = 19.1\text{kHz}$



(c)  $f = 23.9\text{kHz}$



(d)  $f = 28.6\text{kHz}$

Figure 3.42 Comparison of the group velocity  $D_{\mathbf{k}}\omega$  of the 2<sup>nd</sup> out-of-plane bending wave mode of the periodic network and the bending mode of the equivalent homogenized plate

Besides, for the 2<sup>nd</sup> bending mode, we also notice that, the group velocity is negative, which means that group velocity vector is always in the inverse direction of the wave vector  $\mathbf{k}$  (Figure 3.43). In other words, the wave front of this mode propagates backward.

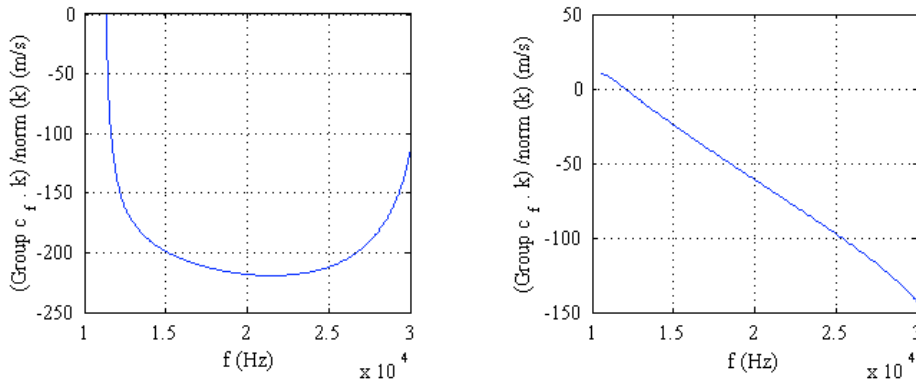


Figure 3.43 Projection of group velocity of the 2<sup>nd</sup> out-of-plane bending wave mode on the direction of the wave vector  $(D_{\mathbf{k}}\omega \cdot \mathbf{k})/|\mathbf{k}|$  (left) Along the axis  $\mathbf{e}_x$ ; (right) Along the axis  $\mathbf{e}_y$

## Conclusion

In this chapter, the numerical simulation of elastic wave propagation, based on the Bloch wave analysis, has been developed in 1D and 2D periodic beam networks. For the 1D network, the dispersion curves have been obtained for both the longitudinal and the bending and transverse shear waves, where the bandgaps of the bending and transverse shear waves was found in a lower frequency range when compared to the longitudinal wave. In the 1D network, we noticed that the more the mismatch between two beams in the primitive cell is present, the larger and stronger the stop bands are.

Then, for the 2D periodic hexagonal and rectangular beam network, the dispersion curves as well as the dispersion surfaces have been obtained both for in- and out-of-plane waves. The first stop band of in-plane waves of the hexagonal network was observed at about  $3 \times 10^5 \text{Hz}$  and the one of out-of-plane waves at about  $3 \times 10^6 \text{Hz}$ , while no frequency bandgaps obtained for the rectangular network. Furthermore, we remarked that the thickness mismatch in the primitive cell of the hexagonal network leads to the disappearance of the first stop band of in-

plane waves. In addition, in-plane waves' stop bands could also be got under different internal angle cases,  $30^\circ$ ,  $45^\circ$ ,  $60^\circ$  and  $75^\circ$ .

In the end, by the wave velocities analysis of the periodic hexagonal beam network, it has been pointed out that the hexagonal beam network provides more and more anisotropic and dispersive characteristics when the frequency moves to a higher range. The homogenized model represented correctly the membrane L-mode and the bending wave mode of the network in LF range but failed in HF range. The wave front of the 2<sup>nd</sup> bending wave mode of the network retro-propagates.

# Wave propagation in honeycomb core sandwich plate

*In this chapter, our numerical approach is applied to the honeycomb thin layer and the honeycomb core sandwich plate. The effect of the strong junction condition on the numerical simulation results is considered first by comparing a beam-sized honeycomb thin layer with the 2D hexagonal beam network. Then the dispersion relation and the corresponding Bloch wave transform eigenmodes are obtained for the thin layer as well as for the sandwich plate. In parallel, the influence of the double-thickness horizontal plate and the internal angle between the horizontal plate and the oblique plates on the dispersion relation for the thin layer is discussed. In the end, the wave propagation velocities are calculated for several main wave modes and compared with the homogenized model in order to analyze the anisotropic and dispersive nature of the honeycomb core sandwich.*

### Summary

---

<b>4.1 Dispersion relation and Bloch wave eigenmodes</b> .....	<b>74</b>
4.1.1 Discussion on the modeling of the junction conditions in the primitive cell.....	74
4.1.2 Dispersion relation.....	75
4.1.3 Influence of structural and geometric characteristics on the dispersion relation.....	77
4.1.4 Bloch wave eigenmodes.....	79
<b>4.2 Wave propagation velocities analysis</b> .....	<b>81</b>
4.2.1 Membrane S-mode and bending modes of honeycomb thin layer.....	81
4.2.2 1 <sup>st</sup> Bloch wave mode of the honeycomb core sandwich plate.....	84
<b>Conclusion</b> .....	<b>86</b>

---

## 4.1 Dispersion relation and Bloch wave eigenmodes

The final purpose arises to apply our numerical approach to analyze elastic wave propagation in the honeycomb thin layer and the sandwich plate. In the literature, there are many research results concerning the periodic beam networks, but relatively little about the periodic plate networks, as the honeycomb thin layer. Nevertheless, we can mention the research work has done for the auxetic tetrachiral honeycombs by Tee et al. in 2010 in order to obtain the dispersion curves and surfaces of the network [Tee (2010)]. Hence, in our present work, it is expected to gain a more precise understanding of the wave behaviors in the hexagonal cell type honeycomb sandwich, especially the interactions between periodic cells and waves. Otherwise, our numerical results based on the Bloch wave analysis are compared with equivalent homogenized models to check whether the homogenized models can represent the dynamic behavior of the honeycomb thin layer and the sandwich plate.

### 4.1.1 Discussion on the modeling of the junction conditions in the primitive cell

We have pointed out in chapter 2 that the condition  $\theta_n = 0$  implies a less flexible junction condition as only the rotation perpendicular to the plane Oxy on the two interface edges,  $\sum_{IW}$  and  $\sum_{IE}$ , is non-zero. Consequently, it is interesting to consider first the influence brought by the condition  $\theta_n = 0$  on the numerical simulation of honeycomb thin layer. Hence, a honeycomb thin layer model, Plate-Hex, with the same geometric and mechanical characteristics as the 2D hexagonal beam network model (Table 4.1) is designed. The Plate-Hex model is used to compare with two 2D hexagonal beam network models, Beam-Hex ( $\theta_n = 0$ ) and Beam-Hex, which respectively means:  $\theta_n = 0$  and  $\theta_n \neq 0$  of the 2D network. For the Plate-Hex model, it is impossible to uncouple the in-plane and out-of-plane waves, thus for the Beam-Hex models, coupled in-plane and out-of-plane waves are considered here as well.

Table 4.1 Geometric and mechanical characteristics of the primitive cell of Plate-Hex and Beam-Hex

	Plate-Hex (Horizontal plate)	Beam-Hex (Horizontal beam)
Young's modulus E (GPa)	70	70
Poisson's ratio $\nu$	0.33	0.33
Density $\rho$ (kg.m <sup>-3</sup> )	2700	2700
Plate/Beam size	3mm×0.12mm	3mm×0.12mm
Thickness H (mm)	0.02	0.02

The first three dispersion curves for the three models have been compared in detail. We remark that for the 1<sup>st</sup> dispersion curve, the model Plate-Hex presents large overlaps with the Beam-Hex ( $\theta_n = 0$ ) as well as the Beam-Hex. Slight differences appear on the point  $Z_1$ ,  $Z_2$  and the points close to the origin. Also, the junction condition does not bring much difference to

the dispersion relation between the two Beam-Hex models (Figure 4.1).

Then looking at the 2<sup>nd</sup> and 3<sup>rd</sup> mode, we notice that, the dispersion curves of Plate-Hex agree in principle with the ones of Beam-Hex ( $\theta_n = 0$ ) along  $Z_0 \rightarrow Z_2$  but not for the  $\mathbf{k}$  around the origin. It is highlighted in the 3<sup>rd</sup> mode that the Plate-Hex shows more similarities with the Beam-Hex in the very beginning of the curve and then is close with the Beam-Hex ( $\theta_n = 0$ ) after a sharp turn. In parallel, the junction condition affects the dispersion curves of the two beam models, where the discretized  $\mathbf{k}$  of Beam-Hex ( $\theta_n = 0$ ) model along  $O \rightarrow Z_0$  and along  $Z_1 \rightarrow Z_2$  gives a higher eigenvalue (Figure 4.1).

The same conclusion can also be obtained by observing the corresponding Bloch eigenmodes. For instance, concerning the 2<sup>nd</sup> mode of the three hexagonal models at point  $Z_0$ , we find the corresponding Bloch eigenmode of Plate-Hex can be identified by the one of Beam-Hex ( $\theta_n = 0$ ) but differs from the one of Beam-Hex (Figure 4.2).

As expected, the dispersion characteristics of the honeycomb thin layer model are very similar with the hexagonal beam network with the condition ( $\theta_n = 0$ ). However, it is also confirmed that the strong junction condition caused by this condition results in higher eigenvalues that affects probably the dispersion relation and also the corresponding Bloch eigenmodes.

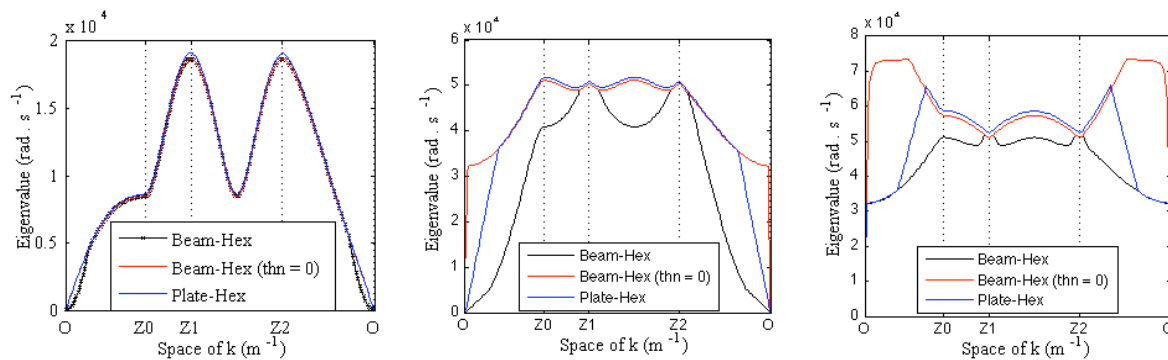


Figure 4.1 Comparison of the dispersion curves between three models: Plate-Hex, Beam-Hex ( $\theta_n = 0$ ) and Beam-Hex (left) 1<sup>st</sup> mode; (middle) 2<sup>nd</sup> mode; (right) 3<sup>rd</sup> mode

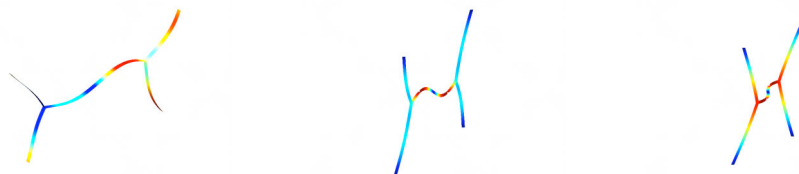


Figure 4.2 2<sup>nd</sup> Bloch wave transform eigenmode for the  $\mathbf{k}$  on the point  $Z_0$  (left) Plate-Hex; (middle) Beam-Hex ( $\theta_n = 0$ ); (right) Beam-Hex

### 4.1.2 Dispersion relation

The geometric and mechanical characteristics of the primitive cells of the honeycomb thin layer and of the skins of sandwich plate are shown in Table 4.2.

Table 4.2 Geometric and mechanical characteristics of the primitive cell of honeycomb thin layer and the skins of sandwich plate

	E (GPa)	$\nu$	$\rho$ (kg.m <sup>-3</sup> )	Plate size	H (mm)
Honeycomb thin layer (Horizontal plate)	70	0.33	2700	3mm×12mm	0.018
Skins	130	0.34	1666.7	5.2mm×5.2mm	1

The 3D dispersion surface and 2D dispersion curve of the honeycomb thin layer and of the sandwich plate are obtained, among which the first ten eigenvalues for coupled in-plan membrane and out-of-plane bending modes is given. Frequency bandgaps are observed neither for the honeycomb thin layer nor for the sandwich plate in the considered frequency range. Besides, we notice that the eigenvalues of the sandwich plate move towards to a higher frequency range when compared to the honeycomb thin layer. Finally, we remark that, as in the case of beam networks, the group velocities become negative in some spatial directions for some modes: from the 6<sup>th</sup> mode in the honeycomb thin layer on the one hand, and from the 4<sup>th</sup> mode in the sandwich plate (Figure 4.3 and 4.4)

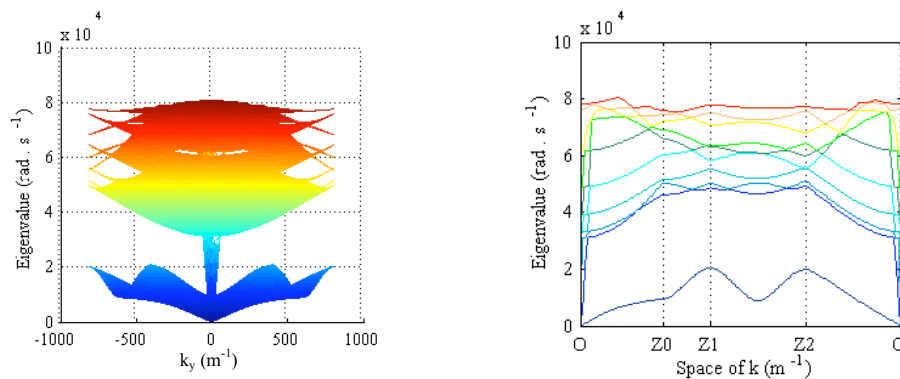


Figure 4.3 Dispersion relation of the honeycomb thin layer (left) 3D dispersion surface; (right) 2D dispersion curve

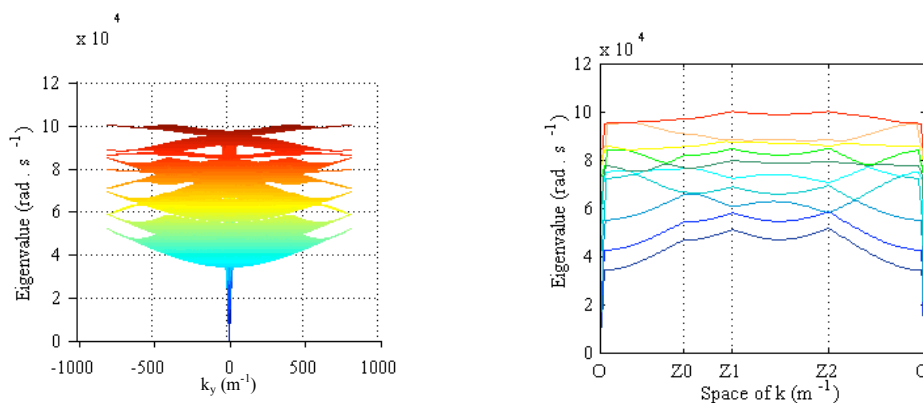


Figure 4.4 Dispersion relation of the honeycomb sandwich plate (left) 3D dispersion surface; (right) 2D dispersion curve

### 4.1.3 Influence of structural and geometric characteristics on dispersion relation

In this section, the parametric study of the mismatch of the thickness and of the internal angle  $\theta$  between the horizontal plate and the oblique plates of the honeycomb thin layer is performed to study their influence on the dispersion relation of the honeycomb thin layer.

#### (a) Influence of double-thickness of horizontal plate

Similar to the 2D hexagonal beam network, the horizontal plate  $P_{CEN}$  of the primitive cell of the honeycomb thin layer normally is a double-thickness plate, with thickness  $H_1$  equal to twice the one of the other four plates  $H_0$  (Figure 4.5). Consequently, two cases,  $H_1 = H_0$  and  $H_1 = 2H_0$ , are considered here for both the honeycomb thin layer and the sandwich plate (Table 4.3).

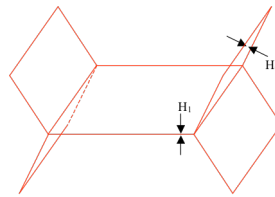


Figure 4.5 Double thickness of the horizontal plate of the honeycomb thin layer

Table 4.3 Thickness,  $H_0$  and  $H_1$

$H_0$ (mm)	$H_1$ (mm)	
0.018	0.018 ( $H_1 = H_0$ )	0.036 ( $H_1 = 2H_0$ )

In the case of the honeycomb thin layer, except the first Bloch eigenmode, the double thickness of the horizontal plate makes the eigenvalues move up to a higher frequency range, also the phase wave velocity (Figure 4.6). It makes sense when we analyze the shape of the Bloch eigenmodes, indeed the first Bloch eigenmode is almost not affected by the variation of the thickness of the horizontal plate as the latter is not mainly involved with bendings (Figure 4.10 and 4.11). Otherwise, in the case of the sandwich plate, all the ten first eigenvalues are influenced by the thickness  $H_1$  of the horizontal plate, they move up to higher frequency range when  $H_1$  increases (Figure 4.7 see also Figure 4.12 and 4.13).

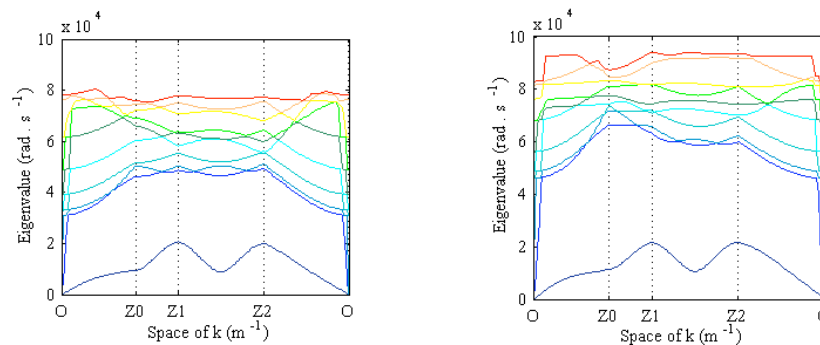


Figure 4.6 Influence of the double thickness of horizontal plate on the dispersion curves of the honeycomb thin layer (left)  $H_1 = H_0$ ; (right)  $H_1 = 2H_0$

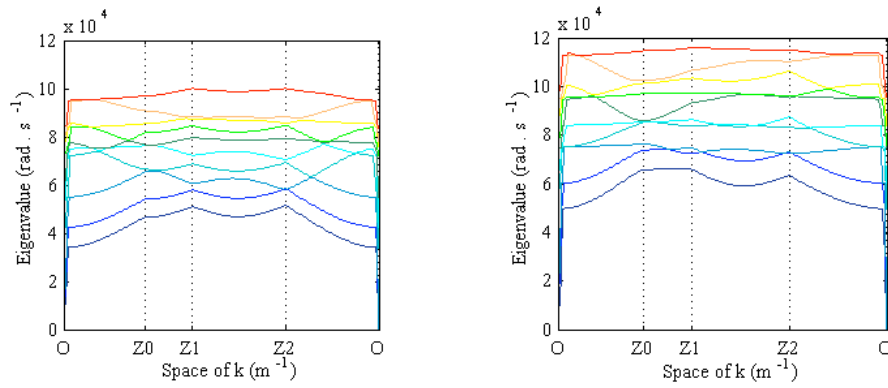


Figure 4.7 Influence of the double thickness of horizontal plate on the dispersion curves of the honeycomb core sandwich plate (left)  $H_1 = H_0$ ; (right)  $H_1 = 2H_0$ ,

**(b) Influence of internal angle on honeycomb thin layer**

Then, we consider the influence of different internal angle  $\theta$  (Figure 4.8), which is swept from  $15^\circ$  to  $90^\circ$  by the step of  $15^\circ$ . Similarly, the  $60^\circ$  is our reference angle (Table 4.4).

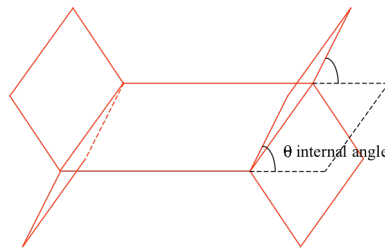
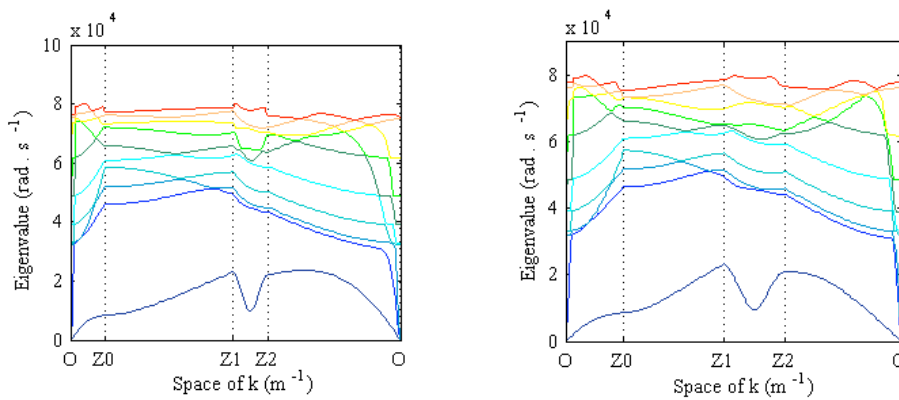


Figure 4.8 Internal angle

Table 4.4 Internal angle,  $\theta$

$\theta$	$15^\circ$	$30^\circ$	$45^\circ$	$60^\circ$ (reference)	$75^\circ$	$90^\circ$
----------	------------	------------	------------	------------------------	------------	------------

We find that the different internal angles do change the dispersion curves of the honeycomb thin layer but do not influence the range of eigenvalue. No stop band is observed for all the six  $\theta$  cases in the considered frequency range (Figure 4.9).



(a)

(b)

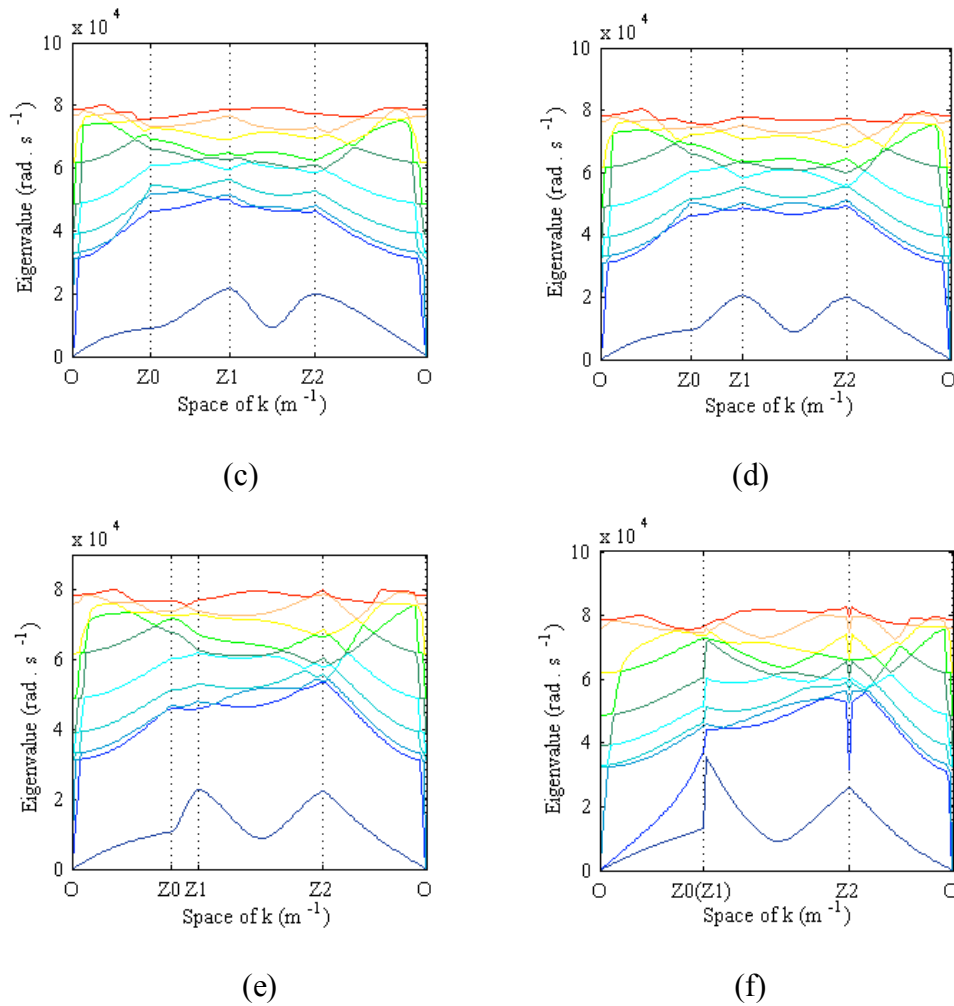


Figure 4.9 Influence of the internal angle on the dispersion curves of honeycomb thin layer (a)  $\theta = 15^\circ$ ; (b)  $\theta = 30^\circ$ ; (c)  $\theta = 45^\circ$ ; (d)  $\theta = 60^\circ$ ; (e)  $\theta = 75^\circ$ ; (f)  $\theta = 90^\circ$

#### 4.1.4 Bloch wave eigenmodes

Six Bloch wave eigenmodes of both the honeycomb thin layer and the sandwich plate are presented respectively for four angular points, O,  $Z_0$ ,  $Z_1$  and  $Z_2$ . The total displacement is displayed in color, where the red color represents the maximal value and the blue color means zero. As expected we firstly notice that on the point O, the first three modes are rigid body modes of the honeycomb thin layer as well as the sandwich plate. Then some classical membrane and bending modes can be found in low-ordered Bloch modes and other complicated modes are observed in higher order. Importantly, we also notice that, for the sandwich plate, due to the large difference between the thickness and the mechanical characteristics of the honeycomb thin layer and the skins, all modes distort mainly the honeycomb thin layer rather than the skins (Figure 4.10, 4.11, 4.12 and 4.13).

**(A) Honeycomb thin layer**

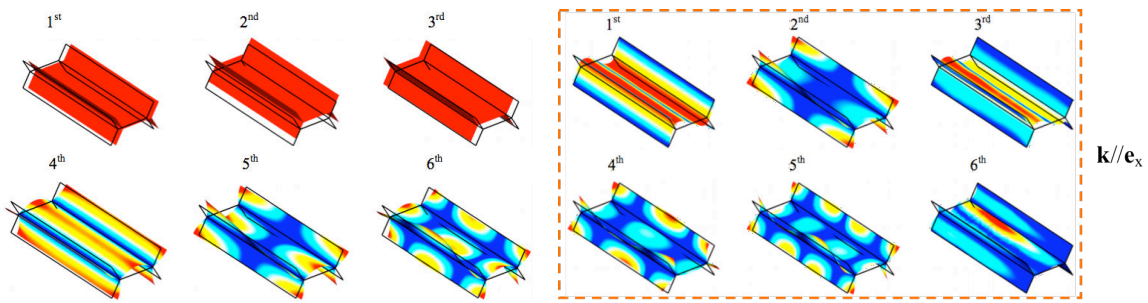


Figure 4.10 Bloch wave eigenmodes of honeycomb thin layer (left) At point O; (right) At point  $Z_0$

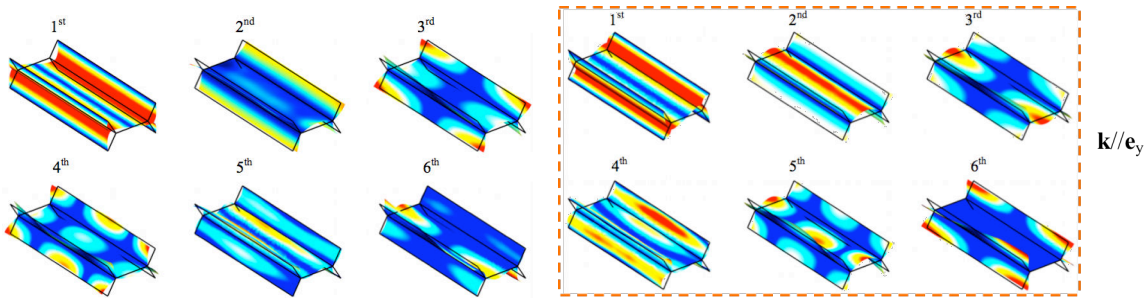


Figure 4.11 Bloch wave eigenmodes of honeycomb thin layer (left) At point  $Z_1$ ; (right) At point  $Z_2$

**(B) Honeycomb core sandwich plates**

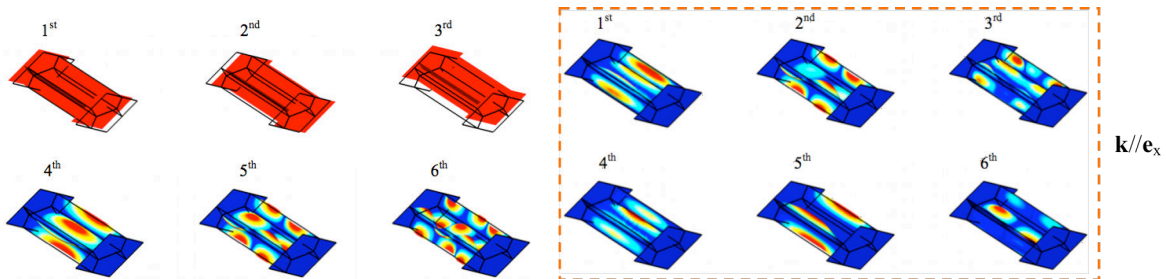


Figure 4.12 Bloch wave eigenmodes of honeycomb core sandwich plate (left) At point O; (right) At point  $Z_0$

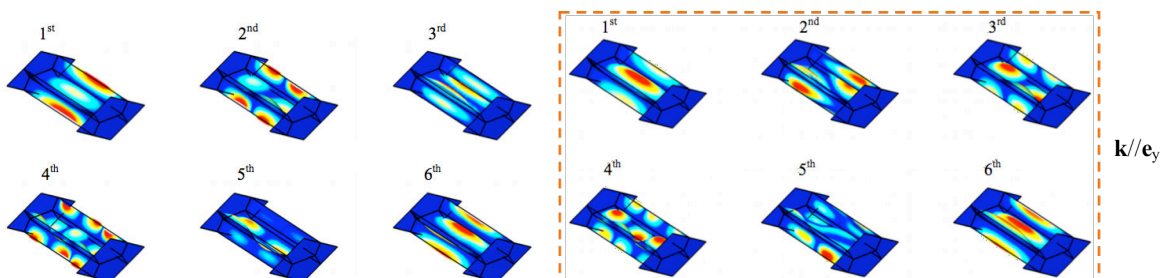


Figure 4.13 Bloch wave eigenmodes of honeycomb core sandwich plate (left) At point  $Z_1$ ; (right) At point  $Z_2$

## 4.2 Wave propagation velocities analysis

Now we look into the phase and group velocities of several main wave modes of the honeycomb thin layer and also of the sandwich plate to analyze the anisotropic and the dispersive characteristics of the networks. The results are compared with the equivalent homogenized models to check whether and in which frequency range the classical homogenized models can represent the dynamic behavior of the honeycomb thin layer and the sandwich plate.

### 4.2.1 Membrane S-mode and bending modes of honeycomb thin layer

Let us first consider the honeycomb thin layer, whose 1<sup>st</sup> Bloch wave mode displays a similarity with the S-mode of the 2D periodic hexagonal beam network. Therefore, it is believed that the 1<sup>st</sup> Bloch wave mode of the honeycomb thin layer should coincide with the membrane shear wave mode (S-mode) of the equivalent homogenized plate (Figure 4.14).

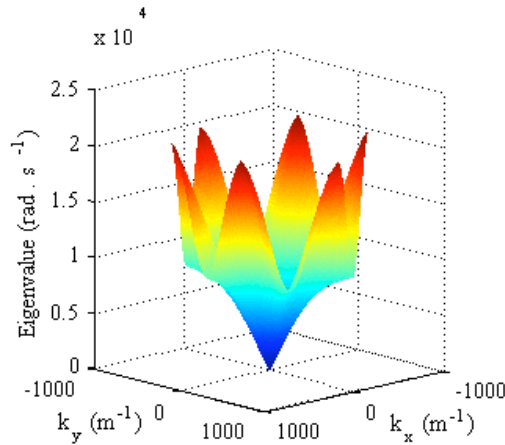


Figure 4.14 Dispersion surface of the 1<sup>st</sup> Bloch wave mode (S-mode) of the honeycomb thin layer

We find that the phase and group velocities of the honeycomb thin layer become more and more anisotropic when the frequency is increased. Complex wave front and group velocity caustics phenomena are observed. Similarly with the 2D beam network, the honeycomb layer shows dispersive characteristics varying in the space except in the six directions corresponding to the hexagonal cellular shape (Figure 4.15).

We compare now the honeycomb thin layer and the equivalent homogenized model. We find that, up to 1100Hz at least, the wave velocities of the two models are not too far, but the S-mode of the homogenized model is not dispersive. Besides, we find that the S-mode of the homogenized model displays anisotropic in  $0^\circ$ ,  $180^\circ$  and  $\pm 90^\circ$ , while the S-mode of the honeycomb thin layer displays more and more anisotropic only in the six directions corresponding to the hexagonal symmetry (Figure 4.15).

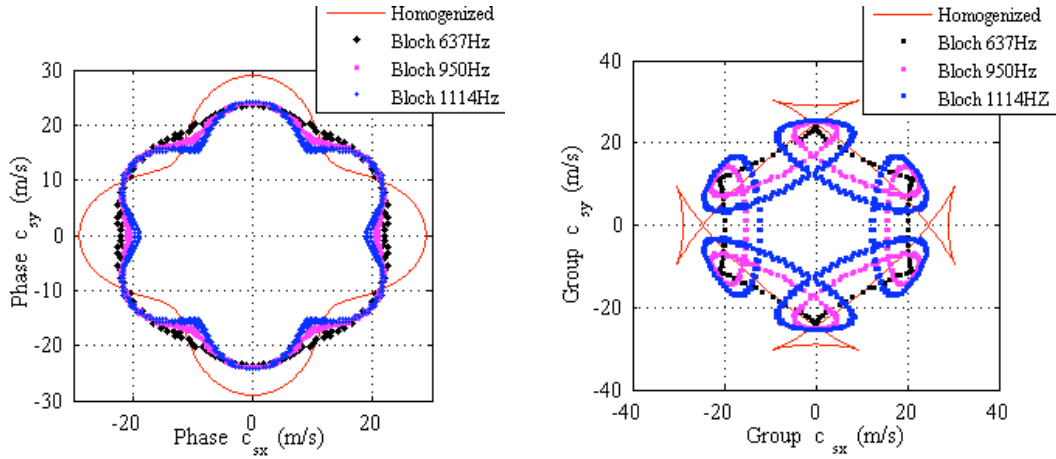


Figure 4.15 Comparison of the wave velocity of the membrane S wave mode between the honeycomb thin layer and its equivalent homogenized plate (left) Phase velocity  $\omega/|\mathbf{k}|$ ; (right) Group velocity  $D_{\mathbf{k}}\omega$

Then, we consider the 2<sup>nd</sup> wave mode of the honeycomb thin layer (Figure 4.16). Since for the honeycomb thin layer, the membrane and bending waves are coupled, it is not as easy as in the 2D periodic hexagonal beam network case to compare the Bloch wave modes and the equivalent homogenized model modes. Here, by comparing the phase wave velocity of the 2<sup>nd</sup> Bloch wave mode with the equivalent homogenized model in LF range, we find that the 2<sup>nd</sup> Bloch wave mode of the honeycomb thin layer is close enough with the bending mode of the homogenized model.

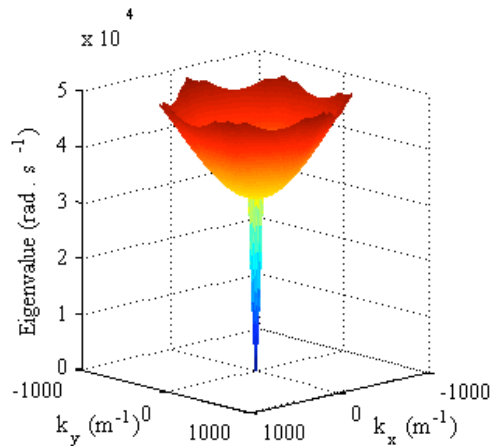
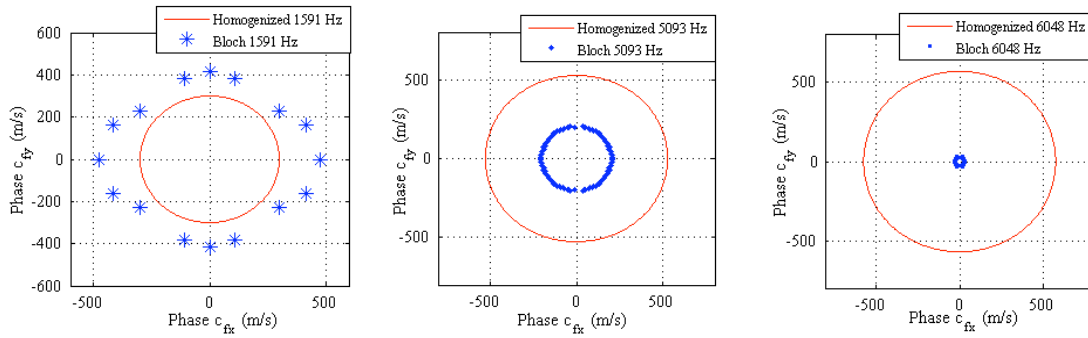


Figure 4.16 Dispersion surface of 2<sup>nd</sup> Bloch wave mode (bending mode) of the honeycomb thin layer

We notice that in the LF range, from 0 to about 5000Hz, the 2<sup>nd</sup> wave mode of the honeycomb thin layer shows slight anisotropic characteristics and its phase wave propagation velocity can be, on the whole, represented by the homogenized plate. However, in HF range, beyond about 5000Hz, both the phase and group velocities decrease rapidly in the honeycomb thin layer but not in the homogenized model, so that the homogenized model totally fails to simulate the honeycomb thin layer (Figure 4.17, 4.18, 4.19(a) and 4.19(b)). Besides, in HF range, the 2<sup>nd</sup> Bloch wave mode of the honeycomb thin layer has complex anisotropic wave fronts (Figure 4.19 (c)).



(a)  $f = 1591\text{Hz}$       (b)  $f = 5093\text{Hz}$       (c)  $f = 6048\text{Hz}$

Figure 4.17 Comparison of the phase velocity  $\omega/|\mathbf{k}|$  of the 2<sup>nd</sup> Bloch wave mode of the honeycomb thin layer and the bending mode of the equivalent homogenized plate

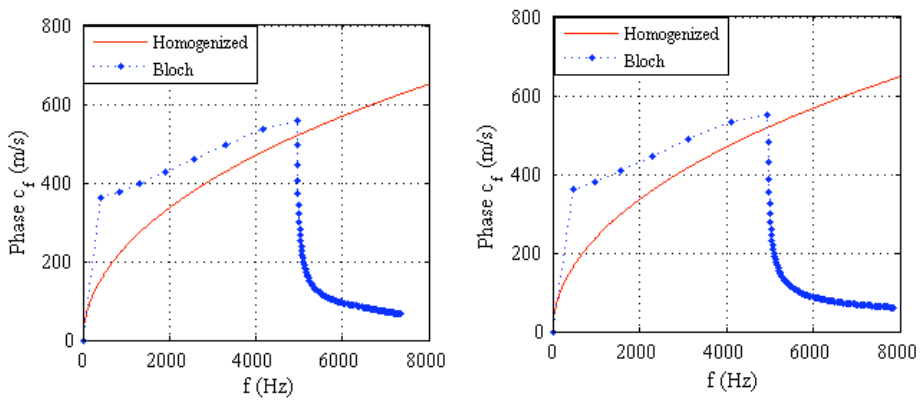
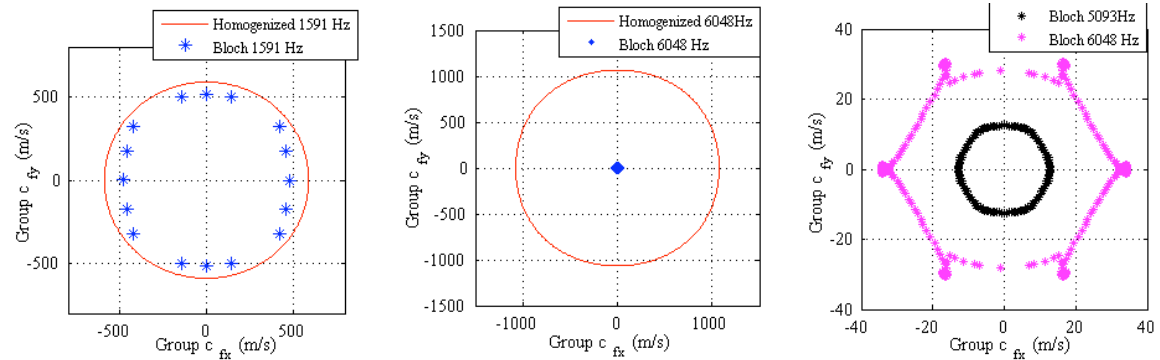


Figure 4.18 Comparison of the phase velocity  $\omega/|\mathbf{k}|$  of the 2<sup>nd</sup> Bloch wave mode of the honeycomb thin layer and the bending mode of the equivalent homogenized plate (left) Along the axis  $\mathbf{e}_x$ ; (right) Along the axis  $\mathbf{e}_y$



(a)  $f = 1591\text{Hz}$ ; (b)  $f = 6048\text{Hz}$ ; (c) the 2<sup>nd</sup> Bloch wave eigenmode,  $f = 5093\text{Hz}$  and  $f = 6048\text{Hz}$

Figure 4.19 Comparison of the group velocity  $D_{\mathbf{k}}\omega$  of the 2<sup>nd</sup> Bloch wave mode of the honeycomb thin layer and the bending mode of the equivalent homogenized plate

### 4.2.2 1<sup>st</sup> Bloch wave mode of the honeycomb core sandwich plate

Let us now consider the 1<sup>st</sup> Bloch wave mode of the honeycomb core sandwich plate (Figure 4.20). Being similar with the 1<sup>st</sup> Bloch wave mode of the honeycomb core thin layer, we still compare it to the bending mode of its equivalent homogenized model.

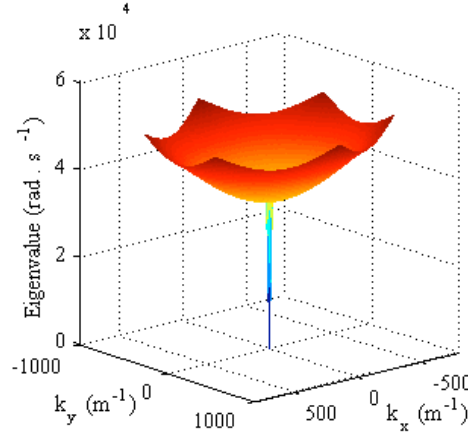
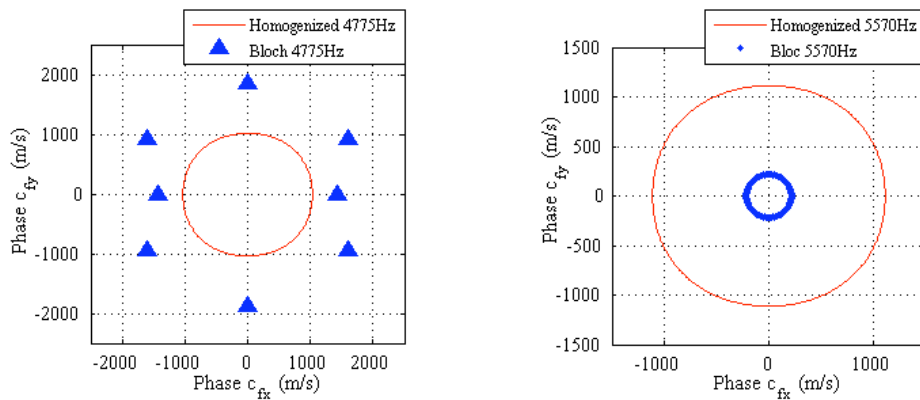


Figure 4.20 Dispersion surface of the 1<sup>st</sup> Bloch wave mode of the honeycomb core sandwich plate

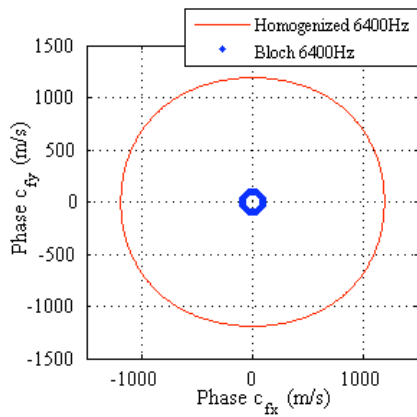
We first notice that in this case, the 1<sup>st</sup> Bloch wave mode of the honeycomb sandwich plate shows anisotropic characteristics in the frequency range from 0 to about 5000Hz, while from about 5000Hz to 7000Hz, it displays more isotropic properties. After 7000Hz, complex wave fronts take place. Second, we notice that significant wave velocity caustics phenomena occur in about 5500Hz for the phase and group velocities varying in the space.

Finally, when the phase wave velocity of the first Bloch eigenmode is compared to the one of the equivalent homogenized model, we remark that in the LF range, up to about 5000Hz, the tendency is similar but quantitatively the comparison is not satisfactory. A relatively coarse discretization of  $k$  and the strong junction conditions used in our modeling may partly explain difference. Then in the HF range, beyond about 5000Hz, both the phase and group velocities decrease rapidly, so that the homogenized model totally fails to simulate the sandwich plate. Hence, we recognize that the previously presented property of the second bending mode of the homogenized thin layer, which confirms the important role played by the honeycomb core in the bending behavior of sandwich plate (Figure 4.21, 4.22 and 4.23).

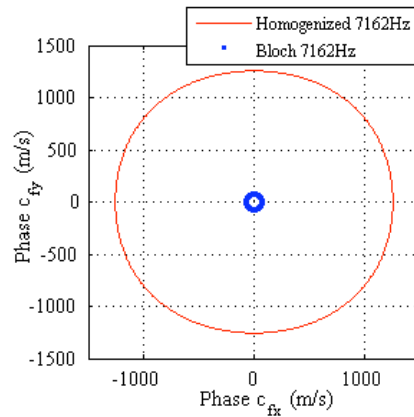


(a)  $f = 4775\text{Hz}$

(b)  $f = 5570\text{Hz}$



(c)  $f = 6400\text{Hz}$



(d)  $f = 7162\text{Hz}$

Figure 4.21 Comparison of the phase velocity  $\omega/|\mathbf{k}|$  of the 1<sup>st</sup> Bloch wave mode of the honeycomb core sandwich plate and the bending mode of the equivalent homogenized plate

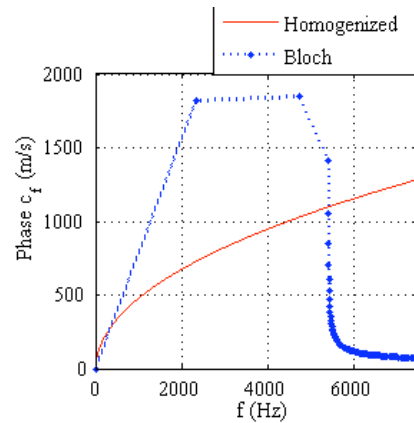
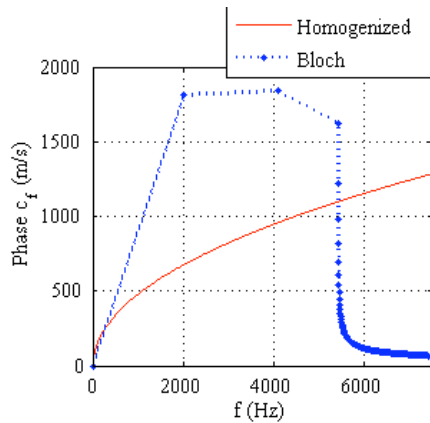
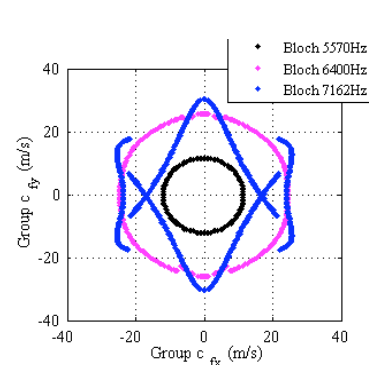
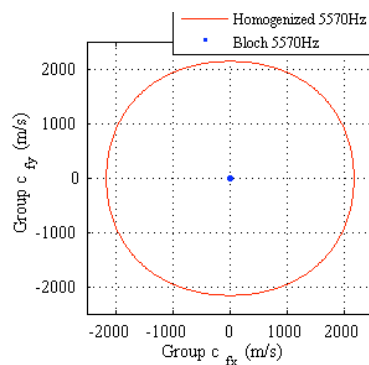
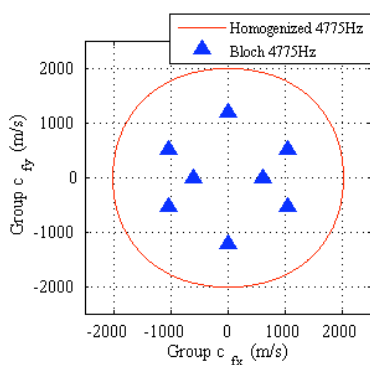


Figure 4.22 Comparison of the phase velocity  $\omega/|\mathbf{k}|$  of the 1<sup>st</sup> Bloch wave mode of the honeycomb core sandwich plate and the bending mode of the equivalent homogenized plate (left) Along the axis  $\mathbf{e}_x$ ; (right) Along the axis  $\mathbf{e}_y$



(a)  $f = 4775\text{Hz}$ ; (b)  $f = 5570\text{Hz}$ ; (c) 1<sup>st</sup> Bloch wave eigenmode,  $f = 5570\text{Hz}$ ,  $f = 6400\text{Hz}$  and  $f = 7162\text{Hz}$

Figure 4.23 Comparison of the group velocity  $D_{\mathbf{k}}\omega$  of the 1<sup>st</sup> Bloch wave mode of the honeycomb core sandwich plate and the bending mode of the equivalent homogenized plate

## Conclusion

In this chapter, we focus on the numerical results of the elastic wave propagation in the honeycomb thin layer as well as in the honeycomb core sandwich plate.

First of all, the strong junction between the plates caused by the condition  $\theta_n = 0$  in globally in the whole primitive has been analyzed. It has been confirmed that apart from the first Bloch wave eigenvalue, the way to model the junction affects all the other Bloch wave eigenvalues of the honeycomb thin layer.

Then, the dispersion relation and the Bloch wave eigenmodes have been obtained for both the honeycomb thin layer and the sandwich plate. It has been studied that the variation of the thickness of the horizontal plate makes the Bloch wave eigenvalues of the honeycomb thin layer and the sandwich plate move to higher frequency ranges, except the first mode of the honeycomb thin layer, which is a membrane S-mode. In parallel, it has also been investigated that the internal angle that indicates the cellular shape of the primitive cell does not affect significantly the dispersion relation of the honeycomb thin layer. We note that, for the considered frequency range up to about 12kHz, no stop band has been found for all cases considered here.

In the end, through wave velocities analysis of the 1<sup>st</sup> and 2<sup>nd</sup> Bloch wave modes, we find that the honeycomb thin layer provides more and more anisotropic and dispersive characteristics with the frequency increases. The equivalent homogenized model represents correctly the membrane S-mode, while for the bending wave mode, it is correct only in the frequency range from 0 to about 5000Hz. For the higher frequency range, an interesting rapid decreasing of wave velocities occurs, the mode tends to be “localized” or locally “trapped”, as its propagation velocity tends to zero. For the honeycomb core sandwich plate, the 1<sup>st</sup> Bloch wave mode is considered. Significant wave velocity caustics phenomena take place at about 5500Hz. We believe that the first Bloch wave mode is a bending mode. Its phase and group velocities are then compared to the ones of the classical equivalent homogenized model. It is found that in the LF range, up to about 5000Hz, the tendency is similar but quantitatively the comparison is not satisfactory, and in the HF range, beyond about 5000Hz, both the phase and group velocities decrease rapidly, so that the homogenized model totally fails to simulate the sandwich plate. Hence, important role played by the honeycomb core in the bending behavior of the sandwich plate is confirmed.

# Conclusion

Honeycomb core sandwich composite panels, composed of two skins with a honeycomb core thin layer, are commonly applied in aviation or aeronautic engineering. Based on the industrial requirements, previously a numerical modeling of HF shock wave propagating in the considered honeycomb core sandwich shells by using the classical homogenized models has been undertaken. The studies have indicated that the homogenized models can simulate the membrane wave behaviors of the sandwich in a large frequency range but fail to give accurate simulation results for the HF bending and transverse shear waves behaviors.

It has been analyzed that the bending and transverse shear waves of the sandwich are mostly controlled by the honeycomb core thin layer, which in our case is produced by bonding several corrugated sheets, which allows the thin layer to contain hexagonal cavities, where complicated wave propagation takes place through the sandwich. Especially in HF range, much more interactions occur between the wave and the honeycomb cells since the involved wavelength is small enough with respect to each cell.

Therefore, a more accurate numerical model has been proposed with the introduction of the honeycomb thin layer microstructure. Since the honeycomb sandwich may be considered as a periodic network, the Bloch wave theory has been proposed, according to which the calculation can be reduced to look for the periodic Bloch wave eigenmodes in a primitive cell instead of looking for the wave solution in the whole sandwich network.

Our study has been focused on giving the complete definition of the Bloch eigenproblem respectively for a 1D periodic beam network, 2D periodic hexagonal and rectangular beam networks, the honeycomb core thin layer and the honeycomb core sandwich plate. By solving the Bloch eigenproblem of the periodic networks, important informations, such as the dispersion relation between the Bloch wave vector and the eigenvalue, the Bloch wave eigenmodes and the phase and group velocities of the wave propagation in the networks have been obtained and analyzed.

For the 1D periodic beam structure, the dispersion relation has been obtained for the longitudinal wave and the bending and transverse shear waves. For the longitudinal wave, it has been found that the more different from one the acoustic impedance ratio, the larger the stop bands and the stronger the attenuation. The frequency bandgaps move to low frequency range with the decrease of Young's modulus. For the bending and transverse shear waves, it has been found that their bandgaps begin in a lower frequency range when compared to the ones of longitudinal wave. The more the mismatch of Young's modulus is, the larger the stop bands. The decrease of Young's modulus makes the bandgaps move to lower frequency range. Besides, it has also been found that for the bending and transverse shear waves there is a relation between the order of magnitude of the eigenvalue and the order of magnitude of beam's thickness.

For the 2D periodic hexagonal beam structure, emphasis has been dedicated to the analysis of the dispersion relation of the in-plane membrane and the out-of-plane bending waves of the network. The first stop band of the in-plane waves has been found at about  $3 \times 10^5$  Hz and the one of out-of-plane waves at about  $3 \times 10^6$  Hz. The influence of the Young's modulus, the beam's thickness  $H$ , the double-thickness horizontal beam and the internal angle on the bandgaps has been studied. For the Young's modulus, we have obtained the same kind of conclusion as in the 1D study, while for the beam's thickness, we notice that, with the

decrease of the thickness, the in-plane waves' bandgaps decrease to low frequency range but the location of the first stop band remains fixed. For the double-thickness horizontal beam, we notice that the first stop band of the in-plane waves observed in the case of single-thickness horizontal beam could not be obtained in this case. For the internal angle, the first stop band of the in-plane waves could be obtained when  $\theta = 30^\circ, 45^\circ, 60^\circ$  and  $75^\circ$  in the considered frequency range and no stop band has been produced for the out-of-plane waves. By analyzing the wave velocities of several main wave modes of the network, it has been pointed out that the periodic hexagonal network provides more and more anisotropic and dispersive characteristics in the six corresponding hexagonal symmetric directions when the frequency moves to higher range. In HF range, complex wave front takes place and the wave velocity caustic phenomenon occurs. Equivalent homogenized model can simulate the in-plane membrane waves and also the out-of-plane bending waves in LF range.

In parallel, the same kind of study has also been done to obtain the dispersion relation of the 2D periodic rectangular beam network. It has been noticed that no complete frequency bandgaps has been observed for both the in-plane membrane and the out-of-plane bending waves in the considered frequency range.

Finally, the investigation has been extended to the honeycomb thin layer and the honeycomb core sandwich plate. We have first discussed the influence of the strong junction condition caused by the condition of the drilling rotation around the axis  $\mathbf{n}$ ,  $\theta_n = 0$ , in each local plate's basis. It has been noticed that the junction condition does not affect the first Bloch eigenmode, while it changes the dispersion curves of the other higher-order modes and makes the eigenvalue move to higher frequency range. Then, the dispersion surfaces as well as the curves of the honeycomb thin layer and the sandwich plate have been obtained. The effects of the double-thickness horizontal plate and the internal angle have been investigated. We have found that the double-thickness horizontal plate makes the dispersion curves of the honeycomb thin layer as well as the sandwich plate move to higher frequency range and the internal angle does change the shapes of the dispersion curves. Finally, the anisotropic and dispersive nature of the honeycomb thin layer and the sandwich has been studied by analyzing the phase and group velocities of several main modes. Similar conclusions can be obtained as in the 2D hexagonal beam case, but now the homogenized model gives acceptable results for the bending wave of the honeycomb thin layer before 5000Hz and fails to coincide with the sandwich.

In the further, we hope to improve the classical homogenized models according to our approach. Then we also wish to further develop our numerical approach in several aspects such as: applying viscoelastic mechanical characteristics to the honeycomb sandwich, taking into account curvature effects and the design of the honeycomb sandwich with respect to vibration control.

# Reference

- [Atkins (2005)] P. Atkins and R. Friedman. *Molecular quantum mechanics*. Oxford University Press, 2005.
- [Barbarosie (2004)] C. Barbarosie and M. M. Neves. *Periodic structures for frequency filtering: analysis and optimization*. Computers & Structures, 82, 1399-1403, 2004.
- [Bloch (1928)] F. Bloch. Über die Quantenmechanik der Elektronen in Kristallgittern, 52:555–600, 1928.
- [Boullard (2009)] A. Boullard. Propagation des ondes dans les coques simples ou en nid d'abeille soumises à des charges mobiles: Application au lanceur Ariane 5 sous chocs pyrotechniques. Thesis, Ecole centrale Paris, France, 2009.
- [Bouzit (1995)] D. Bouzit and C. Pierre. *Localization of vibration in disordered multi-span beams with damping*. Journal of sound and vibration, 187(4), 625-648, 1995.
- [Brillouin (1946)] L. Brillouin. *Wave propagation in the periodic structures*. Dover Publication, 1946.
- [Burton (1997)] W. S. Burton and A. K. Noor. *Assessment of continuum models for sandwich panel honeycomb cores*. Computational methods in applied mechanics and engineering, 145, 341–360, 1997.
- [Chen (1998)] J. Y. Chen, Y. Huang and M. Ortiz. *Fracture analysis of cellular materials: a strain gradient approach*. Journal of the mechanics and physics of solids, 46, 789-828, 1998.
- [Clouteau (2000)] D. Clouteau, D. Aubry, M. L. Elhabre and E. Savin. *Periodic and stochastic BEM for large structure embedded in an elastic half-space*. Chapman & Hall/CRC Research Notes in Mathematics: Mathematical aspects of boundary element methods, 414, 91-102, 2000.
- [Collet (2011)] M. Collet, M. Ouisse, M. Ruzzene and M. N. Ichchou. *Floquet–Bloch decomposition for the computation of dispersion of two-dimensional periodic, damped mechanical systems*. International journal of solids and structures, 48, 2837–2848, 2011.
- [Cotoni (2008)] V. Cotoni, R. S. Langley and P. J. Shorter. *A Statistic energy analysis subsystem formulation using finite element and periodic structure theory*. Journal of sound and vibration, 318, 1077-1108, 2008.
- [Cremer (1967)] L. Cremer, M. Helk and B. A. T. Petersson. *Structure-Borne Sound, 3<sup>rd</sup> edition*. Springer, Berlin, 2005.
- [Dal Maso (1993)] G. Dal Maso. *An introduction to  $\Gamma$ -convergence*. Birkäuser, Boston, 1993.
- [Davini (2011)] C. Davini and F. Ongaro. *A homogenized model for honeycomb cellular materials*. Journal of Elasticity, 104, 205–226, 2011.
- [Floquet (1883)] M. G. Floquet. *Sur les équations différentielles linéaires à coefficients périodiques*. Annales de l'Ecole Normale, 12, 47-88, 1883.
- [Florens (2010)] C. Florens. Modeling of the viscoelastic honeycomb panel equipped with

piezoelectric patches in view of vibroacoustic activecontrol design. Thesis, Ecole Centrale Paris – ONERA, 2010.

[Gibson (1988)] L. J. Gibson and M. F. Ashby. *Cellular solids: Structures and properties*. International Series on Material Science & Technology, Pergamon Press, 1988.

[Gonella (2008)] S. Gonella and M. Ruzzene. *Analysis of in-plane wave propagation in hexagonal and re-entrant lattices*. Journal of sound and vibration, 312, 125–139, 2008.

[Grédé (2006)] A. Grédé, B. Tie and D. Aubry. Elastic wave propagation in hexagonal honeycomb sandwich panels: Physical understanding and numerical modeling. Journal de Physique, 134, 507–514, 2006.

[Grédé (2009)] A. Grédé. Modélisation des chocs d’origine pyrotechnique dans les structures d’Ariane 5: développement de modèles de propagation et d’outils de modélisation. Thesis, Ecole Centrale Paris, 2009.

[Ho (2003)] K. M. Ho, C. K. Cheng, Z. Yang, X. X. Zhang and P. Sheng. *Broadband locally resonant sonic shields*. Applied physics letter, 83(26), 5566-5568, 2003.

[Inquiété (2008)] G. Inquiété. Simulation numérique de la propagation des ondes dans les structures composites stratifiées. Thesis, Ecole Centrale Lyon, France, 2008.

[Jensen (2002)] J. S. Jensen, O. Sigmund, J. J. Thomsen and M. P. Bendsoe. *Design of multi-phase structures with optimized vibrational and wave transmitting properties*. 15<sup>th</sup> Nordic Seminar on Computational Mechanics, 63-66, 2002.

[Jeong (2004)] S. M. Jeong and M. Ruzzene. *Analysis of vibration and wave propagation in cylindrical grid-like structures*. Shock and Vibration, 11, 311–331, 2004.

[Jones (2007)] I. S. Jones and A. B. Movchan. *Bloch-Floquet waves and controlled stop bands in periodic thermo-elastic structures*. Waves in Random and Complex Media, 17(4), 429-438, 2007.

[Kittel (1962)] C. Kittel. Elementary solid state physics: A short course, 1<sup>st</sup> edition, Wiley, 1962.

[Langley (1995)] R. S. Langley. Wave transmission through one-dimensional near periodic structures: optimum and random disorder. Journal of sound and vibration, 188(5), 717-743, 1995.

[Langley (1997)] R. S. Langley, N. S. Bardell and H. M. Ruivo. The response of two-dimensional periodic structures to harmonic point loading: a theoretical and experimental study of a beam grillage. Journal of sound and vibration, 207, 521–535, 1997.

[Langley (1997)] R. S. Langley, J. R. D. Smith and F. J. Fahy. *Statistic energy analysis of periodically stiffened damped plate structures*. Journal of sound and vibration, 208(3), 407-426, 1997.

[Leclère (2001)] J. –M. Leclère. Modélisation parallèle de la propagation d’ondes dans les structures par éléments finis adaptatifs. Thesis, Ecole centrale Paris, 2001.

[Legay (2009)] A. Legay and J. –F. Deü. Simulation de la réponse aux chocs de structures sandwich de révolution: Application à la découpe pyrotechnique d’un adaptateur de charge utile. In 9e Colloque National en Calcul des Structures, Giens, France, 2009.

- [Liu (2000)] Z. Y. Liu, X. X. Zhang, Y. Mao, Y. Y. Zhu, Z. Y. Yang, C. T. Chan and P. Sheng. *Locally resonant sonic materials*. Science, 289, 1734-1736, 2000.
- [Martinsson (2003)] P. G. Martinsson and A. B. Movchan. *Vibrations of lattice structures and phononic bandgaps*. The Quarterly Journal of Mechanics and Applied Mathematics, 56, 45–64, 2003.
- [Mead (1970)] D. J. MEAD. *Free wave propagation in periodically-supported infinite beams*. Journal of sound and vibration, 11, 181-197, 1970.
- [Mead (1973)] D. J. MEAD. A general theory of harmonic wave propagation in linear periodic system with multiple coupling. Journal of sound and vibration, 27(2), 235-260, 1973.
- [Mead (1979)] D. J. MEAD and S. Parthan. *Free wave propagation in two-dimensional periodic plates*. Journal of sound and vibration, 64(3), 325-346, 1979.
- [Mead (1983)] D. J. MEAD and S. MARKUS. *Coupled flexural-longitudinal wave motion in periodic beam*. Journal of sound vibration, 90, 1-24, 1983.
- [Mead (1987)] D. J. Mead and N. S. Bardell. *Free vibration of a cylindrical shell with periodic circumferential stiffness*. Journal of sound vibration, 111(2), 499-520, 1987.
- [Mead (1991)] D. J. MEAD and Y. YAMAN. The harmonic response of rectangular sandwich plates with multiple stiffening: a flexural wave analysis. Journal of sound vibration, 145, 409-428, 1991.
- [Mencik (2005)] J. M. Mencik, M. Ichchou and L. Jézéquel. *Propagation multi-modale dans les systèmes périodiques couples*. In 7e Colloque National en Calcul des Structures, Giens (Var), France, 2005.
- [Richards (2003)] D. Richards and D. J. Pines. *Passive reduction of gear mesh vibration using a periodic drive shaft*. Journal of sound and vibration, 264, 317-342, 2003.
- [Ruzzene (2003)] M. Ruzzene, F. Scarpa and F. Soranna. *Wave beaming effects in two-dimensional cellular structures*. Smart Materials and Structures, 12, 363–372, 2003.
- [Sanchez-Palencia (1989)] E. Sanchez-Palencia and J. Sanchez Hubert. *Vibration and coupling of continuous systems*. Asymptotic methods, Ed. Springer, Berlin, 1989.
- [Sigalas (1992)] M. Sigalas and E. N. Economou. *Elastic and acoustic wave band structure*. Journal of sound and vibration, 158(2), 377-382, 1992.
- [Sigalas (1993)] M. Sigalas and E. N. Economou. *Band structure of elastic waves in two dimensional systems*. Solid State Communications, 86(3), 141-143, 1993.
- [Sigalas (1998)]: M. Sigalas. Defect states of acoustic waves in a two-dimensional lattice of solid cylinders. Journal of applied physics, 84, 26-30, 1998.
- [Sigalas (2005)] M. Sigalas, M. S. Kushwaha, E. N. Economou, M. Kafesaki, I. E. Psarobas and W. Steurer. *Classical vibrational modes in phononic lattices: theory and experiment*. Z. Kristallogr, 220, 765 – 809, 2005.
- [Sigmund (2003)] O. Sigmund and J. S. Jensen. *Systematic design of photonic band-gap materials and structures by topology optimization*. Philosophical Transactions of the Royal Society London Series A (Mathematical, Physical and Engineering Sciences), 361, 1001–1019, 2003.

- [Sjöberg (2005)] D. Sjöberg, C. Engström, G. Kristensson, D. J. N. Wall and N. Wellander. *A Floquet-Bloch decomposition of Maxwell's equations, applied to homogenization*. Multiscale Modeling & Simulation, 4(1), 149-171, 2005.
- [Sorokin (2004)] S. V. Sorokin. *Analysis of wave propagation in sandwich plates with and without heavy fluid loading*. Journal of sound and vibration, 271, 1039-1062, 2004.
- [Spadoni (2009)] A. Spadoni, M. Ruzzene, S. Gonella and F. Scarpa. *Phononic properties of hexagonal chiral lattices*. Wave motion, 46, 435-450, 2009.
- [Srikantha Phani (2006)] A. Srikantha Phani, J. Woodhouse and N. A. Fleck. *Wave propagation in two-dimensional periodic lattices*. Journal of the Acoustical Society of America, 119(4), 1995-2005, 2006.
- [Srikantha Phani (2008)] A. Srikantha Phani and N. A. Fleck. *Elastic boundary layers in two-dimensional isotropic lattices*. Journal of Applied Mechanics, 75(2), 1-8, 2008.
- [Tawfik (2004)] M. Tawfik, J. Chung and A. Baz. *Wave attenuation in periodic helicopter blade*. In 5<sup>th</sup> Jordan International Mechanical Engineering Conference, Amman, Jordan, 2004.
- [Tee (2010)]: A. Tee, A. Spadoni, F. Scarpa and M. Ruzzene. *Wave propagation in auxetic tetrachiral honeycombs*. Journal of vibration and acoustics, 132, 031007-8, 2010.
- [Tian (2011)] B. Y. Tian, B. Tie, D. Aubry and X.Y. Su. *Elastic Wave Propagation in Periodic Cellular Structures*. Computer modeling in engineer & science, 76(4), 217-234, 2011.
- [Tie (2009)] B. Tie, D. Aubry, A. Grédé, J. Philippon, B. Y. Tian and P. Roux. *Predictive numerical modeling of pyroshock propagation in payload adaptors of space launcher*. 11th ECSSMMT European Conference on Spacecraft Structures, Materials & Mechanical Testing (CNES ESA DLR), Toulouse, France, 2009.
- [Tie (2012)] B. Tie, D. Aubry and B. -Y. Tian. *Bloch wave modal analysis and numerical investigation of HF elastic wave propagation in periodic assemblies of thin structures*. DYNACOMP 2012 1<sup>st</sup> International Conference on Composite Dynamics, Arcachon, France, 2012.
- [Wang (2012)] J. W. Wang, G. Wang, J. H. Wen and X. S. Wen. *Flexural vibration band gaps in periodic stiffened plate structures*. Mechanika, 18(2), 186-191, 2012.
- [Wolfe (1998)] J. P. Wolfe. *Imaging Phonons: acoustic wave propagation in solids*. Cambridge University Press, 1998.
- [Wu (2002)] F. -G. Wu and Y. -Y. Liu. *Acoustic bandgaps and defect states in two-dimensional composite materials*. Chinese physics letters, 51(7), 1434-1438, 2002.
- [Yeh (1977)] P. Yeh, A. Yariv and C. -S. Hong. *Electromagnetic propagation in periodic stratified media. I. General theory*. Journal of the optical society of america B, 67, 423-437, 1977.
- [Yeh (1977)] P. Yeh, A. Yariv and C. -S. Hong. *Electromagnetic propagation in periodic stratified media. II. Birefringence, phase matching, and x-ray lasers*. Journal of the optical society of america B, 67, 438-448, 1977.
- [Zhang (2005)] W. Zhang, N. Vlahopoulos and K. Wu. *An energy finite element formulation*

for high-frequency vibration analysis of externally fluid-loaded cylindrical shells with periodic circumferential stiffeners subjected to axi-symmetric excitation. *Journal of sound and vibration*, 282, 679-700, 2005.

[Zhong (1995)] W. X. Zhong and F. W. Williams. *On the direct solution of wave propagation for repetitive structures*. *Journal of sound and vibration*, 181(3), 485-501, 1995.

## Appendix A

# Bending wave velocity in homogenized model

According to the equilibrium equation (1.3), we have the equilibrium equation of the bending and transverse shear waves:

$$\begin{aligned} \xi_s \cdot (\mathbf{C}_{st} \cdot \mathbf{U}_{1s}) &= i[\rho\omega^2 - \xi_s \cdot (\mathbf{C}_{st} \cdot \xi_s)]U_{0n} \\ \frac{12}{H^2}iU_{0n}(\mathbf{C}_{st} \cdot \xi_s) &= \left[ \rho\omega^2 \mathbf{I}_{2d} - \mathbf{Q}_s(\xi_s, \xi_s) - \frac{12}{H^2} \mathbf{C}_{st} \right] \cdot \mathbf{U}_{1s} \end{aligned} \quad (\text{A.1})$$

where  $\mathbf{U}_{1s} = U_{1s1}\mathbf{e}_1 + U_{1s2}\mathbf{e}_2$ . Therefore, (A.1) which can be written as:

$$[\mathbf{B}] \begin{Bmatrix} U_{0n} \\ U_{1s1} \\ U_{1s2} \end{Bmatrix} = 0 \quad (\text{A.2})$$

with the coefficient matrix  $\mathbf{B}$ :

$$[\mathbf{B}] = \begin{bmatrix} \|\xi_s\|^2(C_{55}a^2 + C_{44}b^2) - \omega^2\rho & -i\|\xi_s\|C_{55}a^2 & -i\|\xi_s\|C_{44}b^2 \\ i\|\xi_s\|C_{55}a^2 & \frac{H^2}{12}(\|\xi_s\|^2(C_{11}a^2 + C_{66}b^2) - \omega^2\rho) + C_{55} & \frac{H^2}{12}\|\xi_s\|^2(C_{12} + C_{66})ab \\ i\|\xi_s\|C_{44}b^2 & \frac{H^2}{12}\|\xi_s\|^2(C_{12} + C_{66})ab & \frac{H^2}{12}(\|\xi_s\|^2(C_{66}a^2 + C_{22}b^2) - \omega^2\rho) + C_{44} \end{bmatrix} \quad (\text{A.3})$$

To ensure that the system (A.2) admits nontrivial solutions, the determinant of matrix  $\mathbf{B}$  should vanish:  $\det(\mathbf{B}) = 0$ , which gives rise to the equations (1.5) and (1.6).